Order Number 9029993

Generalization of the Weinbaum-Jiji bioheat equation and studies of whole limb heat transfer

Zhu, Min, Ph.D.

City University of New York, 1990

U·M·I
300 N. Zeeb Rd.
Ann Arbor, MI 48106

GENERALIZATION OF THE WEINBAUM-JIJI BIOHEAT EQUATION

AND STUDIES OF WHOLE LIMB HEAT TRANSFER

by

MIN ZHU

A dissertation submitted to the Graduate Faculty
in Engineering in partial fulfillment of the
requirements for the degree of Doctor of
Philosophy, The City University of New York

1990

This manuscript has been read and accepted for the Graduate Faculty in Engineering in satisfaction of the dissertation requirement for degree of Doctor of Philosophy.

3/19/90

Date

Professor Sheldon Weinbaum
Chair of Examining Committee

3/26/90

Date

Professor Gerard G. Lowen
Executive Officer

Professor Sheldon Weinbaum

Professor Latif M. Jiji

Professor Daniel E. Lemons

Professor Zeev Dagan

Professor Caleb K. Charny

Supervisory Committee

The City University of New York

Abstract

GENERALIZATION OF THE WEINBAUM-JIJI BIOHEAT EQUATION AND STUDIES OF WHOLE LIMB HEAT TRANSFER

by

Min Zhu

Advisers: Professor Sheldon Weinbaum

Professor Latif M. Jiji

In this dissertation the Weinbaum-Jiji bioheat equation (1985) is generalized to vessels of unequal size and then combined with a new theory for asymmetric countercurrent heat transfer to develop a three-dimensional variable geometry model for whole limb heat transfer. An experimental study is also conducted to verify the predictions of this theoretical model and to provide the input values for model parameters for a human arm.

A brief introduction to blood-tissue heat transfer is given in Chapter 1. In Chapter 2 an asymptotic analysis is derived to elucidate the relationship between the near field temperature of an unequal artery-vein pair and the local average tissue temperature. This analysis is used to rigorously prove the closure approximation relating the local arterial-venous temperature difference and the mean tissue temperature which had been derived by Weinbaum & Jiji (1985) using a more heuristic approach. Based on these results, the Weinbaum-Jiji bioheat equation is generalized for vessels of unequal size.

In Chapter 3 a three dimensional approximate analytic solution technique is developed for treating unequal countercurrent heat

exchange. The solution describes the heat transfer between parallel paired countercurrent vessels with a laminar velocity profile asymmetrically embedded in a long cylinder with surface convection. In Chapter 4 this solution is extended to formulate a three dimensional variable geometry model for whole limb heat transfer. This model is not limited by the restriction in the model by Song et al. (1988) which assumes that the heat loss to the surroundings is small compared to the heat exchange between the central vessels. The local microvascular temperature field in the muscle tissue is described by a new approach in which the Pennes (1948) and Weinbaum-Jiji equations are applied in different flow regions. This model also allows for an arbitrary axial variation of the cross-sectional area and blood distribution between the muscle and cutaneous tissue. Furthermore, the computational time for the present model is much shorter than that of the model by Song et al. (1988). Representative solutions for the axial variation of the average skin and central artery and vein temperatures are in much better agreement with available experimental data than previous solutions.

In the experimental study described in Chapter 5, a plethysmograph-calorimeter apparatus has been constructed to measure the blood flow rates of the human arm and hand and the heat loss of the hand. The relationship between blood flow and heat transfer when the hand is placed in a water bath at different temperatures is examined. Also, the skin surface temperature distribution of the arm is measured and compared with the theoretical predictions of the whole limb model described in Chapter 4.

To My Wife

Ming-Xu

Acknowledgements

The author wishes to express his deepest gratitude and appreciation to Professor Sheldon Weinbaum, Professor Latif M. Jiji and Doctor Daniel E. Lemons for their constant support, encouragement and guidance which made it possible for the author to enter the frontier of this promising and challenging field of research.

The author would also like to thank Doctor Caleb K. Charny for many helpful discussions and to thank Ms. Susan Teitelbaum and Mr. Yulong Wu for their help and cooperation during the course of the experimental study of this research.

The author is grateful to professor Gerard G. Lowen for handling administrative details in such a warm and friendly manner.

This research was supported by NIH Grant HL 26090 and NSF Grant CBT-8702582.

Table of Contents

List of Symbols

a	vessel radius of muscle layer
a^*	variable, defined in equation (4.48)
a_a	radius of artery in chapter 2; radius of central artery
a_{ai}	radius of central artery at entrance of limb
a_v	radius of vein in chapter 2; radius of central vein
A_{ij}	component of eigenvector, defined by equations (3.20) and (3.21)
b^*	variable, defined in equation (4.48)
B_a	shape factor, defined by (2.26)
B_i	Biot number of tissue cylinder
B_v	shape factor, defined by (2.27)
B_{it}	Biot number of arm
c^*	variable, defined in equation (4.48)
c	specific heat of tissue
c_b	specific heat of blood
c_w	specific heat of water
C_i	constant, defined by equations (3.20) and (3.21) in chapter 3; given in Table 3 in chapter 4
d_a	distance from origin to artery
d_v	distance from origin to vein
F	variable, defined by equation (A1)

g_a	blood bleed-off from artery per unit vessel surface area
G	variable, defined by (2.13); dimensionless shape function representing axial variation of arm geometry in chapter 4
h	heat transfer coefficient of tissue cylinder
h_t	heat transfer coefficient of arm
$H_{1,2,3}$	variables, defined by equation (4.52)
J_c	rate of water flow through coil in Plethcal
J_v	rate of water flow through vessel A_{in} in Plethcal
k	thermal conductivity
k'	blood conductivity/tissue conductivity
$(k_{ij})_{eff}$	tensor of effective conductivity
k_{eff}	effective conductivity
k_{em}	radial effective conductivity in entire muscle layer
k"	radial effective conductivity in entire muscle layer/tissue conductivity
l	distance between artery and vein
l_i, l_j	directional cosine of vessel axis with respect to direction i,j
l_r	directional cosine of vessel axis with respect to radial direction
L	characteristic length of macroscopic temprature gradient, length of arm in chapter 4
L_e	thermal equilibration length of vessel
n	number density of vessel pairs of muscle layer
N_u	Nusselt number of central vessel

p	shape factor, defined by (2.19)
P	shape factor, defined by (2.34)
P_e	Peclet number of vessel in muscle; Peclet number of central artery in chapter 3
P_{ei}	inflow Peclet number of central artery at entrance of limb
q	rate of energy transfer by conduction between vessel pair per unit length of vessel
q_a	rate of energy transfer by conduction at artery wall per unit length
q_e	net heat lose to far field tissue from countercurrent vessels
q_{ev}	rate of energy transfer by evaporation per unit area of skin surface
q_H	total heat transfer rate on extremity surface
q_m	metabolic heat production of muscle layer
q_v	rate of energy transfer by conduction at vein wall per unit length
Q_a	variable, defined by equation (3.12)
Q_v	variable, defined by equation (3.13)
r	radial coordinate
r_o	radius of tissue cylinder surrounding microvessel pair
R	radial coordinate in w plane in chapter 2; radius of arm or tissue cylinder
R_a	radius of artery in w plane, Fig. 2
R_A	blood flow rate of arm
R_H	blood flow rate of hand

s	distance along microvessel pair in chapter 2; distance between central vessels
s_a	distance from origin to central artery
s_v	distance from origin to central vein
S	dimensionless distance along microvessel pair
t	time
T	temperature
T_{ai}	blood bulk temperature of central artery at entrance of limb
$T_{i,ov}$	temperature of water entering, leaving vessel A_{in} in Plethcal
$T_{i,oc}$	temperature of water entering, leaving coil in Plethcal
T_m	temperature, defined by (2.31)
T_w	water temperature to which hand exposed
T_∞	environmental temperature
u	Cartesian coordinate in w plane, Fig. 2 in chapter 2; blood velocity in vessels of muscle layer
U	dimensionless blood velocity of central vessels
v	Cartesian coordinate in w plane, Fig. 2
V	mean blood velocity of central vessels
V'	mean blood velocity of central artery/mean blood velocity of central vein
V_{ai}	blood velocity of central artery at entrance of limb
V_H	volume of hand
W_b	volumetric blood perfusion rate per unit volume in muscle
x,y	Cartesian coordinate in z plane, Fig. 2
x_i,x_j	general Cartesian coordinate

z	dimensionless axial coordinate
Z	axial coordinate
α	polar angle in w plane, Fig. 2
β	reciprocal of inflow Peclet number of limb or tissue cylinder
$\Phi_{0,1,2}$	variables, defined by equation (4.32)
ϵ	normalized thermal equilibration length, defined by equation (2.39) or (4.29)
$\lambda_{1,2}$	eigenvalue, defined by (3.22)
λ_m	dimensionless metabolic heat production of muscle layer
λ_{pm}	dimensionless volumetric blood perfusion rate in muscle
λ_{pc}	dimensionless blood perfusion coefficient in inner cutaneous layer
φ	polar angle in cylindrical coordinate
φ_{av}	polar angle of central artery in cylindrical coordinate
ψ	blood supply to arm/blood supply to whole limb
ω	blood supply to muscle layer/blood supply to arm
μ	square root of λ_{pc}
ρ	density of tissue in chapter 2; dimensionless radial coordinate
ρ_b	density of blood
ρ_w	density of water
ρ_R	dimensionless radius of arm or tissue cylinder
γ	shape factor given by (32); dimensionless evaporation heat loss in chapter 4
θ	average tissue temperature in chapter 2; dimensionless temperature

θ_p	variable, defined by equation (3.14)
θ_c^*	temperature of blood entering cutaneous layer
σ	shape factor of vessels of muscle layer
σ_c	shape factor between vessels
σ_t	shape factor between vessel pair and surroundings
δ_{ij}	Kroneker delta
δ_m	thickness of inner region of cutaneous layer of arm
δ_s	thickness of outer region of cutaneous layer of arm

Superscript

-	dimensionless

Subscripts

a	artery
b	bulk, blood
i	entrance of limb
o	zeroth order
t	tissue
v	vein
w	vessel wall
1	core
2	deep muscle layer
3	surrounding muscle layer
4	inner cutaneous layer

List of Tables and Figures

Chapter 1. Introduction

The quantitative analysis of living tissue heat transfer has been the subject of numerous investigations since the work of Pennes [1]. Most of these studies, which are summarized in [2], have been based on the simplified bioheat equation proposed by Pennes,

$$\rho c \frac{\partial T}{\partial t} = \nabla \cdot k_t \nabla T + W_b \rho_b c_b (T_a - T) + q_m \qquad (1.1)$$

The crucial term in the Pennes equation is the blood perfusion term which describes the local heat transfer between blood and tissue. This term is treated as a volumetric and isotropic heat source which derives from the assumption that primary thermal equilibration between blood and tissue occurs in the capillary bed and the small arterioles and venules that feed and drain these smallest microvessels because of their very large surface area for heat exchange. However, this assumption has been questioned by several investigators [3,4,5]. The paper by Chen and Holmes [5] is of special importance since they showed that because the thermal conductivity coefficient is typically three orders of magnitude larger than the gaseous diffusion coefficient, thermal equilibration could not possibly occur in single vessels which are less than 50 μm under normal conditions.

A new fundamental bioheat equation has been derived by Weinbaum and Jiji [6] in which an important new blood-tissue heat transfer mechanism is described: the imperfect countercurrent heat exchange of the larger thermally significant artery-vein pairs of the microcirculation. This new equation is

$$\rho c \frac{\partial \theta}{\partial t} - \frac{\partial}{\partial x_i}\left[(k_{ij})_{eff} \frac{\partial \theta}{\partial x_j}\right] = -\frac{\pi^2 n a_a^2 k_b^2}{4\sigma_c k_t} P_e^2 l_j \left(\frac{\partial l_i}{\partial x_j}\right)\left(\frac{\partial \theta}{\partial x_j}\right) + q_m \qquad (1.2)$$

where the effective tissue conductivity due to the combined effect of both the countercurrent convection in the vessel pairs and small vessel bleed off from the countercurrent vessels is defined by

$$(k_{ij})_{eff} = k_t(\delta_{ij} + \frac{\pi^2}{4\sigma_c k_t^2} n a_a^2 k_b^2 P_e^2 l_i l_j) \tag{1.3}$$

This equation, which is considered a major advance in living tissue heat transfer analysis, differs from the Pennes equation in that the macroscopic local average temperature is related for the first time to the local microvascular geometry and flow and that the basic mechanism for blood-tissue heat transfer is not due to capillary heat exchange, but due to countercurrent heat exchange and the small vessel bleed off mechanism just mentioned.

Recently, Charny et al. [7] have used a full three-equation one-dimensional model to compare the Weinbaum-Jiji equation and the Pennes equation. The results show that the Weinbaum-Jiji equation provided very good agreement with the three-equation model for the vessels which are located in the outer half of the muscle tissue layer of a limb, where the vessels diameters are under 500 μm and the Pennes equation yields a better description of heat transfer for the vessels whose diameters are greater than 500 μm. The analysis of the results in [7] has led to a new interpretation of the source term in the Pennes bioheat equation. Instead of describing blood tissue heat transfer in the smallest microvessels and capillary beds, as has been commonly assumed, this analysis shows that the Pennes equation actually described small vessel bleed off (20-40 μm thermally equilibrated microvessels) from the largest countercurrent vessels of the microcirculation. However, in the initial study [6] the criteria for the validity of the Weinbaum-Jiji

equation and its region of applicability for the larger branching countercurrent vessels were not clear.

The original derivation in [6] is based on two fundamental hypotheses: (1) the primary vessels that control blood-tissue heat transfer are at least 50 and more likely over 100 μm diameter and that virtually all vessels of this diameter in muscle tissue occur as countercurrent pairs and (2) the local temperature field in the vicinity of each thermally significant countercurrent pair is determined principally by the tissue conduction field in the cross-sectional plane and the local average tissue temperature equals the mean temperature of the artery-vein pair. The first hypothesis was initially supported by a detailed microvascular model for surface tissue energy exchange [8] and [9], which theoretically predicted the variation of the local arterio-venous temperature difference in a model simulation of a branching microvascular network. This theoretical prediction was strongly supported by an extensive series of experiments reported in Lemons et al. [10] in which the local thermal field surrounding vessels > 100μm was measured. The second hypothesis was based on a physically reasonable intuitive argument that did not have any rigorous theoretical or experimental verification at the time it was first proposed.

The second hypothesis involves both (i) the relationship between the local average tissue temperature and the average temperature of the artery and vein and (ii) the closure approximation introduced in the Weinbaum-Jiji equation relating the local arterial-venous temperature difference and the local mean tissue temperature gradient. This hypothesis and the closure condition, which determine the validity of the Weinbaum-Jiji equation, are subtle and were not carefully examined using asymptotic analysis in the original formulation in [6]. The

hypothesis has been critically questioned by Wissler [11] who believed that the axial variation of the artery and vein temperatures in microcirculation were uncoupled from the axial variation of the local average tissue temperature. A reply to his objection is given in a short paper by Weinbaum and Jiji [12], which shows that it is possible using rigorous asymptotic analysis to prove both the assumption about the definition of the local average tissue temperature and the closure approximation. For mathematical convenience the countercurrent vessels were assumed to be of equal size in the derivation in [6] and the analysis in [12].

The results of the experiments [10] showed that the countercurrent arteries produced more than three times the number of positive thermal identifications as the countercurrent veins and that the latter needed to be significantly larger to be detected. An analysis of the conduction field in the plane perpendicular to the vessel axes in [10] shows that this behavior could be accounted for if the local solutions took into account the significant difference in size between the countercurrent artery and vein in the microcirculation and a new local average tissue temperature introduced to describe the far field temperature several diameters removed from the thermal disturbance of the vessel pair. In particular, it was shown that the temperature fluctuation about the correct far field temperature was approximately 2.7 times as large for the countercurrent artery as for the vein when the diameter of the latter was three times the former and about 1.8 times as large when the diameter ratio was 2. Nearly all of the countercurrent vessel pairs examined in the experiment fell between these two diameter ratios. It is evident from these results that the new bioheat equation in [6] needs to be extended to artery-vein pair interactions where the difference in

size between the vessels is accounted for and a revised definition of the local mean tissue temperature is required in the derivation of the new equation.

The Weinbaum-Jiji bioheat equation has been already successfully applied in developing a more sophisticated model of peripheral tissue heat transfer [13] and as the basis for the formulation of a new generation of combined macro and microvascular model for whole limb heat transfer [14]. The model in [14] has been developed with the flexibility to treat limbs of continuously varying cross-sectional area and an unknown surface temperature distribution, where the local distribution of the central arterial blood supply to the muscle and cutaneous tissue are considered for the first time.

The models for a whole limb, before [14], have either been based on simple one-dimensional models for a countercurrent heat exchanger [15,16] or on multi-compartment models using the Pennes equation in each compartment [17,18]. The prototype of the former is the paper by Mitchell and Myers [15]. This model treated the central artery and vein as a countercurrent heat exchanger which experiences heat losses to a uniform temperature external environment along its length. The arterial and venous temperatures are set equal at the end of the limb since the effect of the extremity is neglected. In the multi-compartment models the limbs are treated as different radii cylinders in which the concentric layers of tissue are described by a Pennes equation with different capillary perfusion rates. The junctions between cylinders were matched by the overall energy balance on the blood entering and leaving each cylinder.

The model in [14] predicts a radial temperature profile which agrees well with the experimental data in [1] but inadequately describes

the axial temperature variation of the central vessels or the skin surface temperature. The inadequacy of the previous model [14] stems from an approximation used to describe the central vessels in the core which assumes that the heat loss to the surrounding is small compared to the heat exchange between the central vessels. In general, the results of [14] and [15] indicate that the heat loss to the environment is comparable or larger than the heat exchange between the central vessels when there is significant convective cooling at the skin surface. Furthermore, excessive computational time is required in [14] to solve the boudary value problem for the axial interaction. In order to couple the energy equation for the central vessels to the tissue cylinder, the arm is discretized into 20 disk like elements in the axial direction and a trial and error method is used in the solution procedure for each element. This leads to a large computation time (approximately 20 CPU minutes on an IBM 4381 for each boundary value problem). Thus, a new approach to modeling countercurrent heat transfer between parallel paired vessels embedded in a tissue cylinder is needed.

The bioheat equation which is used to describe the local microvascular temperature field in the muscle tissue in [14] is the Weinbaum-Jiji equation. However, the study in [7] reveals that the Weinbaum-Jiji equation overestimates the magnitude of the countercurrent microvascular heat source term in the tissue region surrounding the first or first and second generations of vessel branching from the central vessels depending on the Peclet number of the blood flow in the veesels, and a "hybrid" model which combines the Weinbaum-Jiji and Pennes equations in different regions should provide a better description of the temperature distribution in the muscle tissue. Thus, in the more accurate whole limb heat transfer model developed herein the

local microvascular temperature field in the muscle tissue is described by a new approach in which the first or first and second generations of vessel branching, depending on the blood flow conditions, are described by the Pennes equation and all subsequent generations by the Weinbaum-Jiji equation.

A theoretical model for whole limb heat transfer needs experimental studies to provide the prescribed input parameters and to test the predictions of the model. Bazett et al. [19] has measured the axial temperature distribution in the major central vessels of the human arm and Pennes [1] has measured the radial temperature profiles in the human forearm and brachial arterial blood temperature. Because such measurements are invasive and potentially dangerous, few studies have attempted similar measurements. However, the skin surface temperature distribution of the arm is not difficult to measure and it also provides important data to confirm the predictions of the theoretical model. There is some previous available data for the temperature distribution in the arm [1] and the heat production from the hand [20]. There is also available data for the blood flow rates of the arm and hand under different conditions, which are summarized in [21]. However, experiments in which all of these data are acquired simultaneously have not been reported previously, and it was decided that to adequately test the theoretical model the input parameters, temperature measurments and blood flow rates should be gathered in a single experiment.

It is well recognized since the classic intravascular temperature measurements of Bernard [22] in dogs and Bazett et al. [19] in the radial artery and vein of the wrist that the extremities play a vital role in whole limb heat transfer. The early work of Brengelmann and Brown [23] showed that the blood flow to the hand in the resting state

was only partly due to the oxygen demand of the tissue and that its most important role was thermoregulation. Raman and Vanhuyse in a series of papers [16], [20], [24] and [25] provided the first detailed quantitative experimental and theoretical studies exploring the relative importance of the deep tissue and cutaneous circulations in the human hand. Their experiments measured the total blood flow to and heat loss from the hand when immersed in a stirred water bath in the steady state. From the relationship between blood flow and heat transfer from the hand at different skin temperatures of the hand and assumptions about the blood temperature entering the hand, they concluded that the redistribution of blood flow within the hand as the skin temperature changed occurred. However, this conclusion has been questioned by Ducharme [26] and still remains to be confirmed or disproven.

The objectives of this research are: (a) Generalize the Weinbaum-Jiji bioheat equation to treat countercurrent artery-vein pairs of unequal size. (b) Present an analytic solution for the countercurrent heat transfer between parallel paired vessels embedded in a cylinder with surface convection. (c) Develop a three-dimensional variable geometry macro and microvascular model for whole limb heat transfer. (d) Conduct an experimental study to verify the proposed theoretical model, to provide the model parameters and to examine the relationship between blood flow and heat transfer when the hand is placed in a bath at different temperatures. This dissertation is divided into four major chapters, one devoted to each of the four related principal objectives mentioned above.

Chapter 2. Generalization of the Weinbaum-Jiji Bioheat Equation to Microvessels of Unequal Size

To generalize the Weinbaum-Jiji bioheat equation [6] and the conductivity tensor that appears in this equation for vessels of unequal size, a solution for an unequal countercurrent artery vein pair at infinite Nusselt number with heat loss to the far field will be presented in this chapter using the superposition technique developed in Baish et al [27]. An asymptotic analysis will also be developed to elucidate the relationship between the near field temperature of the artery-vein pair and the local average tissue temperature. This analysis is used to rigorously prove the closure approximation relating the local arterial-venous temperature difference and the mean tissue temperature gradient which had been derived in [6] using a more heuristic approach.

2.1 Background

The Weinbaum-Jiji new bioheat equation [6] differs fundamentally from the traditional bioheat equation in that the macroscopic local average tissue temperature is related to the local vascular geometry and flow and that it describes an important new mechanism for blood-tissue heat transfer due to microvascular counterourrent heat exchange. The original derivation in [6] assumes that the thermally significant countercurrent vessels are of equal size and also introduces the two fundamental hypotheses mentioned in the general introduction. The detailed temperature profiles in the vicinity of the countercurrent vessels measured in [10] indicate that large asymmetries in the local temperature field can result from the significant differences in size between the countercurrent artery and vein. The diameter ratio of nearly

all the countercurrent pairs examined in [10] in the microcirculation fell between 2-3. Therefore, the Weinbaum-Jiji equation needs to be generalized for countercurrent arteries and veins of unequal size.

A detailed experimental verification of the first hypothesis relating to the size of the microvessels involved in thermal equilibration has been completed and reported in [10]. Fine wire thermal traverses were analyzed in proximity to 137 vascular elements taken from all regions of the rabbit thigh. The precise trajectory of the thermocouple wire was established by using a tissue clearing technique in which the wire was left in place after the animal was sacrificed so that its relationship to vascular elements could be ascertained when the tissue was made translucent by treatment with glycerin and examined in serial sections. The result showed that rarely did the blood-tissue temperature difference exceed 0.2°C, even when temperature differences between the center of the limb and the skin surface were raised to the order of 10°C, except for the large central vessels. The smallest artery with a measurable temperature fluctuation field was approximately 100μm, whereas the smallest vein was slightly greater than 300μm. These measurements showed that the thermal equilibration of even the largest countercurrent vessels of the microcirculation (500μm) was very efficient and that thermal equilibration occurred primarily in vessels larger than 100μm diameter. Furthermore, the order of magnitude of the measured blood-tissue temperature difference agreed well with the predictions of the theoretical model simulation for a branching countercurrent microvascular network in [9].

The second hypothesis involving the relationship between the local average tissue temperature and the mean temperature of the artery vein pair is discussed in a short paper by Weinbaum and Jiji [12] for vessels

of equal size. This paper, which is based on the model equations in Baish et al. [27, 28], shows that if the equations are expanded in a parameter ϵ defined as the ratio L_e/L (normalized thermal equilibration length), where L_e is the thermal equilibration length of the vessel pair and L the characteristic length of the macroscopic tissue temperature gradient, then to $O(\epsilon)$, $\theta=(T_a+T_v)/2$ and the local arterial-venous temperature difference $T_a-T_v=-\epsilon\partial\theta/\partial s$, where s is the axial coordinate. This asymptotic analysis, which is considerably more complicated for vessels of unequal size, will be presented herein.

Although the countercurrent heat exchanger is a classic problem that has been addressed in numerous previous investigations, there is no existing rigorous analytic formulation or solution for the case where the tubes are of unequal size and there is a net heat flux to the far field. For the case of a perfect countercurrent heat exchanger, where all the energy leaving one tube reenters the other, one can use the well known solution for the bicircular isotherms to compute the interaction shape factor for the conduction heat transfer in the cross-sectional plane and also the local average temperature T_m of the surrounding medium. When the heat exchange is imperfect and there is a heat loss to the far field because T_m is not the same as the local far field temperature θ, these isotherms are distorted and the interaction shape factors describing the heat transfer between the tubes and the total heat loss from each tube are altered. A solution to this classic unsolved problem is presented herein. These solutions are then used to formulate a new set of model equations describing the heat exchange

between the countercurrent vessels and the heat loss from these vessels to the tissue in the far field of the vessel pair.

2.2 Relation Between the Local Average Tissue Temperature and Microvessel Temperatures

2.2.1 Basic Equations

After writing some elementary mass and energy balances for a differential control volume which is penetrated by n countercurrent vessel pairs per unit area, one ends up with the following equations which provide the starting point for the derivation of the new bioheat equation in [6]

$$\bar{\rho}\bar{c}\frac{\partial\theta}{\partial t} - \nabla\cdot k_t\nabla\theta = n(q_a - q_v) + 2\pi\rho_b c_b n a_a g_a (T_a - T_v) + q_m \tag{2.1}$$

$$\pi\rho_b c_b a_a^2 u_a \frac{dT_a}{ds} = -q_a \tag{2.2a}$$

$$\pi\rho_b c_b a_v^2 u_v \frac{dT_v}{ds} = -q_v \tag{2.2b}$$

These results correspond to equations (17) and (19a,b) in [6]. Similar equations are also presented in Chen and Holmes [5]. T_a and T_v are the local arterial and venous temperatures which are assumed to be constants in the plane perpendicular to the vessel axes, θ is some mean tissue temperature that still needs to be defined, q_a and q_v are the conduction heat transfer per unit vessel length, g_a is the local capillary bleed-off per unit area of vessel wall leaving the countercurrent artery, q_m is the metabolic heat release per unit volume, s is distance along the countercurrent vessel pair and the other symbols have their usual meaning. In (2.1) we have assumed that the local bleed-off from the

countercurrent artery re-enters the adjacent vein since the loss to the lymphatics is very small. These equations are not useful as they now stand since they involve three different temperatures and the primary objective of the derivation in [6] is to reduce (2.1), (2.2a) and (2.2b) to a single equation in one unknown temperature, the local average tissue temperature. The first term on the right hand side of (2.1) results from the incomplete countercurrent exchange between the vessels and is the crucial term that gives rise to the effective conductivity tensor. In general, it is assumed that when a vessel pair crosses a surface there is no net mass flow, $\dot{m} = u_a a_a^2 - u_v a_v^2$, but there is energy transfer since the artery and vein having come from opposite directions retain a different memory of the neighboring tissue temperature. The second term on the right hand side (2.1) is the energy loss to the tissue due to the directed small vessel blood perfusion between the vessels.

To derive the local relationship between T_a, T_v and θ, we consider a small tissue cylinder of radius r_o surrounding the vessel pair. The radius r_o is an asymptotically defined distance from the vessel pair at which the thermal fluctuation from the vessel vanishes and one returns to the temperature of the surrounding tissue. Temperature measurements in [10] indicate that this is at most several vessel diameters. θ can therefore be viewed as the far field temperature of an inner region containing the vessels in which there are large thermal gradients in the plane perpendicular to the vessel axes. From equations (2.2a) and (2.2b) the net heat flux crossing r_o and entering the interstitial space is

$$q_e = q_a - q_v = \dot{m} c_b \frac{d}{ds}(T_v - T_a) \qquad (2.3)$$

θ can vary in general as an arbitrary function of s and the important question is to see how the axial variation of T_a and T_v are related to this variation of the surrounding tissue temperature. These axial gradients, however, will be much smaller than the thermal gradients in the cross-sectional plane for $r < r_o$.

2.2.2 Decomposition of Boundary Value Problem

Following the approach of Baish et al. [27] the boundary value problem for conduction in the plane perpendicular to the vessel axes can be exactly decomposed into two problems A and B as shown in Fig. 1. In problem A both vessels are the same temperature T_m and the boundary temperature at r_o is θ, which is a constant. The temperature T_m is unknown and must be determined as part of the solution to problem B by requiring that in this problem the temperature vanish and there be no heat flux crossing r_o. In this way the original problem has been split into two components, one describing the total heat loss q_e to the far field in which there is no heat transfer between the vessels and the second describing the total heat exchange q between the vessels with no heat loss to the tissue. This superposition exactly satisfies the original boundary conditions and is strictly valid since the equations are linear. The expression for q can be written as

$$q = \sigma_c k_t (T_a - T_v) \qquad (2.4)$$

where σ_c is a conduction shape factor that must be determined along with T_m as part of the solution to the second boundary value problem.

In view of the foregoing superposition the interaction for the conduction loss from each vessel can be written as the sum of two contributors

$$-q_a = \dot{m}c_b\frac{dT_a}{ds} = -\sigma_c k_t(T_a - T_v) - p\sigma_t k_t(T_m - \theta) \tag{2.5}$$

$$-q_v = \dot{m}c_b\frac{dT_v}{ds} = -\sigma_c k_t(T_a - T_v) + (1 - p)\sigma_t k_t(T_m - \theta) \tag{2.6}$$

Here σ_c and σ_t are the conduction shape factors for problem A and B and the factors p and 1-p describe the fraction of the heat loss to the far field from each of the two vessels. For equal sized vessels p=1/2. All together there are four unknown parameters in equations (2.5) and (2.6) σ_c, σ_t, T_m and p. When (2.5) and (2.6) are subtracted and equated to (2.3) one obtains

$$q_a - q_v = -\dot{m}c_b\frac{d}{ds}(T_a - T_v) = \sigma_t k_t(T_m - \theta) \tag{2.7}$$

2.2.3 Solution to Boundary Value Problem A

The solution to boundary value problem A is somewhat subtle since it involves an asymmetric and unequal dipole heat source near the origin. To solve this problem we introduce the transformation

$$W = \frac{z - d_v + a_v b}{-b(z - d_v) - a_v} \tag{2.8}$$

where d_v is defined in Fig. 2, 1/b is the distance of the infinity point from the origin in the transformed w plane and b is given by

$$b = \frac{l^2 + a_v^2 - a_a^2 + \sqrt{[(l+a_a)^2 - a_v^2][(l-a_v)^2 - a_v^2]}}{2a_v l} \tag{2.9}$$

Equation (2.8) is a variation of the general bicircular transformation that maps the artery into a unit circle as shown in Fig. 2. The expression for R_a is

$$R_a = \frac{1^2 - a_v^2 - a_a^2 - \sqrt{[(1+a_a)^2 - a_v^2][(1-a_a)^2 - a_v^2]}}{2a_a a_v} \tag{2.10}$$

Similarly, the circle of radius r_o defining the far field maps into a small circle of radius R_o defined by

$$(u + \frac{1}{b})^2 + v^2 = R_o^2 \tag{2.11}$$

where,

$$R_o = \frac{a_v^2(b^2 - 1)}{b^2 r_o} \tag{2.12}$$

Since a_v is much smaller than r_o, the circle of radius R_o can be treated as a point in the w plane and the sink in the far field represented by a logarithmic singularity at distance 1/b from the origin. This singularity is given by $G(u,v) = (q_e/k_t)g(u,v)$ where $g(u,v)$ is the unit line sink

$$g(u,v) = \frac{1}{4\pi} \ln[(u + \frac{1}{b})^2 + v^2] \tag{2.13}$$

This simplification greatly reduces the complexity of the boundary value problem sketched in Fig. 2. One seeks a solution for T_A which can be written as the superposition of three terms, a harmonic function F which is valid in region R<1, the singularity G in (2.13) and T_m

$$T_A = F + G + T_m \tag{2.14}$$

The boundary conditions for F are

$$F(R_a,\alpha) = -G(R_a,\alpha), \qquad F(1,\alpha) = -G(1,\alpha) \tag{2.15}$$

A solution summary for the boundary value problem defined by (2.13-2.15) is given in the Appendix including the expressions for the various coefficients. We shall present only the principal results here. The solution for the temperature field is

$$T_A = \frac{q_e}{k_t}[a_o + b_o \ln R + \sum_{k=1}^{\infty} (a_k R^k + b_k R^{-k})\cos k\alpha + (c_k R^k + d_k R^{-k})\sin k\alpha] \tag{2.16}$$

The contribution of the heat flux from the artery and vein to the sink at infinity can be obtained by performing a contour integration for the radial temperature gradient on the circles $R=R_a$ and $R=1$, respectively. This integration is readily performed using residue theory. There are no singularities which lie in the region $R<R_a$ and the only singularity that lies within the unit circle is the G function at $(-1/b,0)$. The final result for the heat loss from each vessel is

$$q_a = q + pq_e \tag{2.17}$$

$$q_v = q - (1-p)q_e \tag{2.18}$$

where,

$$p = -\frac{\ln b}{\ln R_a} \tag{2.19}$$

For equal vessels $R_a = 1/b^2$ and $p = 1/2$.

The far field flux q_e is determined by evaluating (2.16) at $r=r_o$ or the circle of radius R_o defined by equations (2.11) and (2.12) in the w plane where $T_A = T = \theta$

$$\theta = T_m - \frac{q_e}{\pi k_t}\left[\ln \frac{b\gamma_o}{a_v(b^2-1)} + \frac{q_e}{k_t}\left[a_o - b_o \ln b + \sum_{k=1}^{\infty} (-1)^k \left(\frac{a_k}{b^k} + b_k \cdot b^k\right)\right]\right] \qquad (2.20)$$

Equation (2.20) can be written in the form

$$q_e = \sigma_t k_t (T_m - \theta) = \left[\frac{1}{\pi}\left[\ln \frac{b\gamma_o}{a_v(b^2-1)} - a_o + b_o \ln b\right.\right.$$

$$\left.\left. + \sum_{k=1}^{\infty} (-1)^k \left(\frac{a_k}{b^k} + \frac{b_k}{b^{-k}}\right)\right]^{-1} k_t (T_m - \theta)\right. \qquad (2.21)$$

which provides the solution for the shape factor σ_t. T_m at this point is still unknown but will be determined next as part of the solution to boundary value problem B.

2.2.4 Solution to Boundary Value Problem B

The classical solution to the boundary value problem shown in Fig. 1B for the perfect conduction heat exchange q between two unequal circular pipes is

$$T_B = \frac{q}{4\pi k_t} \ln\left[\frac{y^2 + (x-\delta)^2}{y^2 + (x+\delta)^2}\right] \qquad (2.22)$$

where δ defines the origin of a bicircular coordinate system is given by

$$\delta = \sqrt{(d_a^2 - a_a^2)} = \sqrt{(d_v^2 - a_v^2)} \qquad (2.23)$$

Equation (2.22) can be evaluated at the innermost point of the wall of each vessel. Using the algebraic identities for the inverse cosh, one obtains

$$T_a - T_m = \frac{q}{2\pi k_t} \cosh^{-1} B_a \qquad (2.24)$$

$$T_v - T_m = \frac{-q}{2\pi k_t} \cosh^{-1} B_v \qquad (2.25)$$

where B_a and B_v are geometrical shape factors

$$B_a = \frac{d_a}{a_a} = \frac{(1/a_a)^2 - (a_v/a_a)^2 + 1}{2(1/a_a)} \tag{2.26}$$

$$B_v = \frac{d_v}{a_v} = \frac{(1/a_v)^2 - (a_a/a_v)^2 + 1}{2(1/a_v)} \tag{2.27}$$

The sum and difference of equations (2.24) and (2.25) are, respectively,

$$T_a + T_v - 2T_m = \frac{q}{2\pi k_t}(\cosh^{-1}B_a - \cosh^{-1}B_v) \tag{2.28}$$

$$T_a - T_v = \frac{q}{2\pi k_t}(\cosh^{-1}B_a + \cosh^{-1}B_v) \tag{2.29}$$

If equation (2.29) is written in the form of (2.4) one obtains the desired expression for the shape factor σ_c

$$\sigma_c = \frac{2\pi}{\cosh^{-1}B_a + \cosh^{-1}B_v} \tag{2.30}$$

Substituting (2.4) and (2.30) into (2.28) and solving for T_m one obtains

$$T_m = \frac{1}{2}\left[(1-\gamma)T_a + (1+\gamma)T_v\right] \tag{2.31}$$

where γ like σ_c is a geometric shape factor given by

$$\gamma = \frac{\cos^{-1}B_a - \cosh^{-1}B_v}{\cosh^{-1}B_a + \cosh^{-1}B_v} \tag{2.32}$$

One can readily show from symmetry considerations that the principal value of the integral

$$\int_{-\infty}^{\infty}\int_{-\infty}^{\infty} T_B(x,y)\,dx\,dy = 0 \tag{2.33}$$

taken over the entire plane vanishes when T_m is given by equation (2.31). One, therefore, concludes from (2.22) and (2.33) that both the far field and average tissue temperatures for problem B are zero.

Multiplying equations (2.5) and (2.6) by $(1-\gamma)/2$ and $(1+\gamma)/2$, respectively, adding these results and introducing the expression of T_m from (2.31), one obtains

$$\dot{m}c_b\frac{dT_m}{ds} = -\sigma_c k_t(T_a - T_v) + P\sigma_t k_t(T_m - \theta) \tag{2.34}$$

where $P = (1+\gamma)/2-p$ is a factor that depends only on the vessel geometry.

2.2.5 Derivation of Closure Hypothesis and Relation between θ and T_m

Equations (2.7) and (2.34) are the two key relations coupling the axial variation of the local arterial-venous temperature difference $T_a - T_v$ and T_m to the local far field tissue temperature θ. These equations will first be rewritten in a form which is more suitable for asymptotic analysis and then put in a dimensionless form in which a small perturbation parameter can be identified. One differentiates each equation once, treating the geometric parameters as constants, and eliminates the first derivative terms of $T_a - T_v$ and T_m on the right hand side of the resulting equations using (2.7) and (2.34). One obtains after some algebraic rearrangement

$$\left(\frac{\dot{m}c_b}{\sigma_c k_t}\right)^2\frac{d^2T_m}{ds^2} = \left(\frac{\sigma_t}{\sigma_c}\right)(T_m - \theta) + P\left(\frac{\dot{m}c_b}{\sigma_c k_t}\right)\left(\frac{\sigma_t}{\sigma_c}\right)\frac{d}{ds}(T_m - \theta) \tag{2.35}$$

$$\left(\frac{\dot{m}c_b}{\sigma_c k_t}\right)^2\frac{d^2(T_a - T_v)}{ds^2} = \left(\frac{\sigma_t}{\sigma_c}\right)\left[T_a - T_v + \left(\frac{\dot{m}c_b}{\sigma_c k_t}\right)\frac{d\theta}{ds}\right] - P\left(\frac{\sigma_t}{\sigma_c}\right)^2(T_m - \theta) \tag{2.36}$$

Equations (2.35) and (2.36) are now cast in dimensionless form by introducing a scaled coordinate S=s/L where L is a length characteristic of the macroscopic temperature gradient. The desired dimensionless equations are

$$\epsilon^2 \frac{d^2 T_m}{dS^2} = \left(\frac{\sigma_t}{\sigma_c}\right)(T_m - \theta) + P\epsilon\left(\frac{\sigma_t}{\sigma_c}\right)\frac{d}{dS}(T_m - \theta) \tag{2.37}$$

$$\epsilon^2 \frac{d^2 (T_a - T_v)}{dS^2} = \left(\frac{\sigma_t}{\sigma_c}\right)(T_a - T_v + \epsilon\frac{d\theta}{dS}) - P\left(\frac{\sigma_t}{\sigma_c}\right)^2 (T_m - \theta) \tag{2.38}$$

where,

$$\epsilon = \frac{\dot{m} c_b}{\sigma_c k_t L} = \frac{\pi a_a P_{ea}}{2\sigma_c L k'}, \qquad P_{ea} = \frac{2\rho_b c_b u_a a_a}{k_b} = \frac{a_a}{a_v} P_{ev} \tag{2.39}$$

Equations (2.37) and (2.38) contain three dimensionless factors, σ_t/σ_c, P and ϵ. σ_t/σ_c is of O(1) and 0<P<1. A typical radial dimension L for a human limb is about 5 cm. For this value of L, ϵ is always small compared to unity for vessels under 500 μm of the microcirculation. Representative values of ϵ are given in Table 1 for several artery-vein pairs of different dimensions. One situation where ϵ may not be small compared to unity is where there is highly localized heating or blood flowing due to exercise as discussed in [28].

When $\epsilon << 1$, equations (2.37) and (2.38) are immediately recognized to be of boundary layer type, that is a small parameter multiplies the highest order derivative terms. Except for narrow regions of thickness $O(\epsilon)$ near the ends of the integration interval these highest derivative terms will not be important and the behavior is given by the reduced equations obtained by setting the right hand sides of (2.37) and (2.38)

equal to zero. For vessels of equal size P=0 since p=1/2 and γ=0. The reduced equations in this case become

$$\theta = T_m + O(\epsilon^2) = \frac{T_a + T_v}{2} + O(\epsilon^2) \tag{2.40}$$

$$T_a - T_v = -\epsilon\frac{d\theta}{dS} + O(\epsilon^2) \tag{2.41}$$

These two results for countercurrent vessels of equal size were previously derived in [12]. Result (2.40) confirms the validity of the mean tissue temperature approximation $\theta=(T_a+T_v)/2$ when $a_a=a_v$ that had been strongly attacked in [11] based on an incorrect set of model equations whereas (2.41) is the closure approximation relating the local arterial-venous temperature gradient in the far field of the vessels (equation (25) in [6]) that had been obtained using a more physically motivated approach in the original formulation of the Weinbaum-Jiji bioheat equation for vessels of equal size.

For vessels of unequal size we shall modify the above approach since equation (2.38) contains an additional term on its right side when P≠0. Multiplying (2.37) by $e^{S/P\epsilon}/P\epsilon$, one obtains

$$\frac{d}{dS}[(T_m - \theta)e^{S/P\epsilon}] = \epsilon\left(\frac{\sigma_c}{\sigma_t P}\right)\frac{d^2T_m}{dS^2}e^{S/P\epsilon} \tag{2.42}$$

The first integral of equation (2.42) is

$$T_m(S)-\theta(S) = [(T_m(0)-\theta(0)]e^{-S/P\epsilon} + \epsilon\frac{\sigma_c}{\sigma_t P}\int_0^S \frac{d^2T_m}{dy^2}\, e^{-y/P\epsilon}dy \tag{2.43}$$

The mean value theorem can now be applied to the last term in (2.43).

$$\int_0^S \frac{d^2T_m}{dy^2}e^{-y/P\epsilon}dy = \frac{d^2T_m}{dy^2}\Big|_{y=\xi S}\cdot(e^{-\xi S/P\epsilon})S \tag{2.44}$$

where $0<\xi<1$. The first term on the right hand side of (2.43) describes the decay of the initial difference between T_m and θ that might have existed at the boundary, whereas the second term determines the deviation between T_m and θ that arises from the physiological situation there is no significant initial difference between T_m and θ since the microvessels form a continuous branching network. However, even if such an initial difference did exist as an entrance condition it would disappear over a distance of order ϵPL.

From (2.43) and (2.44) it is apparent that, except for a small exponential correction, θ is related to T_m by

$$\theta(S) = T_m(S) + O(e^{-\xi S/P\epsilon}) \simeq (\frac{1-\gamma}{2})T_a + (\frac{1+\gamma}{2})T_v \qquad (2.45)$$

and thus the right hand side of (2.38) reduces to

$$T_a(S) - T_v(S) = -\epsilon\frac{d\theta}{dS} + O(\epsilon^2) \simeq -(\frac{\dot{m}c_b}{\sigma_c k_t})\frac{d\theta}{dS} \qquad (2.46)$$

which is the same as result (2.40) above except that σ_c in the expression for ϵ is now given by equation (2.30) for vessels of unequal size. It is clear from results (2.45) and (2.46) and the previous discussion that the local solution for T_m and T_a-T_v is independent of boundary conditions and the relaxation to the local average tissue temperature and the closure condition is exponential with a decay length that is short compared to the macroscopic length over which the average tissue temperature changes under normal physiological conditions.

In the original formulation in [6] of the new bioheat equation different arguments were used to justify the approximations (2.40) and (2.41) above, which we now see can be demonstrated through much more

rigorous analysis. In this earlier formulation we assumed in the derivation of the closure hypothesis that the heat transfer between the vessels q was much larger than the small, but non-negligible heat loss to the tissue q_a-q_v. It is clear from the present derivation that the first approximation to this heat loss to the tissue is directly related to the closure condition (2.46). Furthermore, this small heat loss described by boundary value problem A does not significantly affect the near field temperature in the vicinity of the vessels and thus the solution for the average near field temperature (2.45) to lowest order in the small parameter ϵ is the same as the far field temperature of the local tissue.

2.3 Generalization of the Weinbaum-Jiji Equation

We are now in a position to express the blood-tissue heat exchange terms in equation (2.1) in terms of the mean tissue temperature θ and its derivatives using result (2.46). Substracting (2.2a) and (2.2b), multiplying this result by n and substituting the resulting expression back in equation (2.1), one obtains

$$\bar{\rho}\bar{c}\frac{\partial\theta}{\partial t} - \nabla\cdot k_t\nabla\theta = -\pi\rho_b c_b n a_a^2 u_a \frac{d}{ds}(T_a - T_v) + 2\pi\rho_b c_b n a_a g_a (T_a - T_v) + q_m \tag{2.47}$$

Using equation (2.46) to express T_a-T_v and its derivatives in (2.47) in terms of θ and introducing the dimensionless Peclet number

$$P_e(s) = P_{ea} = \rho_b c_b a_a(s) u_a(s)/k_b$$

one has,

$$\bar{\rho}\bar{c}\frac{\partial\theta}{\partial t} - \nabla\cdot k_t\nabla\theta = \frac{\pi^2 n a_a^2 k_b}{4k_t} P_e\left[\frac{d}{ds}\left(\frac{a_a P_e}{\sigma_c}\frac{d\theta}{ds}\right) - \frac{2g_a d\theta}{\sigma_c u_a ds}\right] + q_m \tag{2.48}$$

This is the basic new bioheat equation for vessel pairs of unequal size. This result is not in its most useful form since the derivatives on the right hand side of (2.48) are directional derivatives along the vessel axes rather than derivatives with respect to the coordinate axes, the reference frame in which the local mean tissue temperature gradient is measured.

Using tensor notation we can transform equation (2.48) to rectangular Cartesian coordinates x_i, as shown in [6]. After some algebra, regrouping of terms and simplification using the continuity equation,

$$\frac{d}{ds}(na_a^2 u_a) = -2na_a g_a \tag{2.49}$$

one obtains

$$\rho c \frac{\partial \theta}{\partial t} - \frac{\partial}{\partial x_i}[(k_{ij})_{eff} \frac{\partial \theta}{\partial x_j}] = -\frac{\pi^2 na_a^2 k_b^2}{4\sigma_c k_t} P_e^2 l_j (\frac{\partial l_i}{\partial x_j})(\frac{\partial \theta}{\partial x_j}) + q_m \tag{2.50}$$

where

$$(k_{ij})_{eff} = k_t(\delta_{ij} + \frac{\pi^2}{4\sigma_c k_t^2} na_a^2 k_b^2 P_e^2 l_i l_j) \tag{2.51}$$

is the effective tissue conductivity.

It is interesting to note that the final new bioheat equation for vessels of unequal size (2.50) and the expression for the effective conductivity tensor (2.51) are of identical form to equations (34) and (35) in [6] where the vessels were assumed to be of equal size. The two important differences are (i) the shape factor σ_c is now given by (2.30) and (ii) the local average tissue temperature has been generalized to describe the far field conduction temperature of the countercurrent

vessel pair defined by (2.31). Fortunately, the interaction parameters p and σ_t, given by equations (2.19) and (2.21) do not enter into the final equation (2.50) when the parameter ϵ is small, since both these parameters are rather tedious to calculate because of the complicated relationship (2.8) between the coordinates of the w plane and the physical plane. This simplification is possible because equation (2.46) provides a reasonable first order approximation to the net local axial heat loss from the vessel pair to the far field.

2.4 Discussion

In conclusion, the Weinbaum-Jiji bioheat equation is valid for vessels of equal or unequal size provided the value of ϵ^2 is much smaller than unity. To apply equation (2.50) one must first construct a microvascular model for the spatial variation of the vascular parameters that appear in $(k_{ij})_{eff}$. These parameters describe the largest countercurrent vessel pairs in the differential control volume since, as shown in [6], these vessels will dominate the heat transfer in the control volume. In most tissues there is a continuous branching of the microvasculature after leaving the central artery and vein. The initial task is to construct a representative arterial-venous arcade that starts at the branching from the central supply vessels for the tissue in question. One also satisfies a continuity of flow relation along the arcade. This procedure is described in detail for peripheral tissue in [9] and [13] and for an entire limb in [14]. For conditions of uniform capillary perfusion it is possible to separate the geometric parameters from the parameter that describes the inflow velocity at the initial branching. As shown in [13] it is then possible to write equation (2.50)

in a much simplified form that is not much more difficult to solve than the traditional bioheat equation. One then specifies boundary conditions on either the tissue temperature or heat flux at each boundary in the usual fashion. When major supply vessels are presented the tissue outside the core tissue cylinder surrounding these vessels is described by the Weinbaum-Jiji or Pennes bioheat equation and a separate analysis is developed for the core tissue cylinder containing these large vessels. Matching conditions on temperature and heat flux are then satisfied at the interface between regions this procedure will be described in detail for the central vessels of the limb later in chapter 4. While it is a rather simple matter to change the tissue temperature or heat flux conditions at a surface using the new equation, changing the arterial supply temperature leads to a much more difficult boundary value problem since this usually involves changing the inlet temperature of the major supply vessels and not the local tissue temperature directly.

It has been assumed in the derivation of equation (2.50) that the tissue surrounding the thermally significant artery-vein pairs satisfies the usual conduction equation in the cross-sectional plane although this tissue contains numerous capillaries, arterioles, and venules. This assumption was based on the premise that these smaller vessels were for all practical purposes in thermal equilibrium with their surrounding tissue and thus did not contribute to local blood-tissue heat transfer. A large scale laboratory model in [10] duplicating the geometry and flow conditions (Peclet number) of an in vivo experiment was specially constructed in an attempt to confirm this assumption. A purely conducting medium of clear gelatin was used in the laboratory model in [10]. Panel B of Fig. 3 is representative of the highest resolution

tissue temperature profiles achieved by passing a very fine thermocouple wire in close proximity to a countercurrent vessel pair in [10]. Temperature measurements were taken at 20-40 μm intervals as the wire was drawn through by the microdrive system. This in vivo temperature profile was simulated in the laboratory model by the thermocouple traverse shown in panel B. The positioning of the thermocouple wire in the laboratory model was adjusted to take into account the thickness of the tube walls. Also shown in Fig. 3 by the dashed curve is the theoretical solution predicted by equation (2.22) for a perfect countercurrent heat exchanger in which the walls are at uniform but unequal temperatures.

There are two principal sources for the discrepancy between the theoretical and experimental curves in panel A. First in the laboratory model experiment it is not possible to maintain the tube wall at a uniform temperature in each cross-sectional plane. The inner margins of the adjacent tube walls will have a smaller temperature difference than the outer margins. This aspect of the laboratory model replicates what one would anticipate is happening in the in vivo measurements in panel B. The second source of discrepancy is the small heat loss to the far field that is described by boundary value problem A. Since this heat loss was not measured in the laboratory model experiment it is not possible to distinguish between these two sources of error in the theoretical prediction. The close correspondence between the curves in panels A and B attests to the reasonableness of the conduction approximation used in the theoretical model for the heat transfer in the cross-sectional plane.

Chapter 3. Heat Exchange between Countercurrent Vessels Embedded in a Cylinder with Surface Convection

In this chapter a three-dimensional approximate analytic solution will be presented for the unequal countercurrent heat transfer between parallel paired vessels asymmetrically embedded in a long cylinder with surface convection. This solution approach takes into consideration the axial thermal interaction and describes the asymmetric thermal field due to the vessels when their wall temperature is non-uniform in the cross-sectional plane (finite Nusselt number). The theory is needed to more adequately and efficiently describe the heat transfer between the major axial artery and vein in the arm and thereby overcome the serious limitations in the treatment of the axial thermal interaction in the whole limb model in [14].

3.1 Introduction

Countercurrent heat transfer has wide applications in industrial problems involving insulation of power plant steam and water distribution lines and certain types of heat exchangers. These more traditional applications are summarized in [32]. A new area of application which has been the subject of numerous studies in the past decade is the countercurrent heat exchange between the larger countercurrent vessels of the microcirculation [6-10] and [27-31] as well as the major axial arteries and veins that supply the human limbs [14, 15]. The countercurrent heat exchange between the thermally significant vessels of the microcirculation has led to the development of the Weinbaum-Jiji new bioheat equation [6] which has been discussed in the last chapter.

Despite the extensive literature cited above there is no existing three dimensional solution which considers the axial thermal interaction between the fluid in the countercurrent vessels when they are embedded in a cylinder of finite radius with a general convective boundary condition at the cylinder surface. This geometry can be considered as a basic prototype for the axial heat transfer in a human limb. Most previous studies of countercurrent heat exchange are either based on the two dimensional conduction shape factors for embedded vessels and pipes in the cross-sectional plane or are simplified analyses of the axial interaction in which there is a linear axial temperature distribution. In [27, 33, 34] approximate solutions are obtained for the conduction shape factors by superposing solutions for an infinite line source and sink in an infinite medium. Exact solutions for these shape factors in an infinite medium, based on the bicircular coordinate geometry, are presented in [8, 29, 35, 36] for vessels with either constant wall temperature or constant heat flux. A related bicircular solution for a single buried pipe in a half space is given in Bau and Sadhal [37]. The latter solution is novel in that the temperature of the fluid in the pipe is matched with the surroundings and the wall temperature is non-uniform. In [27] the axial interaction equations are formulated for an artery-vein pair and shape factors are derived for two equal sized vessels embedded in a surrounding tissue cylinder with constant wall temperature in the cross-sectional plane. The formulation for the axial interaction is based on a superposition which is a summation of the heat exchange between a perfect countercurrent heat exchanger and the heat loss from the vessel pair to the surface of the surrounding tissue cylinder. This analysis is extended in chapter 2 to vessels of unequal size which are at constant wall temperature.

The motivation for the study in this chapter stems primarily from the model for whole limb heat transfer proposed in [14]. An important restriction on the core energy balance in this model is that it requires that the heat loss from the central vessels of the arm to the surrounding tissue be small compared to the heat exchange between the vessels. The results of [14] and Mitchell and Myers [15] indicate that the heat loss to the environment is comparable or larger than the heat exchange between these central vessels. Therefore, a more general theory is required for countercurrent heat exchange in a cylinder in which there is no restriction on the convective boundary condition at the cylinder surface. The solution in [14] also assumes that the vessel wall temperatures are uniform in the cross-sectional plane and thus neglects the asymmetry in the wall temperature distribution created by the close juxtaposition of the central artery and vein. Recently, Wissler [38] has presented an exact solution for the perfect countercurrent heat exchange between paired vessels in an infinite medium which includes this asymmetry. In this solution there is a linear and equal axial temperature gradient in the medium and vessels, and the physical properties of the fluid and medium are identical and constant throughout the region.

The objective of the study in this chapter is to present a more general three-dimensional approximate analytic solution for the unequal axial countercurrent heat transfer between parallel paired vessels asymmetrically embedded in a long cylinder with surface convection, as shown in Fig. 4. Taking the reciprocal of the Peclet number as a small parameter, a perturbation method is employed to obtain the solution to the temperature distributions both in the vessels and the surrounding cylinder. The analysis introduces several important modifications of

Wissler's [38] basic approach. The line heat source and sink used to replace the convective heat loss/gain from each vessel are unknown functions of the axial coordinate and are related to the local bulk fluid temperature gradients. The surrounding cylinder has a general convective boundary condition, which leads to an unknown axial variation of the heat transfer between the vessels and the vessel pair with environment. The solution also allows for a lowest order asymmetric positioning of the vessels within the cylinder.

Results will be presented for the temperature distributions inside and outside the vessels for several representative cases. The region of biological interest constitutes a small portion of these results. Explicit expressions are obtained for the vessel Nusselt number and the conduction shape factors and the results are compared with the predictions of the models by Baish et al. [27] and Chato [29] for uniform vessel wall temperature. An important and surprising result is that the Nusselt number is the same as for the fully developed flow in a pipe with a constant wall heat flux. The theory is then used to develop a simple prototype model for the axial temperature distributions along the central artery and vein of a human limb in which the skin temperature is unknown and allowed to vary in both the axial and angular directions. The predictions of this model are compared with results of an earlier one-dimensional model by Mitchell and Myers [15] in which the skin temperature variation is not considered. The new model is shown to provide much better agreement with the experimental data of Bazett et al. [19] for the axial variation of the central artery and vein temperature.

3.2 Formulation

A steady state temperature field is assumed in both the vessels and the surrounding tissue cylinder. The analysis further assumes that the velocity profile in the vessels is parabolic (laminar flow)* and the Peclet number is large compared to unity. The vessels are asymmetrically located in the central area of the cylinder, as shown in Fig. 5, and it is assumed that the radius of the cylinder is several times larger than the distances from the origin to the vessels. We shall also assume that the cylinder is sufficiently long for end effects to be neglected.

We introduce nondimensional parameters and variables as follows:

$$P_e = \frac{2\rho_b c_b a_a V_a}{k_b}, \quad k' = \frac{k_b}{k_t}, \quad V' = \frac{V_a}{V_v}, \quad \beta = \frac{1}{P_e}, \quad B_i = \frac{hR}{k_t}, \quad \bar{s} = \frac{s}{a_a},$$

$$\bar{s}_a = \frac{s_a}{a_a}, \quad \bar{s}_v = \frac{s_v}{a_a}, \quad \bar{a}_v = \frac{a_v}{a_a}, \quad \rho_R = \frac{R}{a_a}, \quad \rho = \frac{r}{a_a}, \quad \rho_a = \frac{r_a}{a_a}, \quad \rho_v = \frac{r_v}{a_v},$$

$$z = \frac{Z}{a_a P_e}, \quad \theta = \frac{T - T_\infty}{T_{ai} - T_\infty}$$

Although the theory is much more general in its application, we have used the biological notation where t, a and v represent tissue, an artery and vein respectively. The governing dimensionless equations in the artery and vein can be written as

$$\frac{1}{\rho}\frac{\partial}{\partial\rho}\left(\rho\frac{\partial\theta_a}{\partial\rho}\right) + \frac{1}{\rho^2}\frac{\partial^2\theta_a}{\partial\varphi^2} + \beta^2\frac{\partial^2\theta_a}{\partial z^2} = (1-\rho_a^2)\frac{\partial\theta_a}{\partial z} \qquad \text{for } \rho_a<1 \qquad (3.1)$$

$$\frac{1}{\rho}\frac{\partial}{\partial\rho}\left(\rho\frac{\partial\theta_v}{\partial\rho}\right) + \frac{1}{\rho^2}\frac{\partial^2\theta_v}{\partial\varphi^2} + \beta^2\frac{\partial^2\theta_v}{\partial z^2} = -V'(1-\rho_v^2)\frac{\partial\theta_v}{\partial z} \qquad \text{for } \rho_v<1 \qquad (3.2)$$

In the tissue, where there is no flow, the energy equation is:

* The Reynolds number in the arm or leg is typically 1000 or less.

$$\frac{1}{\rho}\frac{\partial}{\partial\rho}\left(\rho\frac{\partial\theta_t}{\partial\rho}\right)+\frac{1}{\rho^2}\frac{\partial^2\theta_t}{\partial\varphi^2}+\beta^2\frac{\partial^2\theta_t}{\partial z^2}=0 \quad \text{for } \rho_a\geq 1 \text{ and } \rho_v\geq 1 \qquad (3.3)$$

The dimensionless boundary conditions are:

$$\theta_{a,v}=\theta_t \qquad \text{at } \rho_{a,v}=1 \qquad (3.4)$$

$$k'\frac{\partial\theta_{a,v}}{\partial\rho_{a,v}}=\frac{\partial\theta_t}{\partial\rho_{a,v}} \qquad \text{at } \rho_{a,v}=1 \qquad (3.5)$$

$$\frac{\partial\theta_t}{\partial\rho}=-\frac{B_i}{\rho_R}\theta_t \qquad \text{at } \rho=\rho_R \qquad (3.6)$$

Examination of equations and boundary conditions (3.1) through (3.6) reveals that a perturbation solution for $\theta_{a,v}$ and θ_t can be sought of the form $\theta=\theta_o+\beta\theta_1+O(\beta^2)$ since $\beta<<1$ for large P_e number. Equations (3.1), (3.2) and (3.3) reduce to O(1) to

$$\frac{1}{\rho}\frac{\partial}{\partial\rho}\left(\rho\frac{\partial\theta_{ao}}{\partial\rho}\right)+\frac{1}{\rho^2}\frac{\partial^2\theta_{ao}}{\partial\varphi^2}=(1-\rho_a^2)\frac{\partial\theta_{ao}}{\partial z} \qquad \text{for } \rho_a<1 \qquad (3.7)$$

$$\frac{1}{\rho}\frac{\partial}{\partial\rho}\left(\rho\frac{\partial\theta_{vo}}{\partial\rho}\right)+\frac{1}{\rho^2}\frac{\partial^2\theta_{vo}}{\partial\varphi^2}=-V'(1-\rho_v^2)\frac{\partial\theta_{vo}}{\partial z} \qquad \text{for } \rho_v<1 \qquad (3.8)$$

$$\frac{1}{\rho}\frac{\partial}{\partial\rho}\left(\rho\frac{\partial\theta_{to}}{\partial\rho}\right)+\frac{1}{\rho^2}\frac{\partial^2\theta_{to}}{\partial\varphi^2}=0 \qquad \text{for } \rho_a\geq 1 \text{ and } \rho_v\geq 1 \qquad (3.9)$$

Equations (3.7) and (3.8) are complicated by the convective terms on their right hand sides. The partial derivatives $\frac{\partial\theta_{ao}}{\partial z}$ and $\frac{\partial\theta_{vo}}{\partial z}$ are required to describe the entrance and exit regions at the cylinder ends where the temperature profiles develop from their initial conditions. Away from these end regions we assume the local temperature profiles can

be related to the local axial temperature gradients in the fluid in much the same way that a velocity profile can be described by its streamwise pressure gradient. The choice of which temperature gradient to use (centerline, average, bulk etc.) is subtle and will be discussed later. Thus, the temperature gradients in the convection terms on the right hand sides of (3.7) and (3.8) can be approximated by $\frac{d\theta_{ac}}{dz}$ and $\frac{d\theta_{vc}}{dz}$ in the artery and vein respectively, where $\frac{d\theta_{ac}}{dz}$ and $\frac{d\theta_{vc}}{dz}$ are unknown characteristic axial gradients in each vessel. This approximation greatly simplifies the equations since the infinite series of eigenvalues required to describe the axial development of the temperature profiles for the full equations (3.7) and (3.8) will be reduced to two characteristic eigenvalues describing the axial interaction of θ_{ac} and θ_{vc}.

3.3 Solution Procedure

The solution for the θ_{ao}, θ_{vo}, θ_{to}, which we denote by θ_o, can be decomposed into two parts

$$\theta_o = \theta_H + \theta_P \tag{3.10}$$

where θ_H is a homogeneous solution, and θ_P is a particular solution. θ_P is defined as

$$\theta_P = -Q_a\theta_{pa} + Q_v\theta_{pv} \tag{3.11}$$

in which

$$Q_a = -\frac{1}{4}\frac{d\theta_{ac}}{dz} \tag{3.12}$$

$$Q_v = -\frac{1}{4} V' \bar{a}_v^2 \frac{d\theta_{vc}}{dz} \tag{3.13}$$

$$\theta_{pa,v} = \begin{cases} \rho_{a,v}^2 - \frac{1}{4}\rho_{a,v}^4 - \frac{3}{4} & \text{for } \rho_{a,v} < 1 \\ k' \ln \rho_{a,v} & \rho_{a,v} \geq 1 \end{cases} \tag{3.14}$$

To satisfy boundary condition (3.6), we first expand θ_p as a power series in $\bar{s}_{a,v}/\rho$ and neglect terms of $O(\bar{s}^2_{a,v}/\rho_R^2)$. We now require that $\theta_H + \theta_P$ satisfy (3.6) at $\rho = \rho_R$. One obtains the approximate homogeneous solution after the unknown coefficients are evaluated

$$\theta_H = k'\left[\left(\frac{1}{B_i} + \ln\rho_R + \frac{(B_i-1)\bar{s}_a}{(1+B_i)\rho_R^2}\rho\cos(\varphi-\varphi_{av})\right)\right]Q_a$$

$$- k'\left[\left(\frac{1}{B_i} + \ln\frac{\rho_R}{\bar{a}_v} - \frac{(B_i-1)\bar{s}_v}{(1+B_i)\rho_R^2}\rho\cos\varphi\right)\right]Q_v \tag{3.15}$$

Hence, equation (3.10) can be written in the form

$$\theta_o = \frac{1}{4}\left[\left(-\frac{1}{B_i} - \ln\rho_R - \frac{(B_i-1)\bar{s}_a}{(1+B_i)\rho_R^2}\rho\cos(\varphi-\varphi_{av})\right)k' + \theta_{pa}\right]\frac{d\theta_{ac}}{dz}$$

$$+ \frac{1}{4}\bar{a}_v^2 V'\left[\left(\frac{1}{B_i} + \ln\rho_R - \ln\bar{a}_v - \frac{(B_i-1)\bar{s}_v}{(1+B_i)\rho_R^2}\rho\cos\varphi\right)k' - \theta_{pv}\right]\frac{d\theta_{vc}}{dz} \tag{3.16}$$

where θ_{pa} and θ_{pv} differ according to the regions defined in (3.14). It is easily shown that θ_o satisfies (3.4) and (3.7-3.9) with the replacement on the right hand sides of equations (3.7) and (3.8), but can not satisfy (3.5) exactly unless $k'=1$. However, the vessels are much smaller than the cylinder so that θ_o is a reasonable approximate

solution when $k' \approx 1$. Equation (3.16) describes the φ dependence both in the vessels and the surrounding cylinder.

If the solution (3.16) is substituted in (3.7) and (3.8) and the equations are intergrated over the cross-sectional area of each vessel, one finds that the resulting integrated average equation will be satisfied only if θ_{ac} and θ_{vc} are the zeroth order bulk temperatures θ_{abo} and θ_{vbo}. The characteristic axial gradients $\frac{d\theta_{ac}}{dz}$ and $\frac{d\theta_{vc}}{dz}$ therefore are replaced by their corresponding bulk temperature gradients $\frac{d\theta_{abo}}{dz}$ and $\frac{d\theta_{vbo}}{dz}$.

Substituting the solution (3.16) for θ_a and θ_v into the definitions of the bulk temperatures

$$\theta_{a,vb} = \frac{2}{\pi} \int_0^{2\pi} \int_0^1 \theta_{a,v}(1-\rho_{a,v}^2)\rho_{a,v} d\rho_{a,v} d\varphi_{a,v} \tag{3.17}$$

and evaluating these double integrals, one obtains the differential equations for θ_{abo} and θ_{vbo}

$$\theta_{abo} = \frac{1}{4}\left[\left(-\frac{1}{B_i} - \ln\rho_R\right)k' - \frac{11}{24}\right]\frac{d\theta_{abo}}{dz} + \frac{1}{4}\bar{a}_v^2 V' k' \left(\frac{1}{B_i} + \ln\frac{\rho_R}{\bar{s}\bar{a}_v}\right)\frac{d\theta_{vbo}}{dz} \tag{3.18}$$

$$\theta_{vbo} = \frac{k'}{4}\left(-\frac{1}{B_i} - \ln\frac{\rho_R}{\bar{s}}\right)\frac{d\theta_{abo}}{dz} + \frac{1}{4}\bar{a}_v^2 V'\left[\left(\frac{1}{B_i} + \ln\frac{\rho_R}{\bar{a}_v}\right)k' + \frac{11}{24}\right]\frac{d\theta_{vbo}}{dz} \tag{3.19}$$

The coupled linear equations (3.18) and (3.19) have solutions of the form

$$\theta_{abo} = C_1 A_{11} \exp(\lambda_1 z) + C_2 A_{21} \exp(\lambda_2 z) \tag{3.20}$$

$$\theta_{vbo} = C_1 A_{12} \exp(\lambda_1 z) + C_2 A_{22} \exp(\lambda_2 z) \tag{3.21}$$

where eigenvalues λ_i are given by

$$\lambda_{1,2} = \frac{-\tilde{b} \pm \sqrt{\tilde{b}^2 - 16\tilde{a}}}{\tilde{a}} \tag{3.22}$$

with

$$\tilde{a} = \dot{a}_v^2 V' \left[\left(\frac{1}{B_i} + \ln \frac{\rho_R}{\dot{a}_v} \right) k' + \frac{11}{24} \right] \left[\left(-\frac{1}{B_i} - \ln \rho_R \right) k' - \frac{11}{24} \right] - \dot{a}_v^2 V' k'^2 \left(\frac{1}{B_i} + \ln \frac{\rho_R}{\dot{s}\dot{a}_v} \right) \left(-\frac{1}{B_i} - \ln \frac{\rho_R}{\dot{s}} \right)$$

$$\tilde{b} = 2\left(\frac{1}{B_i} + \ln \rho_R + \frac{11}{24} \right) - 2\dot{a}_v^2 V' \left[\left(\frac{1}{B_i} + \ln \rho_R - \ln \dot{a}_v \right) k' + \frac{11}{24} \right],$$

A_{ij} are the eigenvector coefficients of the equations and C_1 and C_2 are constants which are determined by the prescribed bulk temperatures at any station of vessels.

3.4 Results

Since the temperatures within the vessels are non-uniform and the mean temperature of the surrounding cylinder at the cross-sectional plane varies along the axial direction, it is appropriate to compute the mean temperature of the cylinder and to define the heat conduction shape factors in terms of the differences in the bulk temperatures, and mean medium and environmental temperatures. Because the area of the vessels is small compared to the area of the cylinder in the cross-sectional plane, the mean temperature of the cylinder at each cross-section can be approximated by

$$\theta_{tmo} \approx \frac{1}{\pi \rho_R^2} \int_0^{\rho_R} \int_0^{2\pi} \theta_o \rho \, d\varphi \, d\rho = -\frac{k'}{4}\left(\frac{1}{B} + \frac{1}{2} \right)\left(\frac{d\theta_{abo}}{dz} - \dot{a}_v^2 V' \frac{d\theta_{vbo}}{dz} \right) \tag{3.23}$$

The mean excess wall temperatures of the vessels can also be computed as follows

$$\theta_{awo} = \frac{1}{2\pi}\int_0^{2\pi} \theta_{ao}\, d\varphi_a = \frac{k'}{4}\left(-\frac{1}{B_i} - \ln\rho_R\right)\frac{d\theta_{abo}}{dz}$$

$$+\frac{1}{4}\bar{a}_v^2 V' k' \left[\frac{1}{B_i} + \ln\rho_R + \ln\bar{s} - \ln\bar{a}_v\right]\frac{d\theta_{vbo}}{dz} \qquad (3.24)$$

$$\theta_{vwo} = \frac{1}{2\pi\,\bar{a}_v}\int_0^{2\pi} \theta_{vo}\, d\varphi_v = \frac{k'}{4}\left(-\frac{1}{B_i} - \ln\rho_R + \ln\bar{s}\right)\frac{d\theta_{abo}}{dz}$$

$$+\frac{1}{4}\bar{a}_v^2 V' k' \left[\frac{1}{B_i} + \ln\rho_R - \ln\bar{a}_v\right]\frac{d\theta_{vbo}}{dz} \qquad (3.25)$$

The Nusselt number of the artery is defined as

$$N_{uao} = \frac{q_{ao}}{\pi k_b (T_{abo} - T_{awo})} = -\frac{\pi \rho_b c_b a_a^2 \dfrac{dT_{abo}}{dz}}{\pi k_b (T_{abo} - T_{awo})} = \frac{48}{11} \qquad (3.26)$$

It is easily shown that the Nusselt number of the vein, N_{uvo}, has this same value. This value is also the same as for the fully developed temperature profile in a single pipe with a constant heat flux to the environment. For the present solution, the net integrated heat flux from each vessel at any station is determined only by the particular solution in (3.11). This solution is locally the same as the solution for fully developed flow in a pipe with a constant axial temperature gradient. The homogeneous solution (3.15) does not contribute to the net heat flux since it does not contain heat sources or sinks.

Results (3.23) through (3.26) can be used to obtain the expressions for the conduction shape factors σ_{co} and σ_{to} describing the heat

transfer between the vessels, and between the vessel pair and the environment. These expressions are

$$\sigma_{co} = \frac{q_{ao}-q_{vo}}{k_t(T_{abo}-T_{vbo})} = \frac{2\pi}{\frac{11}{24} + k'\ln\bar{s}} \tag{3.27}$$

$$\sigma_{to} = \frac{q_{ao}+q_{vo}}{k_t(T_{tmo}-T_\infty)} = \frac{4B_i\pi}{k'(2+B_i)} \tag{3.28}$$

It is interesting to note that to $O(\bar{s}_{a,v}^2/\rho_R^2)$, σ_{co} depends on the spacing of the vessels only rather than their asymmetry with respect to the origin, and σ_{to} is a simple function of the cylinder Biot number.

For convenience, we let the polar angle $\varphi_{av} = \pi$ and $s_s = s_v$ in all the following calculations. The blood bulk and mean tissue temperature distribution $\theta_{a,vbo}$ and θ_{tmo} along the axial coordinate for B_i=0.5 and 10, which are typical values for the human upper limb in air and water respectively, are shown in Figs. 6 and 7. The solution exhibits a saddle point behavior. For each case, there is a critical bulk temperature of the vein at z=0, $\bar{\theta}_{vb}(0)$, which separates two families of solutions. This critical temperature corresponds to a very long cylinder with the right end maintained at the ambient temperature. As the Biot number is increased from 0.5 to 10, $\bar{\theta}_{vb}(0)$ decreases from 0.45 to 0.32. The dimensionless bulk temperatures grow exponentially positive or negative depending upon whether the bulk temperature $\theta_{vb}(0)$ is greater or less than the critical value. In addition, the mean tissue temperature need not lie between the bulk temperatures of the vessels, as we assumed in chapter 2 for the case of small heat loss from a tissue cylinder in the

microcirculation. Figs. 8 and 9 show the non-uniform circumferential temperature distribution at the vessel walls and the cylinder surface at three different cross-sections for $\theta_{vb}(0)$ =0.5, and B_i=0.5 and 10 respectively.

3.5 Discussion

3.5.1. General Behavior

To evaluate the validity of the assumption that the axial temperature gradients in the convection terms of equations (3.7) and (3.8) can be approximated by the bulk temperature gradients, the normalized difference between the local and bulk axial temperature gradients $(\frac{\partial \theta_{a,v}}{\partial z} - \frac{d\theta_{a,vb}}{dz}) / \frac{d\theta_{a,vb}}{dz}$ has been calculated. Fig. 10 shows the difference distribution across vessel a for the axial boundary condition $\theta_{vb}(0)$=0.9 and $\theta_{vb}(0)$=0.5 at z=0. The maximum value of this normalized difference in the cross-sectional plane occurs at the point in closest proximity to the other vessel. The maximum deviation is less than 19% for the boundary value problems in Figs. 6 and 7. Thus, it is reasonable to approximate the axial temperature gradients in equations (3.7) and (3.8) by their bulk temperature gradients.

lt is interesting to note that the temperature profiles in the vessels do not satisfy the definition of a fully developed temperature profile

$$\frac{\partial}{\partial z} \left(\frac{\theta_{a,v} - \theta_{a,vw}}{\theta_{a,vb} - \theta_{a,vw}} \right) = 0 \qquad (3.29)$$

throughout the vessels even though the Nusselt numbers of the vessels remain constant. The temperature profiles in the vessels continue to

deviate somewhat from a fully developed profile due to the countercurrent axial interaction, regardless of the axial distance from the entrance. However, the fully developed temperature profile defined in (3.29) is satisfied only for a constant axial temperature gradient in the vessels and surrounding medium as shown in [38]. The temperature profile (3.16) can thus be viewed as a quasi fully developed profile in which the Nusselt number does not change but the bulk temperature gradients slowly change to account for the heat loss at the cylinder surface and the axial interaction between the vessels.

Since the present analysis assumes that the vessels are located in the central area of the cylinder and neglects terms of $O(\bar{s}_{a,v}^2/\rho_R^2)$, the heat transfer between vessels and cylinder is determined by the relative spacing of the vessels and not the asymmetry with respect to the cylinder surface. In other words, to $O(\bar{s}_{a,v}^2/\rho_R^2)$ the heat transfer will not change when the vessels are displaced as a pair from the origin. This partly explains why the bulk and mean wall temperatures of the vessels are independent of the asymmetry parameters $\bar{s}_a$ and $\bar{s}_v$ but depend on the distance between the vessels and the ratio of their radii.

From Figs. 6 and 7, one observes that when $\theta_{vb}(0)=0.5$, the bulk temperatures θ_{abo} and θ_{vbo} have a cross over point. The axial position of this point decreases and the temperature distribution changes more significantly along the axial coordinate when the Biot number is increased from 0.5 to 10. Depending on the Biot number and the bulk temperature $\theta_{vb}(0)$, the mean embedding medium temperature θ_{tmo} relative to that of the artery may change along the cylinder. For $B_i=0.5$ and θ_{vb}

(0)=0, θ_{tmo} shifts from a level below the bulk temperature of the artery to one above at z=0.9 as shown in Fig. 6. However, no such crossover is observed for this case when the Biot number is increased to 10 (Fig.7). A similar behavior is obtained for $\theta_{vb}(0)=0.5$. Thus the directions of heat flows between the vessels and between the tissue and vessels may change along the cylinder, depending on $\theta_{vb}(0)$ and the Biot number of the cylinder which describes the heat loss to the environment.

In Table 2 results for σ_{co} for several representative blood vessel pairs are compared with the predictions of Baish et al. [27] and Chato [29]. In [29] the vessels are embedded in an infinite medium whereas in [27] the surrounding cylinder has a uniform surface temperature. In the present solution σ_{co} is based on the difference between the bulk temperature of vessels, while in [27] and [29] it is based on the difference between the vessels surface temperatures which are assumed uniform. This partly explains why the present model gives lower values for σ_{co}. As the spacing between vessels is decreased from 2.5 to 2.1, the effect of surface temperature non-uniformity on σ_{co} becomes more important, resulting in much lower values for σ_{co} than predicted by the uniform wall temperature models [27] and [29]. The solutions in Figs. 8 and 9 clearly show the large variation in wall temperature.

3.5.2. Application to Whole Limb Heat Transfer

In Fig. 11 the experimental data of Bazett et al. [19] for the axial temperature distribution for the artery and vein in a limb is compared with the present model and that of Mitchell and Myers [15]. Both models assume (a) constant radii of the central vessels and the arm, (b) metabolic and perfusion heat sources in the tissue are

negligible, (c) all blood and tissue properties are constant, (d) the temperatures of artery and vein are equal at the wrist end. An important difference between the two models is that the variation of the skin surface temperature is neglected in [15]. Thus in [15] constant overall heat transfer coefficients are assumed to characterize the heat transfer between vessels, and between vessel and the environment for a one-dimensional countercurrent exchange. Using the same geometry parameters, the present theory is applied to determine the artery and vein axial temperature distribution for B_1=1.5, which accounts for the radiation heat transfer, and two values of the Peclet number 7000 and 14000, which are typical of the arm between at rest and during minimal exercise. For the limb the dimensionless coordinate z is typically confined to the region $z<0.07$. Fig. 11, therefore, corresponds only to a small portion of Figs. 6 and 7. It is clear that the present model provides a much better agreement with experimental data for the axial artery and vein temperature distribution than the Mitchell and Myers' model. However, the present non-tapered model can not predict the minimum in the axial variation of the skin surface temperature observed in the experiments which will be discussed later.

The present theory can be used to develop a much more elaborate model, which will not be limited by the restriction in [14] that the heat loss to the surroundings is small compared to the heat exchange between the central vessels, than the simple models just discussed. This new model will be presented in the next chapter.

Chapter 4. A Simplified Three-Dimensional Countercurrent Model for Whole Limb Heat Transfer

In this chapter the theory proposed in chapter 3 is used to develop an improved model for whole limb heat transfer. This model will consider the variable radii of the arm and central vessels and allow for a countercurrent core flow that varies axially to account for the blood supply to the muscle and cutaneous circulations. The local microvascular temperature field in the muscle tissue is described by a new approach in which the first or first and second generations of vessel branching, depending on the value of the local Peclet number, are described by the Pennes equation and all subsequent generations by the Weinbaum-Jiji equation. Representative solutions for the axial variation of the average skin and central artery and vein temperatures and radial variation of the tissue temperature are presented and compared with available experimental data.

4.1 Introduction

A combined macro and microvascular model for whole limb heat transfer has been developed by Song et al. [14] which differs from previous models [15-18] in a number of fundamental aspects. These include: (1) a continuity of flow relation which considers the local arterial bleed off and venous return from the central vessels to the muscle tissue and the cutaneous circulation; (2) the use of a local microvascular equation to describe the radial variation of the effective thermal conductivity of the muscle tissue; (3) an unknown venous return temperature and skin surface temperature distribution which is determined as part of the solution to the overall boundary value

problem; (4) a simplified formulation which allows one to treat a limb with an arbitrary axial variation in cross-sectional area.

The model in [14] predicts a radial temperature profile which agrees well with the experimental data in [1] but inadequately describes the axial temperature variation in the central vessels that was observed in the classic experiments of Bazett et al. [19]. The solutions in [14] do not predict the correct trend for the axial temperature variation of the central vein or the minimum in the axial variation of the skin surface temperature observed in our own recent experiments which will be discussed in the next chapter. The results of our new countercurrent theory developed in chapter 3 suggest that the inadequacy of the previous model [14] stems from an approximation introduced in describing the central vessels in the core of the limb which required that the heat loss to the surrounding be small compared to the heat exchange between the central vessels. Another shortcoming of the model in [14] is that it requires excessive computational time. In order to couple the energy equation for the central vessels to the tissue cylinder, the arm is discretized into 20 disk like elements in the axial direction and a trial and error method is used in the solution procedure for each element. This procedure requires approximately 20 CPU minutes on an IBM 4381 for each boundary value problem.

The bioheat equation which is used to describe the local microvascular temperature field in the muscle tissue in [14] is the Weinbaum-Jiji equation [6]. This equation was developed primarily to describe blood-tissue heat transfer in the microcirculation (vessels under 300μm diameter) and peripheral tissue (outer 2 cm of human limb) [11], and was intended only as a rough estimate of the heat transfer in the deeper tissue where larger countercurrent vessels are present. The

recent study by Charny et al. [7] reveals that the Weinbaum-Jiji equation overestimates the magnitude of the countercurrent microvascular heat source term in the tissue region surrounding the first one or two generations of vessel branching from the central vessels, and a "hybrid" model which applies the Weinbaum-Jiji and Pennes equations in different flow regions provides a better description of the tissue temperature. The analysis of the results in [7] has led to a new interpretation of the source term in the Pennes bioheat equation. Instead of describing blood-tissue heat transfer in the smallest microvessels and capillary beds, as has been commonly assumed, this analysis shows that the Pennes equation actually described small vessel bleed off from the largest countercurrent vessels of the microcirculation. Thus, in the present model the local microvascular temperature field in the muscle tissue is described by a new approach in which the first or first and second generations of vessel branching, depending on the value of the local Peclet number, are described by Pennes equation and all subsequent generations by the Weinbaum-Jiji equation.

In chapter 3, a three-dimensional approximate analytic solution is presented for the unequal countercurrent heat transfer between parallel paired vessels with a laminar Poiseuille velocity profile asymmetrically embedded in a long circular cylinder with surface convection and non-uniform vessel wall temperature. This configuration can be considered as a basic prototype for the axial heat transfer in a human limb. The solution in chapter 3 is for vessels and an embedding cylinder of constant radii and uniform conductivity with a constant axial flow. In this chapter this theory will be extended to include vessels and an embedding cylinder with variable radii, a countercurrent core flow that varies axially to account for the blood supply to the muscle and

cutaneous circulations and muscle tissue with an effective radial conductivity that considers the axial variation of the local bleed off from the central vessels.

The primary objectives of the study in this chapter are to develop an improved asymmetric macro and microvascular model for whole limb heat transfer which: (1) allows for a substantially more efficient and accurate determination of the axial interaction, (2) takes account of the asymmetry of the central vessel wall temperatures due to their interaction, (3) is not limited by the assumption that the heat loss to the surrounding is small compared to the heat exchange between the central vessels, (4) provides an improved description of the heat transfer from the larger countercurrent radial vessels in the deeper muscle tissue where the closure approximation in the Weinbaum-Jiji equation is not valid and (5) still retains the fundamental features of the earlier model [14] mentioned at the beginning of this introduction. The present model is still limited to steady state heat transfer, neglects the axial conduction in the arm, the return circulation from hand in the subcutaneous veins and the bifurcation of the central vessels in the lower portion of the limb and requires a known input for the hand or foot heat transfer to the environment.

4.2 Mathematical Model

It is assumed that the microvascular structure of the tissue is axisymmetric and the major axial artery and vein are located in the central area of the arm, and thus the radius of the arm is several times larger than the distances from the origin to the vessels. As shown in Fig. 12 and 13, the cross-section of the limb perpendicular to its axis can be divided into four basic regions: a) a central region or core of

radius r_1 containing the central artery and vein; b) a deep muscle layer of radius r_2 which contains the first or first and second generations of microvessel branching, depending on the value of the local Peclet number; c) a surrounding layer of muscle and fat tissue which extends to within 2 mm of the skin surface and contains all subsequent microvessel generations; d) a cutaneous layer. The cross-sectional area of the arm and the central vessels can be varied arbitrarily by introducing an axial shape factor G(Z) which when multiplied by the initial radii of the arm or the central vessels provides the local values for these radii.

As with the analysis in chapter 3 a steady state temperature field is assumed in both the central vessels and the tissue of the limb and the velocity profile in the vessels is assumed to be parabolic. Similar nondimensional parameters and variables to those in chapter 3 are introduced as follows:

$$P_{ei}=\frac{2\rho_b c_b a_{ai} V_{ai}}{k_b},\quad k'=\frac{k_b}{k_t},\quad U_a=\frac{V_a}{V_{ai}},\quad U_v=\frac{V_v}{V_{ai}},\quad \beta=\frac{1}{P_{ei}},\quad B_{it}=\frac{h_t R}{k_t},$$

$$\gamma=\frac{q_{ev} a_{ai}}{k_t(T_{ai}-T_\infty)},\quad \bar{s}=\frac{s}{a_{ai}},\quad \bar{s}_a=\frac{s_a}{a_{ai}},\quad \bar{s}_v=\frac{s_v}{a_{ai}},\quad \bar{a}_a=\frac{a_a}{a_{ai}},\quad \bar{a}_v=\frac{a_v}{a_{ai}},$$

$$\rho_R=\frac{R}{a_{ai}},\quad \rho=\frac{r}{a_{ai}},\quad \rho_a=\frac{r_a}{a_a},\quad \rho_v=\frac{r_v}{a_v},\quad z=\frac{Z}{a_{ai}P_{ei}},\quad \theta=\frac{T-T_\infty}{T_{ai}-T_\infty}$$

where the subscript i refers to the entrance of the limb. The inflow Peclet number P_{ei} in the arm or leg is 3500 or larger. Thus the parameter β is much smaller than unity.

(A) The Core

The dimensionless governing equations in the central artery and vein are

$$\frac{1}{\rho}\frac{\partial}{\partial\rho}\left(\rho\frac{\partial\theta_a}{\partial\rho}\right)+\frac{1}{\rho^2}\frac{\partial^2\theta_a}{\partial\varphi^2}+\beta^2\frac{\partial^2\theta_a}{\partial z^2}=U_a(1-\rho_a^2)\frac{\partial\theta_a}{\partial z}$$

$$\text{for } \rho_a<1 \qquad (4.1)$$

$$\frac{1}{\rho}\frac{\partial}{\partial\rho}\left(\rho\frac{\partial\theta_v}{\partial\rho}\right)+\frac{1}{\rho^2}\frac{\partial^2\theta_v}{\partial\varphi^2}+\beta^2\frac{\partial^2\theta_v}{\partial z^2}=-U_v(1-\rho_v^2)\frac{\partial\theta_v}{\partial z}$$

$$\text{for } \rho_v<1 \qquad (4.2)$$

The immediate surrounding tissue, which basically consists of bones and other non-muscle tissues, can be treated as a pure conduction region. Therefore, the tissue temperature field satisfies

$$\frac{1}{\rho}\frac{\partial}{\partial\rho}\left(\rho\frac{\partial\theta_t}{\partial\rho}\right)+\frac{1}{\rho^2}\frac{\partial^2\theta_t}{\partial\varphi^2}+\beta^2\frac{\partial^2\theta_t}{\partial z^2}=0 \qquad \text{for } \rho<\rho_1 \qquad (4.3)$$

The dimensionless boundary conditions at the interfaces between the central vessels and the tissue are:

$$\theta_{a,v}=\theta_t \qquad \text{at } \rho_{a,v}=1 \qquad (4.4)$$

$$k'\frac{\partial\theta_{a,v}}{\partial\rho_{a,v}}=\frac{\partial\theta_t}{\partial\rho_{a,v}} \qquad \text{at } \rho_{a,v}=1 \qquad (4.5)$$

(B) Deep Muscle Layer

The bioheat equation applied in this region, as discussed in the Introduction, is the Pennes equation

$$\frac{1}{\rho}\frac{\partial}{\partial\rho}\left(\rho\frac{\partial\theta_t}{\partial\rho}\right)+\frac{1}{\rho^2}\frac{\partial^2\theta_t}{\partial\varphi^2}+\beta^2\frac{\partial^2\theta_t}{\partial z^2}+\lambda_{pm}(\theta_a^*-\theta_t)+\lambda_m=0$$

$$\text{for } \rho_1\le\rho<\rho_2 \qquad (4.6)$$

where θ_a^* is the local bulk temperature of the blood leaving the central artery, and λ_{pm} and λ_m are the dimensionless blood perfusion and metabolic heat production coefficients in the muscle respectively. The latter are defined as

$$\lambda_{pm} = \frac{W_b c_b a_{ai}^2 \rho_b}{k_t}, \qquad \lambda_m = \frac{q_m a_{ai}^2}{k_t (T_{ai} - T_\infty)}$$

(C) The Surrounding Muscle Layer

The Weinbaum-Jiji bioheat equation is used to describe the local temperature field in this region. From [14] this is given by

$$\frac{1}{\rho}\frac{\partial}{\partial \rho}\left[1+A(\rho)P_e^2)\rho \frac{\partial \theta_t}{\partial \rho}\right] + \frac{1}{\rho^2}\frac{\partial^2 \theta_t}{\partial \varphi^2} + \beta^2 \frac{\partial^2 \theta_t}{\partial z^2} + \beta^2 A(\rho)\frac{\partial P_e^2}{\partial z}\frac{\partial \theta_t}{\partial z} + \lambda_m$$

$$- B(\rho)P_e^2 \frac{\partial \theta_t}{\partial \rho} \qquad \text{for} \quad \rho_2 \le \rho < \rho_3 \qquad (4.7)$$

where

$$A(\rho) = \frac{\pi^2 k' n a^4 u^2 l_r^2}{4\sigma a_2^2 u_2} \qquad (4.8)$$

$$B(\rho) = \frac{\pi^2 k' n a^4 u^2}{4\sigma a_2^2 u_2}\left(\frac{l_r^2}{\rho} + \frac{1}{2}\frac{dl_r^2}{d\rho}\right) \qquad (4.9)$$

Here a is the local vessel radius of the countercurrent microvessels, n is the vessel number density, u is the local blood velocity, l_r is the direction cosine of the vessels in the radial direction, σ is the local shape factor for countercurrent heat transfer, P_e is the local Peclet number and $\rho_3 = \frac{R-\delta_m-\delta_s}{a_a}$ is the dimensionless radial coordinate of the

interface between the muscle layer and the cutaneous layer. The subscript 2 refers to the interface r_2 between the deep muscle layer and the surrounding muscle layer.

(D) The Cutaneous Layer

This layer is treated as in Song et al. [14]. In the inner region of the cutaneous layer, the energy equation is

$$\frac{1}{\rho}\frac{\partial}{\partial\rho}\left(\rho\frac{\partial\theta_t}{\partial\rho}\right)+\frac{1}{\rho^2}\frac{\partial^2\theta_t}{\partial\varphi^2}+\beta^2\frac{\partial^2\theta_t}{\partial z^2}+\lambda_{pc}(\theta_c^*-\theta_t)=0 \qquad \text{for } \rho_3\le\rho<\rho_4 \tag{4.10}$$

where θ_c^* is the temperature at which blood from the central artery arrives at the cutaneous plexus, $\lambda_{pc}=\dfrac{\psi(1-\omega)k'a_{ai}^3P_{ei}}{4\delta_m R_i\int_0^L G(x)dx}$ is the dimensionless blood perfusion coefficient in this inner region and $\rho_4=\dfrac{R-\delta_s}{a_a}$ is the dimensionless radial coordinate of the interface between the inner and outer cutaneous layers. The energy equation for the outer region is simply the conduction equation since all blood vessels are less than 50 μm diameter and in thermal equilibrium with the tissue.

The dimensionless boundary condition at the skin surface of the arm is

$$\frac{\partial\theta_t}{\partial\rho}=-\frac{B_{it}}{\rho_R}\theta_t-\gamma \qquad \text{at } \rho=\rho_R \tag{4.11}$$

where the Biot number B_{it} describes the convective and radiative heat loss and γ is a dimensionless evaporation heat loss.

(E) Hand

Neglecting metabolic energy generation in the hand and the conduction heat transfer between the wrist and the hand, conservation of energy yields

$$T_{ab}(L) - T_{vb}(L) = \frac{q_H}{R_H V_H} = \frac{q_H}{\pi(1-\psi)\rho_b c_b V_{ai} a_{ai}^2} \tag{4.12}$$

where $T_{ab}(L) - T_{vb}(L)$ is the artery-vein bulk temperature difference at the entrance to the hand, R_H is the blood flow rate of the hand, V_H is the hand volume and $1-\psi$ is the fraction of the total blood flow to the limb that enters the hand. The total heat loss from the hand q_H is specified.

(F) Continuity Equation

The muscle tissue in the limb is assumed to be uniformly perfused. The local radial blood bleed-off rate to the muscle and cutaneous layers per unit length of the central artery, $P_m(Z)$ and $P_s(Z)$, can be related to the variation in the local cross-sectional area of the muscle and to the local perimeter for the cutaneous layer. These functions, which are derived in [14], are given by

$$P_m(Z) = \pi\psi\omega a_{ai}^2 V_{ai} G^2(Z) / \int_0^L G^2(x)dx \tag{4.13}$$

$$P_s(Z) = \pi\psi(1-\omega) a_{ai}^2 V_{ai} G(Z) / \int_0^L G(x)dx \tag{4.14}$$

where ψ is the fraction of the total blood flow to the limb that enters the arm as opposed to the hand and ω is the parameter which describes the fraction of the radial blood flow from the central artery that enters the muscle tissue.

Conservation of fluid mass in the central artery then gives

$$\pi\frac{d}{dZ}(a_a^2 V_a) = -P_m - P_s \tag{4.15}$$

or

$$a_a^2 V_a = a_{ai}^2 V_{ai}\{\psi[\frac{\omega\int_Z^L G^2(x)dx}{\int_0^L G^2(x)dx} + \frac{(1-\omega)\int_Z^L G(x)dx}{\int_0^L G(x)dx}] + (1-\psi)\} \tag{4.16}$$

On the other hand, the continuity of fluid mass at the interfaces $r=r_1$ and $r=r_2$ gives

$$P_m = 2\pi^2 r_1 n_1 a_1^2 u_1 \tag{4.17}$$

$$P_m - \pi(r_2^2 - r_1^2)W_b = 2\pi^2 r_2 n_2 a_2^2 u_2 \tag{4.18}$$

The second term on the left hand side of (4.18) represents the blood perfusion in the deep muscle layer. Substituting the expression for P_m in (4.13) into (4.17) and (4.18), one obtains the relationships between the local Peclet number P_{e1} at $r=r_1$, P_{e2} at $r=r_2$ and the Peclet number of the major artery at the entrance to the arm P_{ei}

$$P_{e1} = \frac{\psi\omega a_{ai}}{2\pi a_1 r_{1i} n_1 \int_0^L G^2(x)dx} G(Z)P_{ei} \tag{4.19}$$

$$P_{e2} = [\frac{\psi\omega a_{ai}}{2\pi a_2 r_{2i} n_2 \int_0^L G^2(x)dx} - \frac{(r_{2i}^2 - r_{1i}^2)\lambda_{pm}}{2\pi a_2 a_{ai} r_{2i} u_{ai} n_2}]G(Z)P_{ei} \tag{4.20}$$

4.3 Model Properties and Parameters

The variation of microvascular variables in the muscle layer in [14] are modified herein since the initial vessel branching angles were overestimated in [14]. The angles in [14] were based on an extrapolation of vascular studies for the peripheral tissue layer given in [13].

Further investigation of the deep tissue has revealed that the initial branchings penetrate a small distance and then run parallel to the central vessels providing for an average direction relative to the skin surface that is much shallower. More realistic values of the branching angle measured relative to the radial coordinate are: 80° for the first generation of vessel branching from the central vessels, 70° for the second generation and 60° for the third generation. A linear variation of microvascular variables in the muscle layer is assumed between the first and third generation of vessel branching. Convenient functional forms for the variation of the vascular geometry of the muscle layer in the radial direction and the local blood velocity proposed in [9] can be used from the third generation of vessel branching on. These are:

$$a/a_2 = (1 + C_1\bar{\rho})^{C_2} \tag{4.21}$$

$$n/n_2 = (1 + C_3\bar{\rho})^{C_4} \tag{4.22}$$

$$\sigma = \frac{\pi}{\cosh^{-1}(C_5+C_6\bar{\rho}^{C_7})} \tag{4.23}$$

$$l_r = \cos[C_8(1-\bar{\rho})] \tag{4.24}$$

$$u/u_2 = \frac{n_2a_2^2}{na^2}\left(1 - \frac{r-r_2}{R-r_2}\right) \tag{4.25}$$

where

$$\bar{\rho}=(r-r_2)/(R-\delta_m-\delta_s-r_2) \tag{4.26}$$

The quantities C_i (i=1-8) and a_2 and n_2 are listed in Table 3. The third generation is the start of the true microcirculation (vessels under 300μm diameter) and occurs roughly 2-3 cm from the skin surface, see

Table 4.

A realistic approximation for a tapered arm is a linear axial variation with radius at the shoulder about twice that at the wrist. We thus choose $G(Z)=(1-\frac{Z}{2L})$. The dimensionless velocities in the vessels, U_a and U_v, can be calculated from equation (4.13) using this relationship for G(Z)

$$U_a = \frac{V_a}{V_{ai}} = \frac{8}{7}\omega\psi(1-\frac{Z}{2L})+\frac{4}{3}(1-\omega)\psi-[\psi(\frac{1}{3}-\frac{4}{21}\omega)+\psi-1)]/(1-\frac{Z}{2L})^2 \qquad (4.27)$$

$$U_v = \frac{V_v}{V_{ai}} = \frac{a_a^2}{a_v^2}U_a = \frac{a_a^2}{a_v^2}(\frac{8}{7}\omega\psi(1-\frac{Z}{2L})+\frac{4}{3}(1-\omega)\psi-[\psi(\frac{1}{3}-\frac{4}{21}\omega)+\psi-1)]/(1-\frac{Z}{2L})^2) \qquad (4.28)$$

Several of parameters used herein are the same as those proposed in [14]. The inflow Peclet number P_{ei} ranges from 3500 for a supine resting state to 14000 during minimal exercise* of the limb being modeled. The ratio ψ of the blood supply to the arm (shoulder to wrist) to the total blood supply to the entire limb is taken to be a constant whose value is 0.75. The Biot number, B_{it}, which includes both convective and radiative contributions, is 1.48 and the dimensionless evaporation heat loss γ is 1.524×10^{-3} at standard room conditions. However, the ratio ω of the blood supply to the muscle layer to the total blood supply to the arm was not accurately described in [14]. During exposure to cold the skin blood flow can be reduced to virtually zero, whereas in severe heat stress the skin flow can comprise more than 50% of the total arm blood

* During heavy exercise the blood flow to the muscle can increase by a factor of 100 or more and the expression for the effective conductivities given by the "hybrid" model proposed herein is not accurate because the Pennes equation is no longer valid in the first generation of vessel branching.

flow. During prolonged exercise in the modeled limb the absolute value of the skin blood flow increases but the ratio ω, which is approximately 0.92 under normal conditions [21], does not decrease as assumed in [14].

The validity of the Weinbaum-Jiji bioheat equation is characterized by the normalized thermal equilibration length of the microvessels ϵ in chapter 2. It is defined as

$$\epsilon = \frac{\pi a P_e}{2\sigma(R-r_1)} \tag{4.29}$$

The asymptotic analysis in chapter 2 has shown that the Weinbaum-Jiji equation is valid provided $\epsilon^2 \ll 1$. From Table 4, one sees that the value of ϵ decreases rapidly from the first generation of vessel branching onward. It is less than 0.3 from the third generation of vessel branching on during light exercise or from the second generation on in the supine resting state. This indicates that the deep muscle layer (Pennes Equation) includes the first and second generations of vessel branching during minimal exercise and includes the first generation only in the supine resting state.

The dimensionless metabolic heat production parameter λ_m is assumed to vary linearly with the blood supply to the muscle

$$\lambda_m = C_9 \psi \omega P_{ei} + C_{10} \tag{4.30}$$

where the constants C_9 and C_{10} are determined by evaluating (4.30) at two known conditions; the value $\lambda_m = 2.897\times10^{-4}$ for the supine resting state where $P_{ei}=3500$, and $\lambda_m = 2.897\times10^{-3}$ for minimal exercise where $P_{ei}=14000$. C_9 and C_{10} are found to be 3.598×10^{-7} and -5.795×10^{-4} respectively.

The temperature of the blood from the central artery when it arrives at the cutaneous plexus θ_c^* depends on the prior equilibration in the large isolated riser vessels and is related to the blood flow rate into the cutaneous layer. The relationship between θ_c^* and the temperature of the blood supply to the cutaneous layer, which can be considered as the local blood bulk temperature in the central artery θ_{ab}, is given in [14]

$$\theta_c^*/\theta_{ab} = 1.9\times10^{-4}\psi(1-\omega)P_{ei} + 0.502 \tag{4.31}$$

The experimental results in the next chapter show that the inflow Peclet number is approximately 3500 in the supine resting state and the ratio ψ ranges from 0.729 to 0.772 under normal conditions. Moreover, the artery-vein bulk temperature difference at the entrance to the hand, $T_{ab}(L)-T_{vb}(L)$, can be estimated from the experimental data for the heat loss from the hand in the next chapter when the hand is placed in water.

4.4 Solution Procedure

Examination of the dimensionless tissue bioheat equations (4.3), (4.6), (4.7) and (4.10) reveals that the equations in the different tissue regions can be written in a general form to O(1) if $\beta<<1$ as

$$k_{eff}(\rho,z)\left[\frac{1}{\rho}\frac{\partial}{\partial\rho}\left(\rho\frac{\partial\theta_{to}}{\partial\rho}\right)+\frac{1}{\rho^2}\frac{\partial^2\theta_{to}}{\partial\varphi^2}\right]+\Phi_2\frac{\partial\theta_{to}}{\partial\rho}+\Phi_1\theta_{to}+\Phi_o = 0 \tag{4.32}$$

where k_{eff} and Φ_i(i=0,1,2) are defined differently in different regions: $k_{eff}=k_t$, $\Phi_i=0$ (i=0,1,2) in the core and outer cutaneous layer; $k_{eff}=k_t$, $\Phi_2=0$, $\Phi_1=-\lambda_p$, $\Phi_o=\lambda_{pm}\theta_a^*+\lambda_m$ in the deep muscle layer (Pennes equation);

$k_{eff}=k_t(1+A(\rho)P_{e^2}^2)$, $\Phi_2=\frac{\partial k_{eff}}{\partial \rho}$ - $B(\rho)P_{e^2}^2$, $\Phi_1=0$, $\Phi_o=\lambda_m$ in the surrounding muscle layer (Weinbaum-Jiji equation); $k_{eff}=k_t$, $\Phi_2=0$, $\Phi_1=-\lambda_{pc}$, $\Phi_o=\lambda_{pc}\theta_a^*$ in the inner cutaneous layer. The neglected terms in this approximation are of $O(\beta^2)$.

4.4.1 Solution in Core

According to the theory in chapter 3, the temperature gradients in the convection terms on the right hand side of equations (4.1) and (4.2) can be approximated by the bulk temperature gradients $\frac{d\theta_{abo}}{dz}$ and $\frac{d\theta_{vbo}}{dz}$ in the central artery and vein respectively. Thus, the approximate solution for θ_o to O(1) in the core can be decomposed into two parts

$$\theta_o=\theta_H+\theta_P \tag{4.33}$$

where θ_H is a homogeneous solution, and θ_P is a particular solution. θ_P is given by

$$\theta_P=-\frac{1}{4}U_a\bar{a}_a^2\frac{d\theta_{abo}}{dz}\theta_{pa}+\frac{1}{4}U_v\bar{a}_v^2\frac{d\theta_{vbo}}{dz}\theta_{pv} \tag{4.34}$$

in which $\theta_{pa,v}$ have been defined in (3.14)

The general homogeneous solution can be written as

$$\theta_H=\sum_{n=0}^{\infty} d_n\rho^n\cos(n\varphi)+b_n\rho^n\sin(n\varphi) \tag{4.35}$$

We expand θ_P as a power series in $\bar{s}_{a,v}/\rho$ and require that $\theta_H+\theta_P$ equal $H_1(\rho_1,z)+H_2(\rho_1,z)\cos\varphi+H_3(\rho_1,z)\cos(\varphi-\varphi_{av})+O(\bar{s}_{a,v}^3/\rho_1^3)$ at $\rho=\rho_1$ where

$H_i(i=1,2,3)$ are unknown functions to be determined. One obtains the solution after adding θ_H and θ_p and neglecting terms of $O(\bar{s}_{a,v}^3/\rho_1^3)$

$$\theta_o = D_o + \frac{1}{4} U_a \bar{a}_a^2 [E_1 \rho \cos(\varphi-\varphi_{av}) + \frac{\bar{s}_a^2 k'}{\rho_1^4} \rho^2 \cos 2(\varphi-\varphi_{av}) + \theta_{pa}] \frac{d\theta_{abo}}{dz} +$$

$$\frac{1}{4} \bar{a}_v^2 U_v [D_1 \rho \cos\varphi + \frac{\bar{s}_v^2 k'}{\rho_1^4} \rho^2 \cos 2\varphi - \theta_{pv}] \frac{d\theta_{vbo}}{dz} \qquad \text{for } \rho \le \rho_1 \qquad (4.36)$$

where D_o, D_1, and E_1 are unknown functions of z that need to be determined. Similar to the solution in chapter 3, the solution (4.36) is valid both in the central vessels and in the core tissue where $\theta_{pa,v}$ is defined differently for each region, see (3.14). Note that the vessel wall and core edge temperatures are non-uniform in the cross-sectional plane due to the heat transfer between the vessels. In contrast to the solution in chapter 3, the solution (4.36) retains terms of $O(\bar{s}_{a,v}^2/\rho_1^2)$ since the value of $\bar{s}_{a,v}/\rho_1$ is not <<1. This brings $\cos 2\varphi$ and $\cos 2(\varphi-\varphi_{av})$ terms in (4.36) which are canceled by θ_{pv} and θ_{pa} respectively at $\rho=\rho_1$ to $O(\bar{s}_{a,v}^3/\rho_1^3)$. Although the radial gradients of these terms may not be canceled by θ_{pv} and θ_{pa} at $\rho=\rho_1$, they are of $O(\bar{s}_{a,v}^3/\rho_1^3)$ and can be neglected.

4.4.2 Axial Variation

It is difficult to find the unknown functions D_o, D_1, and E_1 in (4.36). The solutions for these functions is coupled to the solution to the overall boundary value problem in the radial direction for the temperature field in the muscle and cutaneous layers. However, an

approximate solution for these unknown functions can be obtained by estimating the overall heat transfer in the muscle and cutaneous layers instead of calculating the detailed radial temperature field. Note that the square of the local Peclet number appears in the expression for the effective conductivity in the Weinbaum-Jiji equation and the blood perfusion term in the Pennes equation leads to an expression for the effective conductivity which is proportional to the Peclet number P_{el}. One thus assumes the effective conductivity in the entire muscle layer to be a quadratic polynomial involving the local Peclet number. According to the calculation by Charny [39] for his three equation model, the radial effective conductivity of the entire muscle layer without metabolic heat production has an approximate relationship that varies with the local Peclet number of the microvessel at $\rho=\rho_1$

$$k_{em} = k_t(1 + 1.763\times10^{-3}P_{el} + 2.59\times10^{-6}P_{el}^2) \tag{4.37}$$

This expression for k_{em} includes both the blood perfusion term in the Pennes equation in the deep muscle layer and the countercurrent exchange in the Weinbaum-Jiji equation in the surrounding muscle layer.

Substituting the model parameters into relation (4.19) between the local Peclet number P_{el} and the Peclet number P_{ei} at the entrance to the artery, one obtains

$$P_{el} = 0.11\psi\omega P_{ei}(1-\frac{Z}{2L}) \tag{4.38}$$

Substituting (4.38) into (4.37), one finds k_{em} as a function of z

$$k_{em} = k_t[1+1.939\times10^{-3}\psi\omega P_{ei}(1-\frac{Z}{2L})+2.849\times10^{-6}\psi^2\omega^2P_{ei}^2(1-\frac{Z}{2L})^2] \tag{4.39}$$

Using equation (4.39), one can set up a simpler model to approximate the overall axial heat transfer in the limb without using the detailed radial temperature distribution in the muscle and cutaneous layers given by equation (4.32). In this simpler model, the temperature field in the core still satisfies equations (4.1-4.3) and thus has the solution (4.36). However, in the muscle layers equation (4.32) is replaced by the single equation

$$k_{em}(z)\left[\frac{1}{\rho}\frac{\partial}{\partial\rho}\left(\rho\frac{\partial\theta_{to}}{\partial\rho}\right)+\frac{1}{\rho^2}\frac{\partial^2\theta_{to}}{\partial\varphi^2}\right]=-\lambda_m \qquad \rho_1\le\rho\le\rho_3 \tag{4.40}$$

for the purpose of determining the axial interaction. The general solution to (4.40) which is required to satisfy the boundary conditions at $\rho=\rho_1$ is

$$\theta_{to}=-\frac{\lambda_m}{4k_{em}}\rho_2+A_o\ln\rho+B_o+(A_1\rho+A_{-1}\rho^{-1})\cos\varphi+(B_1\rho+B_{-1}\rho^{-1})\cos(\varphi-\varphi_{av}) \qquad \rho_1\le\rho\le\rho_3 \tag{4.41}$$

A simplified boundary condition at $\rho=\rho_3$ is needed to determine the unknown functions $A_i(z)$ and $B_i(z)$ $(i=-1,0,1)$ in (4.41). In the inner cutaneous layer equation (4.32) is approximated by

$$\frac{\partial^2\theta_t}{\partial\rho^2}=\lambda_{pc}(\theta_t-\theta_c^*) \tag{4.42}$$

since the curvature of this thin layer can be neglected and the problem treated locally as one dimensional. Thus the general solution in the inner cutaneous layer can be written as

$$\theta_t=\theta_c^*+c_1e^{\mu\rho}+c_2e^{-\mu\rho} \tag{4.43}$$

where

$$\mu = \sqrt{\lambda_{pc}}$$

Since the temperature gradient does not change in the outer cutaneous layer and its thickness is small compared with the radius of the arm, the thermal variation in the outer cutaneous layer can be neglected. Therefore, the convective boundary condition can be considered to be applied on the inner cutaneous layer directly

$$\frac{\partial \theta_t}{\partial \rho} = -\frac{Bi}{\rho_R}\theta_t - \gamma \qquad \text{at } \rho = \rho_4 \tag{4.45}$$

Substituting (4.43) into (4.44), one has

$$\mu(c_1 e^{\mu\rho_4} - c_2 e^{-\mu\rho_4}) = -\frac{Bi}{\rho_R}(\theta_c^* + c_1 e^{\mu\rho_4} + c_2 e^{-\mu\rho_4}) - \gamma \tag{4.45}$$

At $\rho=\rho_3$

$$\theta_t(\rho_3) = \theta_c^* + c_1 e^{\mu\rho_3} + c_2 e^{-\mu\rho_3} \tag{4.46}$$

$$\frac{\partial \theta_t(\rho_3)}{\partial \rho} = \mu(c_1 e^{\mu\rho_3} - c_2 e^{-\mu\rho_3}) \tag{4.47}$$

One obtains a relationship between $\theta(\rho_3)$ and $\frac{\partial \theta_t(\rho_3)}{\partial \rho}$ by eliminating c_1 and c_2 in equations (4.45-4.47)

$$\frac{\partial \theta_t(\rho_3)}{\partial \rho} = a^* \theta_t(\rho_3) + b^* \theta_c^* + c^* \tag{4.48}$$

where

$$a^* = -\mu[(\mu+\frac{B_i}{\rho_3})e^{\mu(\rho_4-\rho_3)} + (\mu-\frac{B_i}{\rho_3})e^{-\mu(\rho_4-\rho_3)}]^{-1}[(\mu+\frac{B_i}{\rho_3})e^{\mu(\rho_4-\rho_3)}$$

$$-(\mu-\frac{B_i}{\rho_3})e^{-\mu(\rho_4-\rho_3)}]$$

$$b^* = \mu[(\mu+\frac{B_i}{\rho_3})e^{\mu(\rho_4-\rho_3)} + (\mu-\frac{B_i}{\rho_3})e^{-\mu(\rho_4-\rho_3)}]^{-1}[(\mu+\frac{B_i}{\rho_3})e^{\mu(\rho_4-\rho_3)} -$$

$$(\mu-\frac{B_i}{\rho_3})e^{-\mu(\rho_4-\rho_3)} - \frac{B_i}{\rho_3}]$$

$$c^* = -\gamma\mu[(\mu+\frac{B_i}{\rho_3})e^{\mu(\rho_4-\rho_3)} + (\mu-\frac{B_i}{\rho_3})e^{-\mu(\rho_4-\rho_3)}]^{-1}$$

Equation (4.48) can be considered as the boundary condition at $\rho=\rho_3$ for the muscle layer. The nine unknown functions D_o, D_1, E_1, A_j and B_j (j=-1,0,1) in (4.36) and (4.41) are determined by applying boundary condition (4.48) and the continuity conditions for the temperature and heat flux at the interface between the core and the muscle layer. There are three boundary and matching conditions for each linearly independent term in (4.36) and (4.41). Note that the boundary conditions on the heat flux have not been satisfied for the $\cos2\varphi$ and $\cos2(\varphi-\varphi_{av})$ terms for the reason discussed following equation (4.36). The solution to this simplified boundary value problem is

$$\theta_o = -\frac{\lambda_m}{2k_{em}}\rho_1^2\ln\frac{\rho_2}{\rho_1} - \frac{\lambda_m}{2k_{em}}(\rho_2^2-\rho_1^2)(\frac{1}{a^*\rho_2}-\frac{1}{2}) - \frac{c^*}{a^*} - \frac{b^*}{a^*}\theta_c^* + \frac{1}{4}U_a\bar{a}_a^2[E_o +$$

$$E_1\rho\cos(\varphi-\varphi_{av}) + \frac{\bar{s}_a^2k'}{\rho_1^4}\rho^2\cos2(\varphi-\varphi_{av}) + \theta_{pa}]\frac{d\theta_{abo}}{dz} + \frac{1}{4}\bar{a}_v^2U_v$$

$$[D_o+D_1\rho\cos\varphi + \frac{\bar{s}_v^2k'}{\rho_1^4}\rho^2\cos2\varphi - \theta_{pv}]\frac{d\theta_{vbo}}{dz} \qquad \text{for } \rho\le\rho_1 \qquad (4.49)$$

in which

$$D_o = -k'\ln\frac{\rho_1}{\bar{a}_v} - \frac{k''}{k'}[\ln\frac{\rho_3}{\rho_1} - \frac{1}{a^*\rho_3}]$$

$$D_1 = \frac{\bar{s}_v}{\rho_1^2} + \left[(k''-1)\left(\frac{1-a^*\rho_3}{1+a^*\rho_3}\right)\frac{\rho_1}{\rho_3^2} - (k''+1)\frac{1}{\rho_1}\right]^{-1}\left[\frac{1-a^*\rho_3}{(1+a^*\rho_3)\rho_3^2} + \frac{1}{\rho_1^2}\right]\frac{2\bar{s}_v k'}{\rho_1}$$

$$E_o = -k'\ln\frac{\rho_1}{\bar{a}_a} + \frac{k''}{k'}\left[-k''\left[\ln\frac{\rho_3}{\rho_1} - \frac{1}{a^*\rho_3}\right]\right.$$

$$E_1 = \frac{\bar{s}_a}{\rho_1^2} + \left[(k''-1)\left(\frac{1-a^*\rho_3}{1+a^*\rho_3}\right)\frac{\rho_1}{\rho_3^2} - (k''+1)\frac{1}{\rho_1}\right]^{-1}\left[\frac{1-a^*\rho_3}{(1+a^*\rho_3)\rho_3^2} + \frac{1}{\rho_1^2}\right]\frac{2\bar{s}_a k'}{\rho_1}$$

where $k''=k_{em}/k_t$.

Substituting the solution (4.49) for θ_{ao} and θ_{vo} into the definitions of the bulk temperatures (3.17) and evaluating those double integrals, one obtains the differential equations for the axial variation of θ_{abo} and θ_{vbo} to $O(\bar{s}_{a,v}^2/\rho_1^2)$

$$\theta_{abo} = -\frac{\lambda_m}{2k_{em}}\rho_1^2\ln\frac{\rho_2}{\rho_1} - \frac{\lambda_m}{2k_{em}}(\rho_2^2-\rho_1^2)\left(\frac{1}{a^*\rho_2} - \frac{1}{2}\right) - \frac{c^*}{a^*} - \frac{b^*}{a^*}\theta_c^* + \frac{1}{4}U_a\bar{a}_a^2\left[E_o - E_1\bar{s}_a - \frac{11}{24}\right]$$

$$\frac{d\theta_{abo}}{dz} + \frac{1}{4}\bar{a}_v^2 U_v\left(D_o - D_1\bar{s}_v\cos\varphi_{av} + k'\ln\bar{s}\right)\frac{d\theta_{vbo}}{dz} \qquad (4.50)$$

$$\theta_{vbo} = -\frac{\lambda_m}{2k_{em}}\rho_1^2\ln\frac{\rho_2}{\rho_1} - \frac{\lambda_m}{2k_{em}}(\rho_2^2-\rho_1^2)\left(\frac{1}{a^*\rho_2} - \frac{1}{2}\right) - \frac{c^*}{a^*} - \frac{b^*}{a^*}\theta_c^* + \frac{1}{4}U_a\bar{a}_a^2\left[E_o + E_1\bar{s}_a + k'\ln\bar{s}\right]$$

$$\frac{d\theta_{abo}}{dz} + \frac{1}{4}\bar{a}_v^2 U_v\left(D_o + D_1\bar{s}_v\cos\varphi_{av} - \frac{11}{24}\right)\frac{d\theta_{vbo}}{dz} \qquad (4.51)$$

where θ_c^* is given by (4.31). Equations (4.50) and (4.51) are now integrated numerically to determine θ_{abo} and θ_{vbo} and these results then substituted in (4.36) to find the vessel and tissue temperatures in the core.

4.4.3 Solution for Radial temperature profile in Muscle and Cutaneous Layers

We are now in the position to determine the detailed radial temperature distribution in the muscle and cutaneous layers since the temperature field in the core is known from (4.36). Evaluating (4.36) at $\rho=\rho_1$, one assumes that the solution to (4.32) in the muscle and cutaneous layers can be written in the functional form

$$\theta_{to} = H_1(\rho,z) + H_2(\rho,z)\cos\varphi + H_3(\rho,z)\cos(\varphi-\varphi_{av}) \qquad \text{for } \rho_1 \le \rho < \rho_R \tag{4.52}$$

Substituting (4.52) into (4.32), one obtains a set of three differential equations for the H_i

$$k_{eff}(\rho,z)\frac{1}{\rho}\frac{\partial}{\partial\rho}\left(\rho\frac{\partial H_1}{\partial\rho}\right) + \Phi_2\frac{\partial H_1}{\partial\rho} + \Phi_1 H_1 + \Phi_o = 0 \tag{4.53}$$

$$k_{eff}(\rho,z)\frac{1}{\rho}\frac{\partial}{\partial\rho}\left(\rho\frac{\partial H_k}{\partial\rho}\right)+\Phi_2\frac{\partial H_k}{\partial\rho}+\Phi_1 H_k - k_{eff}(\rho,z)\frac{H_k}{\rho^2} = 0 \qquad k=2,3 \tag{4.54}$$

The boundary conditions are the continuity conditions of temperature and temperature gradient at $\rho=\rho_1$ and

$$\frac{\partial H_1}{\partial\rho} = -\frac{Bi}{\rho_R}H_1 - \gamma \qquad \text{at } \rho = \rho_R \tag{4.55}$$

$$\frac{\partial H_k}{\partial\rho} = -\frac{Bi}{\rho_R}H_k \qquad \text{at } \rho = \rho_R \quad k=2,3 \tag{4.56}$$

Equation (4.53) and (4.54) are solved numerically to determine the radial temperature profile at any value of Z. These profiles reflect the asymmetry of the central vessels and the non uniformity of the vessel wall temperatures.

4.5 Results and Discussion

Figs. 14 and 15 show representative solutions for the axial variation of the central artery and vein bulk temperatures and skin surface temperature. The corresponding solutions for the radial temperature profiles are shown in Fig. 16. The asymmetric circumferential temperature distributions at the central vessel walls and at the edge of the core $\rho=\rho_1$ are shown in Fig. 17. The experimental data in the next chapter for the axial skin surface temperature profiles when the hand is immersed in 30°C and 35°C water are compared with the theoretical predictions of the model in Fig. 18. Fig. 19 shows the comparison between a representative radial temperature profile of the human forearm [1] and the theoretical predictions of the present model and the models in [1] and [14].

(A) Axial Variation of Central Artery and Vein Bulk Temperatures and Skin Surface Temperature

Fig. 14 shows the axial variation of the dimensionless bulk temperature of the central artery and vein and the average circumferential temperature of skin surface for different blood flow rates to the entire limb as characterized by the inlet flow Peclet number P_{ei}. One observes that the temperatures of the central artery, vein and surface increase with the blood flow rate and there is a higher metabolic heat production. The temperature difference of the central artery and vein and bulk temperature gradient are both small at the high blood inflow rate since the conductive heat loss from the central vessels is low due to the metabolic heating of the core and the longer equilibration length of the central vessels.

A fundamental difference between the present model and the model in [14] is the prediction for the central vein temperature. In the present model, there is a continuous temperature decrease in the central artery and vein in their respective flow directions. This behavior had been predicted by Mitchell and Myers in their one-dimensional model [15] and observed by Bazett et al. in the human arm [19]. The experimental data in [19] for the arm in the resting state at room temperature are also shown in Fig. 14. In contrast, the vein temperature predicted in [14] increases in the flow direction (wrist to shoulder) due to the assumption that the heat loss to the surrounding is small compared to the heat exchange between the central vessels (close to perfect heat exchanger). The results of the present model and the model in [15], however, predict that the heat loss to the environment is larger than the heat exchange between the central vessels both in the resting state and during minimal exercise at standard room conditions (22°C).

As shown in Figs. 14 and 15, the present model predicts a non-monotonic axial skin surface temperature profile that has not previously been reported. The minimum in this variation occurs in the forearm or the elbow. This behavior is believed to be attributable to a contribution of the increasing vein temperature as one proceeds towards the wrist, the tapered geometry of the arm and the non-linear radial effective conductivity in the entire muscle layer $k_{em}(Z)$. The depth of the minimum depends on the inflow Peclet number P_{ei}, the artery-vein bulk temperature difference $\theta_{ab}(L)-\theta_{vb}(L)$ and the axial shape factor $G(Z)$. For the simple non-tapered arm model in chapter 3, this non-monotonic profile appears only when $\theta_{ab}(L)-\theta_{vb}(L)$ is negative, or when the hand absorbs heat from the surroundings.

(B) Radial Temperature Profiles

Fig. 16 shows that the tissue temperature is elevated throughout the arm at the higher blood flow rate due to the higher metabolic heat production. It is also observed that the radial temperature gradient is small in the central region of the arm at the higher flow rate. This effect is due to the significant enhancement of the effective conductivity in the muscle tissue that arises form the microvascular heat exchange. For P_{ei}=3500 and ω=0.92 (resting state), the radial temperature profile inside the arm varies nearly linearly with the radius of the arm outside the core region. This indicates that conduction is more important than countercurrent microvascular tissue heat transfer at the low flow rates characteristic of the supine resting state. This linear relation has been measured by Ducharme et al. [40] for the resting human forearm immersed in water. The non-uniformity of the profile for ρ<0.2 is due to the presence of the central vessels described next.

As shown in Fig. 17 the circumferential temperature distributions at the central vessel walls and the interface between the core and the muscle are non-uniform. Their non-uniformity depends on the bulk temperature difference between the central vessels at the cross-section. The results of the relation for the radial tissue temperature profile show that the asymmetry of the circumferential temperature distribution in the tissue decays rapidly in the radial direction.

(C) Effect of Cutaneous Circulation

The importance of the cutaneous circulation in whole limb heat transfer can be easily seen from the cases for ω=0.50 in Figs. 15 and 16. Fig. 15 shows that the axial temperature profile of the central

vessels and skin surface are altered by increasing the fractional blood supply to the cutaneous layer. Decreasing ω leads to a decrease in temperature of the central vessels but an increase in skin surface temperature and thus more heat is transferred at the skin surface. This effect of the cutaneous circulation can be more easily understood with aid of Fig. 16 which shows the corresponding temperature profiles in the radial direction at Z/L=0.95. Dilating the cutaneous circulation lowers the core tissue temperature but elevates the skin surface temperature since warm blood from the central artery is directly brought to the inner region of the cutaneous layer. The temperature gradient at the skin surface increases significantly at ω=0.50 producing a substantial increase in heat transfer to the surroundings. In contrast, the temperature gradient changes little in the same region for ω=0.99.

(D) Comparison between Theoretical Predictions and Experimental Measurements

In Fig. 18 the predictions of the present model for the axial skin surface temperature distribution are compared with newly obtained experimental data in the next chapter. The latter represent average values from seven healthy men. In the experiment, the arms of subjects were exposed in 22°C air while their hands were immersed in 30°C and 35°C water baths. Several of the input parameters, including ψ and $\theta_{ab}(L)-\theta_{vb}(L)$, in the theoretical model are taken directly from the experimental measurements for each subject. Using the total blood flow to the limb measured in the experiments described in the next chapter and a typical radius of the central artery at the shoulder, the inflow Peclet number P_{ei} is estimated to be 3582 and 4125 for the hand in 30°C and 35°C water respectively. The theoretical results agree well with the

data from the experiment in which the minimum in the average axial skin surface temperature variation has been observed.

The average radial temperature profile of the human forearm of nine subjects [1] is shown by the short and long dashed curve in Fig. 19. The dotted curve, the dashed curve and the solid curve are the theoretically predicted temperature profiles obtained from the Pennes model, the model in [14] and the present model respectively, for the resting state. The theoretical curve based on the Pennes equation is much fuller than the experimental curve due to the overestimation of the blood perfusion source term in the outer muscle layer. The Pennes equation, since it neglects countercurrent microvascular heat exchange, provides a poor description of the outer muscle layer and heat flux at the skin surface. The Weinbaum-Jiji equation allows for a much better description of peripheral tissue heat transfer for the reasons discussed in [7]. While there is a good agreement between the curve based on the model [14] and the experimental profile in the left half of Fig. 19, their agreement for the right half of the figure is not as close. The theoretical curve in [14] has a flat temperature distribution near the axis of the arm arising from the model assumption that the temperature of the core is the mean temperature of this area. The agreement between the present theoretical prediction and the experimental profile is reasonably good in both halves of Fig. 19 since the present model considers the lowest order asymmetric temperature variation and uses the more accurate "hybrid" model to describe the temperature field in the muscle.

In conclusion, the model developed herein has introduced several important modifications of the original model proposed in [14] for whole limb heat transfer. A much improved axial thermal interaction between the central vessels and the environment is described and thus more

realistic axial temperature profiles for the arm are predicted. The CPU time for calculating each boundary value problem is less than 1 minute on an IBM 4381 compared to 20 minutes for the model in [14]. A more appropriate "hybrid" model which applies the Pennes and Weinbaum-Jiji bioheat equations in different flow regions is used to describe the temperature field in the muscle tissue. The present model also predicts the first approximation for the asymmetric temperature field of the arm and provides a rational explanation for the minimum in the average axial skin temperature variation that has been observed for the human limb. The new model has the flexibility for some important future refinements. These include a more realistic treatment of the central vessel location and its bifurcation in the lower arm, the inclusion of a separate superficial venous return circulation from the extremity and a separate model for heat transfer in the extremity.

Chapter 5. Experimental Study

5.1 Objectives

In this study several of the important input parameters of the proposed whole limb heat transfer model were directly measured or indirectly determined, including the fraction of the total limb blood flow entering the hand, the blood perfusion parameter in the arm, the inflow Peclect number of the arm and the artery-vein bulk temperature difference at the wrist. The axial skin surface temperature distribution of the arm was also measured to test the theoretical predictions. The experiments were carried out under steady state thermoneutral conditions in which the hand was immersed in water at temperatures ranging from 10 to 40°C while the arm was exposed to the air at room temperatures of 21 to 23°C. The relationship between blood flow and heat transfer at different skin temperatures of the hand was examined. Studies were carried out in accordance with guidelines of and with the approval of the Columbia University committee on human investigation. The subjects were seven healthy men between 22 and 38 years of age.

5.2 Method

An electrically calibrated mercury-in-rubber strain gauge (made by Hokanson Company) was placed around the forearm to measure the arm blood flow. A water filled plethysmogragh-calorimeter (Plethcal) apparatus (modified from the design of Raman and Vanhuyse [24]) was constructed to measure hand blood flow and heat transfer of the hand simultaneously. Both blood flow measurements were based on the venous occlusion technique whereby the changing volume of the tissue following proximal occlusion reflects the inflow rate. The Plethcal apparatus was fed by

temperature controlled water bath and the difference between the inlet and outlet temperatures combined with the flow rate gave the hand heat loss.

The principle of the apparatus is shown in Fig. 20. Vessel A consisted of two concentric cylinders (A_{in} and A_{out}), the inner one, A_{in}, (inner diameter 14cm, length 24cm) had an aperture that allowed the introduction of the hand. A_{in} was partly filled with water to a level slightly above the hand. Between the two cylinders was a copper pipe coil (inner diameter 0.7cm) in which there was a water circulation of the same temperature as inside A_{in}. The coil kept the air temperature between the cylinders uniform and equal to the water temperature inside A_{in}, and reduced the heat exchange between vessel A and the room. The whole Plethcal apparatus was covered by foam rubber in order to reduce the heat exchange between the Plethcal and the surroundings to a very small amount. An Harvard infusion pump was connected to the lower part of vessel A_{in}. A_{in} was connected via another vessel B (inner diameter 20cm, length 35cm) to a sensitive pressure transducer of the linear differential type F (LCCD Model made by Celesco Transducer Productions, INC.); V and R are the amplifier and recorder, which were connected to computer C. The purpose of vessel B was to minimize the pressure increase during blood flow measurements so that the blood flow was not disturbed in the hand by the measuring procedure. Vessel B contained some water in order to have it saturated with water vapor as was the case with vessel A. The other side of the transducer was connected to reservoir C which maintained atmospheric pressure. Before a measurement was started A and B were brought to atmospheric pressure by opening a

computer controlled solenoid S which was then closed during the measurement interval.

For blood flow measurements, venous occlusion was accomplished with two pneumatic cuffs. One cuff was placed on the upper arm above the strain gauge and another one at the wrist as near as possible to the Plethcal. The cuffs were rapidly inflated to a pressure of 50-60 mmHg which was sufficient to stop venous return from the limb while still allowing arterial inflow. The cuff on the wrist and the cuff on the upper arm stopped the venous return from the hand and the upper arm respectively so that the blood flow of the hand and the arm could be measured independently. The cuffs were fully inflated in 0.5 second and cuff pressure was maintained for 10 seconds. A time interval of about 70 seconds was allowed between successive cuff inflations. The outputs of the strain gauge and the Plethcal were recorded and the initial linear part of the slopes of these recordings are used to calculate the blood flow rates of the arm and the hand respectively.

During the hand blood flow measurements at each water temperature to which the hand was exposed, one or two calibrations were carried out depending on the experiment time. The water was injected uniformly in vessel A_{in} by the infusion pump (injection rate is known) providing a linear change in volume over time. The slope of this recording was used as a standard output of the inflow rate to vessel A_{in} to calculate the hand blood flow rate by comparing this slope to the initial slope of the Plethcal output during the venous occlusion.

Heat loss from the hand was found by measuring the temperatures of the water entering and leaving vessel A_{in}, T_{iv} and T_{ov}, and the coil, T_{ic} and T_{oc}, and the rates of the water flow through vessel A_{in}, J_v, and

the coil, J_c (J_v=J_c in the actual measurements). Flow was maintained with precision flow meters. No major temperature gradients built up in vessel A_{in} as the water was slightly stirred via the recirculation. Taking into account the adaptation period prior to data collection which was about 30 minutes for each water temperature, we confirmed that the heat exchange between the hand and the water reached steady state so that the rate of heat flux q_H from hand to the water could be determined by means of the equation

$$q_H = c_w\rho_w[(T_{ov} - T_{iv})J_v + (T_{oc} - T_{ic})J_c] \qquad (5.1)$$

where c_w and ρ_w are the specific heat and the density of the water.

Eight calibrated 36 gauge copper-constantan thermocouples referenced to a distilled water crushed ice slurry were placed axially on both sides of the arm while two other thermocouples were placed on the finger and the palm respectively. The measured temperatures were obtained with a resolution of 0.01°C when the thermocouples were connected to an HP3478A multimeter and HP3488A scanner. The HP3478A had integrating analog to digital converter and 5 1/2 digit display. The output of the HP3478A was connected to a computer for real time display and storage.

5.3 Results

Fig. 21 gives the mean ±1 standard deviation (SD) values of heat loss from the hand q_H for all subjects as a function of the water temperature T_w, which is between T_{ov} and T_{iv} and can be considered uniform in vessel A_{in} since the difference between T_{ov} and T_{iv} is less

than 1°C. As expected, q_H was positive or negative depending on whether the water temperature, T_w, was lower or higher than 37°C. The graph of the figure shows a minimum for q_H at T_w of about 15°C and a maximum at T_w of about 25°C. For one subject the minimum value for q_H occurred at T_w=20°C.

In Fig. 22 the mean ± SD rate of the blood flow to the hand R_H in ml blood$\cdot min^{-1}\cdot 100ml^{-1}$ tissue for all subjects is shown as a function of the water temperature T_w. R_H increased gradually as T_w increased from 15°C to 35°C, but when the water temperature reached 40°C there was a large R_H increment. When the water temperature was decreased to lower than 15°C R_H also increased. In the theoretical model in chapter 4, the axial conduction heat transfer was neglected in the arm. Thus, the artery-vein bulk temperature difference at the entrance of the arm to the hand which was an important boundary condition in the model, was approximated by substituting the values of q_H and R_H into equation (4.12) since the metabolic heat production of the hand is negligible which will be discussed later.

Fig. 23 shows the mean ±1 SD of arm blood flow per unit tissue R_A in $ml\cdot min^{-1}\cdot 100ml^{-1}$. Although the arm was exposed to the air at a constant room temperature 22°C, the blood flow rate to the arm changed as the water temperature in which the hand was immersed was altered. The arm blood flow rate increased when the hand blood flow rate increased. This effect shows that the blood flow of the arm is influenced by the hand temperature. The value of R_A provides the blood perfusion parameter

in the Pennes bioheat equation which is used to describe the deep muscle layer heat transfer in the theoretical model in chapter 4. The total blood flow rate to the arm, which is used to estimate the inflow Peclet number of the arm in the model, is obtained by multiplying R_A by the total volume of the arm.

The ratio of the blood supply to the hand to the total blood supply to the entire limb is shown in Fig. 24. It verifies that the value of this ratio, 0.25, which is used in the theoretical model is reasonable at standard room conditions.

The average skin surface temperature distributions along the arm (in a dimensionless axial coordinate with ±1 SD) for the water temperature at 10, 25 and 40 °C are shown in Fig. 25. The average skin temperature at the Z/L=0.93 (about 5 cm from the wrist) changed with the water temperature more significantly than those at other stations. The axial temperature gradient became considerable in the forearm when the water temperature was lower than 25°C. Results of the temperature measurements from the thermocouples on the palm and the finger show that the skin surface temperature of the hand was little different from the water temperature to which the hand was exposed.

5.4 Discussion

As shown in Fig. 25 the axial temperature gradient is expected to be small compared to the radial temperature gradient in the arm when the water temperature, T_w, to which the hand was exposed is from 25°C to 40°C. In the experiment by Raman and Vanhuyse [20] the conduction heat transfer from arm to the hand was found to be less than 20% of the total heat loss from the hand when T_w was in this range. Therefore, these

results confirm that the proposed whole limb heat transfer model, in which the axial conduction is neglected, is valid under these conditions. The total heat loss from hand consists of the conduction heat transfer from the arm to the hand, the metabolic heat production in the hand and the heat transfer due to blood flow. As the metabolic heat production is only about 4% of the total heat loss value [41] for a resting hand, it is reasonable to assume that possible changes of such a small value will be negligible. Assuming a doubling of hand metabolism with 10°C tissue temperature increase (Q_{10} of 2), metabolic heat production could be eight times as high at 40°C as at 10°C. Since heat transfer due to blood flow is also increased over this temperature range, the metabolic heat would still be a small percentage of total hand heat loss. It is thus reasonable to estimate the artery-vein bulk temperature difference at the entrance of the hand by substituting the measured heat loss q_H in (4.12) when the water temperature T_w is from 25°C to 40°C. The comparison of the predictions of the axial skin surface temperature distribution by the theoretical model with the measurements in the experiment is discussed in chapter 4. As shown in Fig. 18 the theoretical results for the water temperature at 30 and 35°C agree well with the experimental data. The minimum in the axial variation of the skin temperature, which was observed for the water temperature was equal to or larger than 30°C, has been predicted by the model in chapter 4. However, when the water temperature is lower the model is not valid due to the considerable axial temperature gradient in the forearm and the wrist.

The blood flow rate and the heat loss rate of the hand measured here agree with the measurements by Raman and Vanhuyse [20]

qualitatively. However, this does not necessarily confirm their conclusion that the blood circulation patterns must be different when the hand is immersed in warm and cold water. The heat loss from the hand due to blood flow is determined by

$$q_B = \rho_b c_b R_H V_H (T_{bi} - T_{bo}) \tag{5.2}$$

where ρ_b and c_b are the density and the specific heat of the blood respectively, V_H is the hand volume and T_{bi} and T_{bo} are the average blood temperatures entering and leaving the hand. The conclusion in [20] was based on the assumption that T_{bi} and T_{bo} are of the body temperature and the water temperature respectively. However, as shown in Fig. 25 the temperature of forearm can be cooled to lower than 20°C when the water temperature is at 10°C. The blood temperature is thus very likely to be precooled before it enters the hand. In fact, cooling of radial arterial blood to 22°C at 9°C room temperature was observed by Bazett et al. [19] in human arm. Moreover, the blood temperature leaving the hand usually is not the water temperature either. The theoretical prediction in chapter 4 for the hand immersed in the 30°C water shows that the blood temperature leaving the hand is higher than 30°C. A larger difference between the water temperature and the blood temperature leaving the hand is expected when the water temperature is lowered.

In conclusion, whether the circulation pattern is changed when the hand is immersed in cold water is still not clear. More information about the blood temperature in the arm is required to confirm or disprove this hypothesis since the theoretical model developed in chapter 4 is not valid due to the considerable axial conduction heat transfer in the arm in this case.

Chapter 6. Conclusion

The work presented in chapter 2 has completed an important step in the development of the Weinbaum-Jiji new bioheat equation [6]. A revised relationship between the local average tissue temperature and the artery vein temperatures for countercurrent microvessels of unequal size has been derived. A rigorous derivation is also presented for the closure approximation relating the local arterial-venous temperature difference and the mean tissue temperature gradient. Based on these results, the Weinbaum-Jiji bioheat equation has been generalized for microvessels of unequal size. The equation is valid provided the square of the normalized thermal equilibration length of the vessels ϵ^2 is much smaller than unity. In chapter 4 the Pennes equation is implemented to describe the tissue temperature field in the muscle regions where $\epsilon>0.3$ in the resting state and during minimal exercise. However, during heavy exercise, which may cause the muscle blood flow to increase more than 100 times, the Pennes equation is no longer valid in the deep tissue layer [39]. Therefore, a more general approach is still needed to describe the tissue temperature field under all possible conditions, including heavy exercise. Note that equation (2.47) is exact without any approximations and assumptions. One may derive a more general bioheat equation by exploring a general relationship between the arterial-venous temperature difference T_a-T_v and the local mean tissue temperature θ (in the Weinbaum-Jiji equation this relationship is given by equation (2.46) with the restriction that $\epsilon^2<<1$).

An approximate three-dimensional analytic solution for describing the countercurrent heat transfer between a vessel pair embedded in a

tissue cylinder of constant cross-section with surface convection has been presented in chapter 3. The solution is the first to describe the axially varying asymmetric thermal field that develops in both the vessels and in the surrounding tissue cylinder. The primary objective in obtaining this new solution is to develop a three dimensional variable geometry macro and microvascular model for whole limb heat transfer. However, the new solution approach is of more general interest since it attempts to lay the foundation for the heat transfer analysis of quasi-thermal fully developed flows (a flow whose axial temperature gradient varies across the vessel cross section, but its Nusselt number is constant). In this new approach the axial temperature gradients in the convection terms in the governing energy equations for the vessels are approximated by the bulk temperature gradients in the respective vessels while the wall temperatures are allowed to be non-uniform in the cross-sectional plane. This approximation greatly simplifies the equations since the infinite series of eigenvalues required to describe the axial development of the temperature profiles for the full governing equations in the vessels are reduced to two characteristic eigenvalues describing the axial interaction of the bulk temperatures. The theory is easily extended to any number of vessels in an embedding medium of more general cross-sectional geometry. Furthermore, the approach can be generalized to consider an arbitrary location of the embedding vessels and different conductivities of the fluid in the vessels and the embedding medium. This will be important in developing a more accurate whole limb heat transfer model in which the major axial artery and vein are located far from the axis of the arm.

The new model of whole limb heat transfer developed in chapter 4 has provided a major improvement on the first combined macro and

microvascular model proposed in [14] in that (i) it is not limited by the assumption that heat loss to the environment is small compared to the heat transfer between the vessels (ii) predicts an axial temperature distribution for the central vein which agrees much better with the experimental data in [19] (iii) provides a rational explanation for the minimum in the average axial skin temperature variation that has been observed for the human arm (iv) describes the asymmetric axial interaction between vessels of non-uniform wall temperature and (v) despite these added complexities requires two orders of magnitude less computer time. This substantial improvement in computational efficiency results from a greatly simplified and yet more accurate description of the axial interaction. Furthermore, the model has the flexibility for some important refinements. These include a more accurate treatment of the asymmetric location of the major axial vessels and their bifurcation in the lower arm, the inclusion of a separate superficial venous return circulation from the extremity, a model for the extremity heat transfer and the consideration of time dependent behavior.

The minimum in the average axial skin temperature variation for the human arm predicted by the theoretical model has been observed in the experimental study discussed in chapter 5. Several of the important parameters for the model were directly measured or indirectly determined by the experiment. The relationship between the blood flow and the heat transfer at different hand skin temperatures indicates that more information is required to confirm or disprove the hypothesis that the circulation pattern is changed when the hand is placed in a cold environment (such as in cold water) but the arm is in warm air. For this case the present model for whole limb heat transfer developed in chapter

4 is not accurate because there is significant axial conduction heat transfer in the wrist and forearm.

Similar experimental studies can be carried out for the rat tail and the human finger. The theoretical models for these appendages and the model for the cremaster muscle can constructed based on a theory that is an extension of the analysis in chapter 3. In conclusion, the present research has set the stage for a new generation of macro and microvascular heat transfer models. It has led to a better understanding of the fundamental mechanisms of microvascular heat transfer and a more accurate description of macro and microvascular heat transfer and their coupling in the human limbs.

Appendix

The function F which appears in equations (2.14) and (2.15) satisfies the differential equation

$$\frac{\partial^2 F}{\partial R^2} + \frac{1}{R}\frac{\partial F}{\partial R} + \frac{1}{R^2}\frac{\partial^2 F}{\partial \alpha^2} = 0 \tag{A1}$$

and boundary conditions

$$F(R_a,\alpha) = \frac{q_e}{k_t} g(R_a,\alpha), \qquad F(1,\alpha) = \frac{q_e}{k_t} g(1,\alpha) \tag{A2}$$

Where $g(u,v)$ is the unit line sink defined in equation (2.13). This boundary value problem can be solved by separation of variables in the cylindrical coordinates R, α of the w plane. This solution is

$$F(R,\alpha) = \frac{q_e}{k_t}[a_o + b_o \ln R + \sum_{k=1}^{\infty} (a_k R^k + b_k R^{-k})\cos k\alpha + (c_k R^k + d_k R^{-k})\sin k\alpha] \tag{A3}$$

The coefficients a_i and b_i are determined by the boundary conditions (A2) and are given by

$$a_0 = \frac{1}{2\pi}\int_0^{2\pi} -g(1,\alpha)\,d\alpha \tag{A4}$$

$$a_0 + b_0 \ln R_a = \frac{1}{2\pi}\int_0^{2\pi} -g(1,\alpha)\,d\alpha \tag{A5}$$

$$a_k R_a^k + b_k R_a^{-k} = \frac{1}{\pi}\int_0^{2\pi} -g(R_a,\alpha)\cos k\alpha\,d\alpha \tag{A6}$$

$$a_k + b_k = \frac{1}{\pi}\int_0^{2\pi} -g(1,\alpha)\cos k\alpha\,d\alpha \tag{A7}$$

$$c_k R_a^k + d_k R_a^{-k} = \frac{1}{\pi}\int_0^{2\pi} -g(R_a,\alpha)\sin k\alpha\,d\alpha \tag{A8}$$

$$c_k + d_k = \frac{1}{\pi}\int_0^{2\pi} -g(1,\alpha)\sin k\alpha\,d\alpha \tag{A9}$$

The fraction of the heat transfer leaving the artery or vein and entering the far field is most conveniently determined using residue theory. These heat transfer fractions pq_e and $(1-p)q_e$ (see equations (2.17) and (2.18)) are given by

$$pq_e = -k_t \int_0^{2\pi} \frac{\partial T}{\partial R} \Big|_{r=Ra} \cdot R_a \, d\alpha = -2\pi b_0 q_e \tag{A10}$$

and

$$(1-p)q_e = k_t \int_0^{2\pi} \frac{\partial T}{\partial R} \Big|_{R=1} \cdot 1 \cdot d\alpha = (1+2\pi b_0) q_e \tag{A11}$$

The coefficient b_0 can be determined from equations (A4) and (A5) and also evaluated using residue theory

$$\ln R_a \cdot 2\pi b_0 = \int_0^{2\pi} g(1,\alpha) - g(R_a,\alpha) \, d\alpha = -\ln \frac{1}{b} \tag{A12}$$

Substituting (A12) into (A10) and (A11) and comparing with equations (2.17) and (2.18) one finds that p is given by

$$p = \frac{\ln \frac{1}{b}}{\ln R_a} \tag{A13}$$

which is result (2.19). One can show from equations (2.9) and (2.10) that p must fall in the range $0<p<1/2$.

Table 1 Typical Values of Parameter ϵ

Artery diam. μm	Vein diam. μm	Peclet number of artery	σ_c	ϵ
300	300	120	5.06	.112
200	200	40	5.06	.024
250	500	120	5.83	.081
100	200	40	5.83	.011
150	450	120	6.20	.046
100	300	40	6.20	.010

Table 2 Shape Factor σ_c for Equal Sized Vessels

Type of vessel	a_a μm	ρ_R	$\bar{s}$	σ_c Present	σ_c Ref. [27]	σ_c Ref. [29]
Large artery	1500	40	2.5	4.571	5.275	5.284
Medium artery	500	35	2.5	4.571	5.268	5.284
Small artery	200	20	2.1	5.234	9.924	9.975

Table 3 Model Properties and Constants

$L = 70$ cm	$C_1 = -0.933$
$R_i = 7$ cm	$C_2 = 0.7$
$r_{1i} = 1.5$ cm	$C_3 = -0.867$
$\varphi_{av} = \pi$	$C_4 = -2$
$\dot{s}_a = \dot{s}_v = 1.25$	$C_5 = 2.5$
$a_{ai} = 0.3$ cm	$C_6 = 9.5$
$a_1 = 0.05$ cm	$C_7 = 16$
$n_1 = 0.14$ pair/cm^3	$C_8 = 1.047$
$a_2 = 0.015$ cm	$C_9 = 3.598\times10^{-7}$
$n_2 = 0.56$ pair/cm^3	$C_{10} = -5.795\times10^{-4}$
$\rho_b = 1.05$ g/cm^3	
$c_b = 3800$ J/kg °C	
$k_b = k_t = 0.5$ W/m °C	
$T_\infty = 22$°C	
$\delta_m = \delta_s = 0.1$ cm	
$W_b = 2.17$ ml/min/100g	

Table 4 Values of Vascular Variables and Normalized Thermal Equilibration Length ϵ

generation of vessel branching	r/R	a cm	n #pairs/cm^2	l_r	ϵ P_{ei}=14000 ω=0.92	ϵ P_{ei}=3500 ω=0.92
1st	0.214	0.05	0.14	0.174	2.872	0.718
2nd	0.398	0.027	0.28	0.342	0.692	0.173
3rd	0.528	0.015	0.56	0.5	0.184	0.046

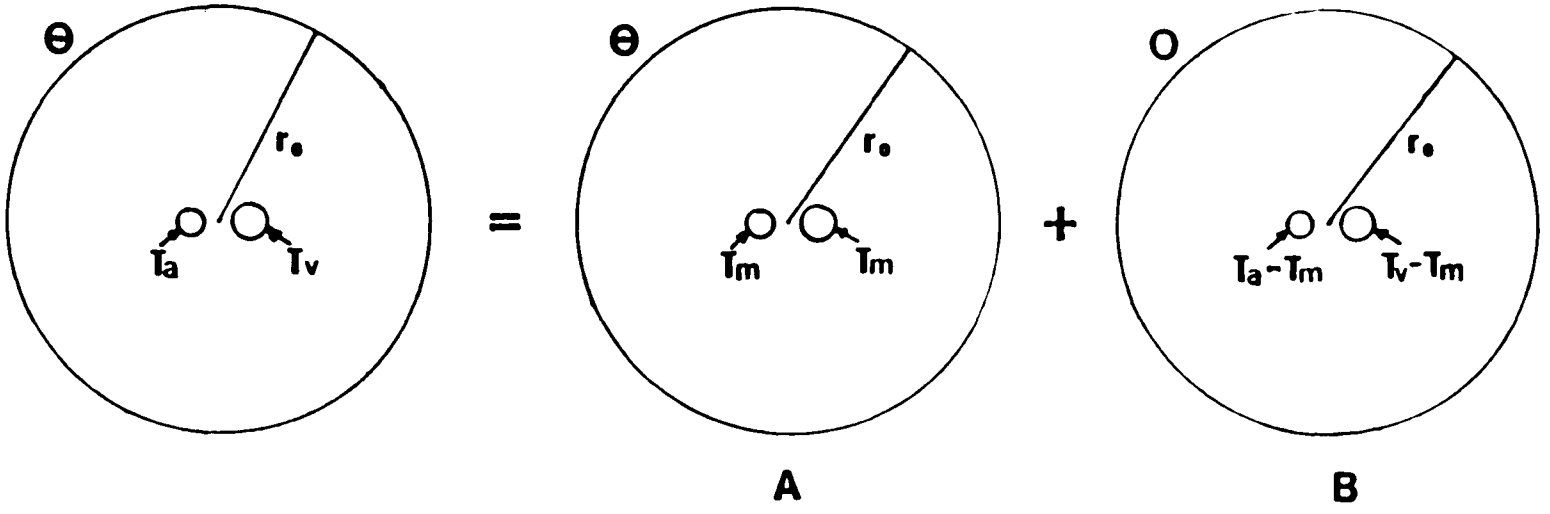

Fig. 1 Superposition of boundary problems of countercurrent vessel pair in cross-section plane

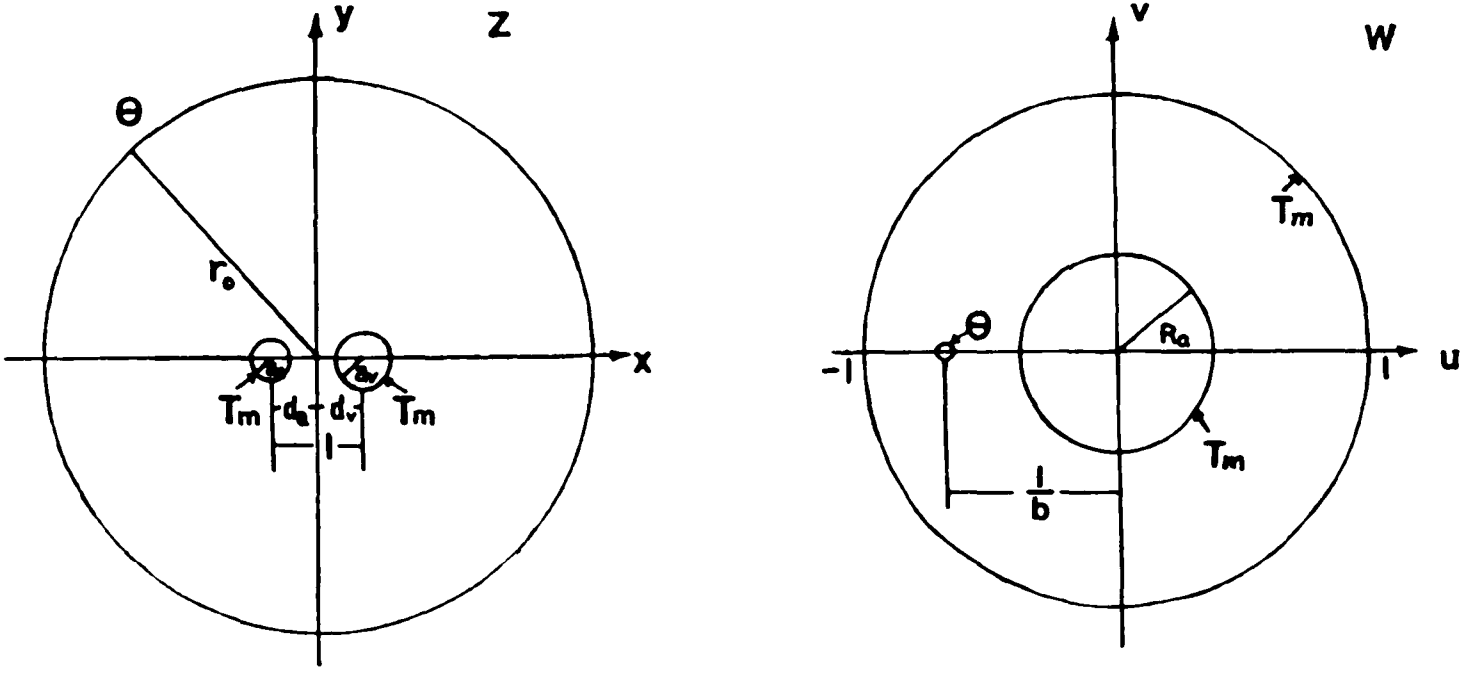

Fig. 2 Transformation from Z to W plane for boudary value problem A

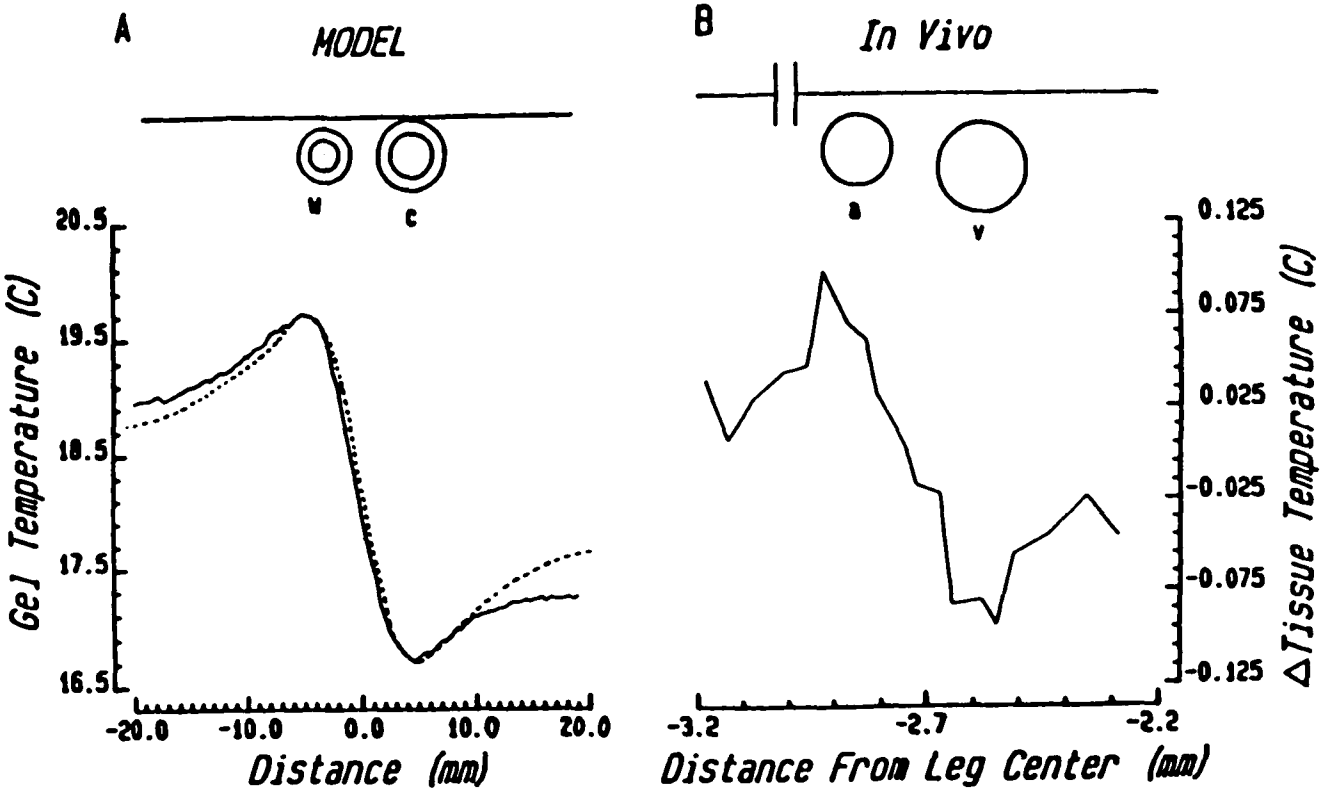

Fig. 3 Model and in vivo temperature measurments [10]. Panel A: Temperature Profile through gelatin block with countercurrent tube flow. Dimensions of tubes and location of wire shown in upper part of diagram scaled relative to dimensions of vessels and position of wire for in vivo traverse shown in Panel B. Solid curve is experimentally measured profile in [10], dashed curve is theoretically predicted profile. Panel B: In vivo measurements [10] taken at 20 to 40 μm intervals and data points connected by straight lines.

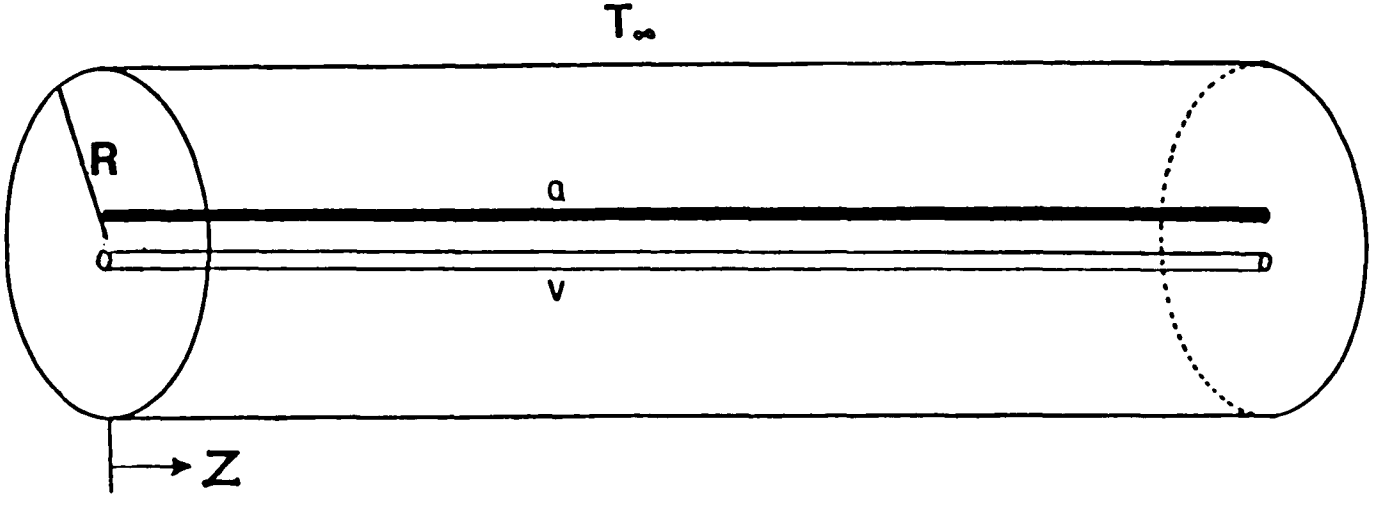

Fig. 4 Schematic of tissue cylinder surrounding countercurrent vessel pair

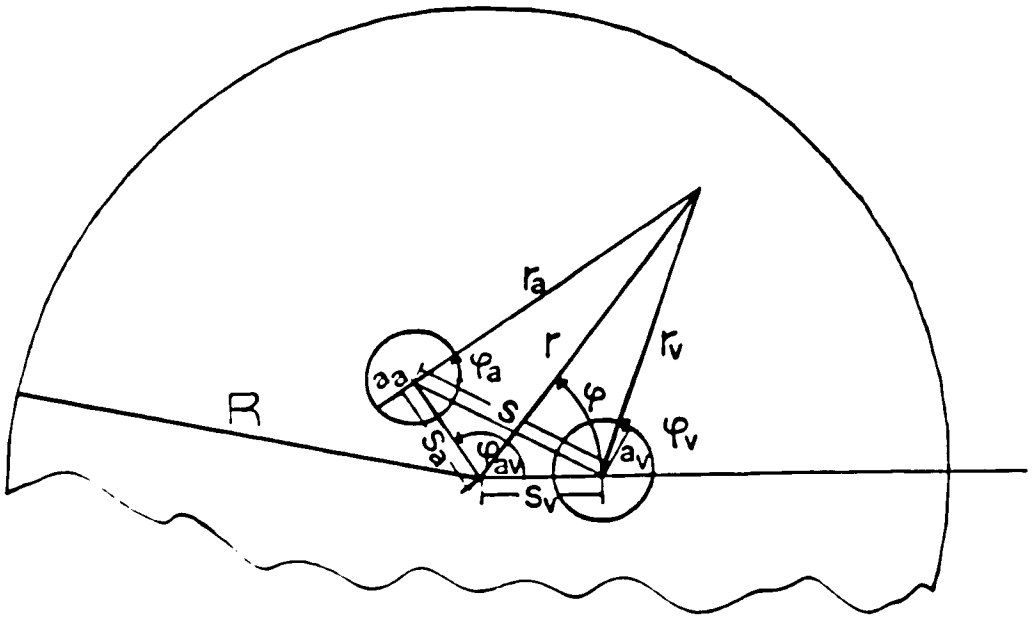

Fig. 5 Geometry of cross-sectional plane and coordinate system

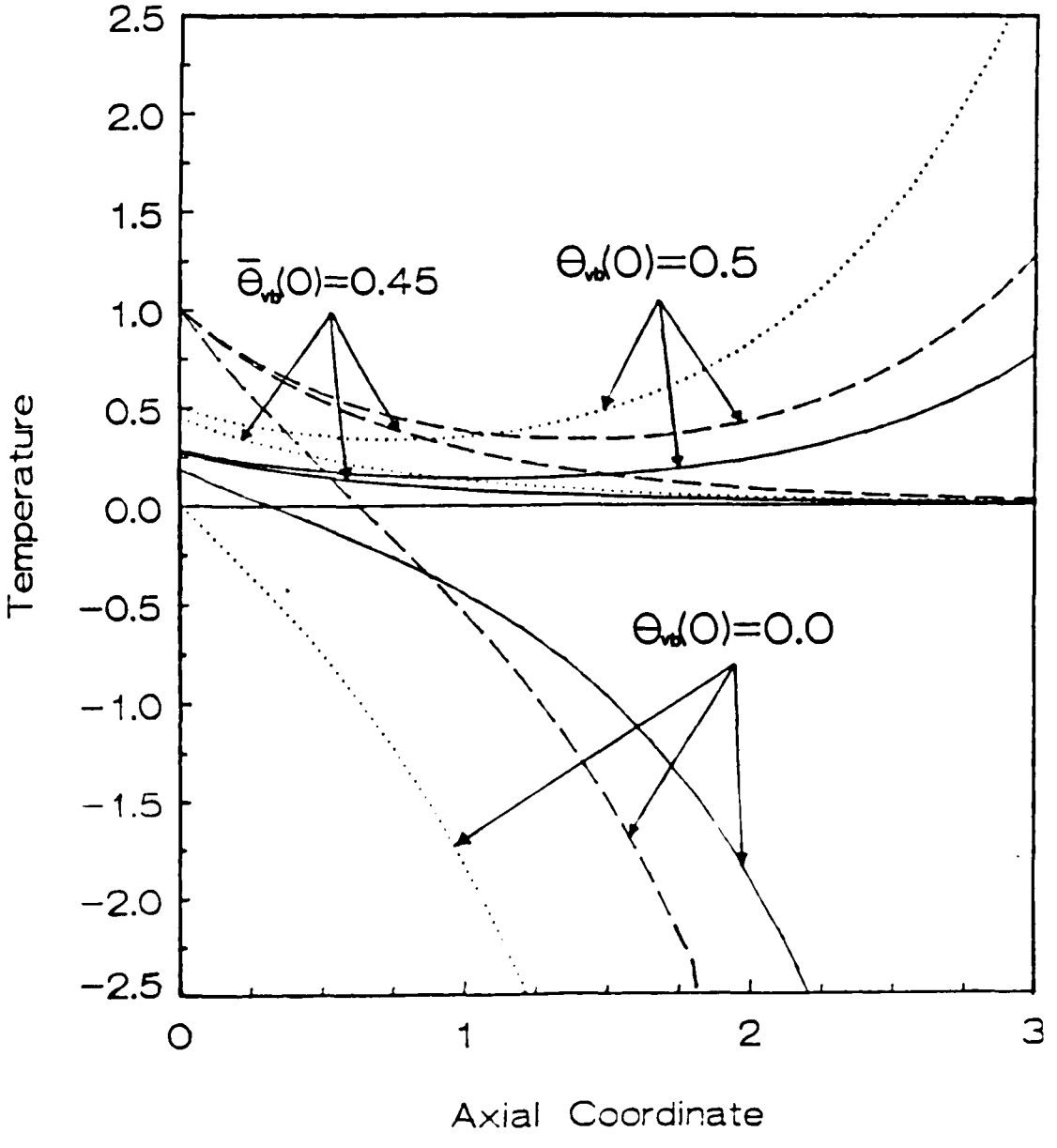

Fig. 6 Bulk temperature distribution in vessels and axial profile of mean tissue temperature for three different axial boundary conditions $\theta_{vb}(0)$. Bi=0.5, k'=1, $\bar{s}$=2.1, ρ_R=10, $\bar{a}_v$=1.
--- artery, ... vein, —— tissue.

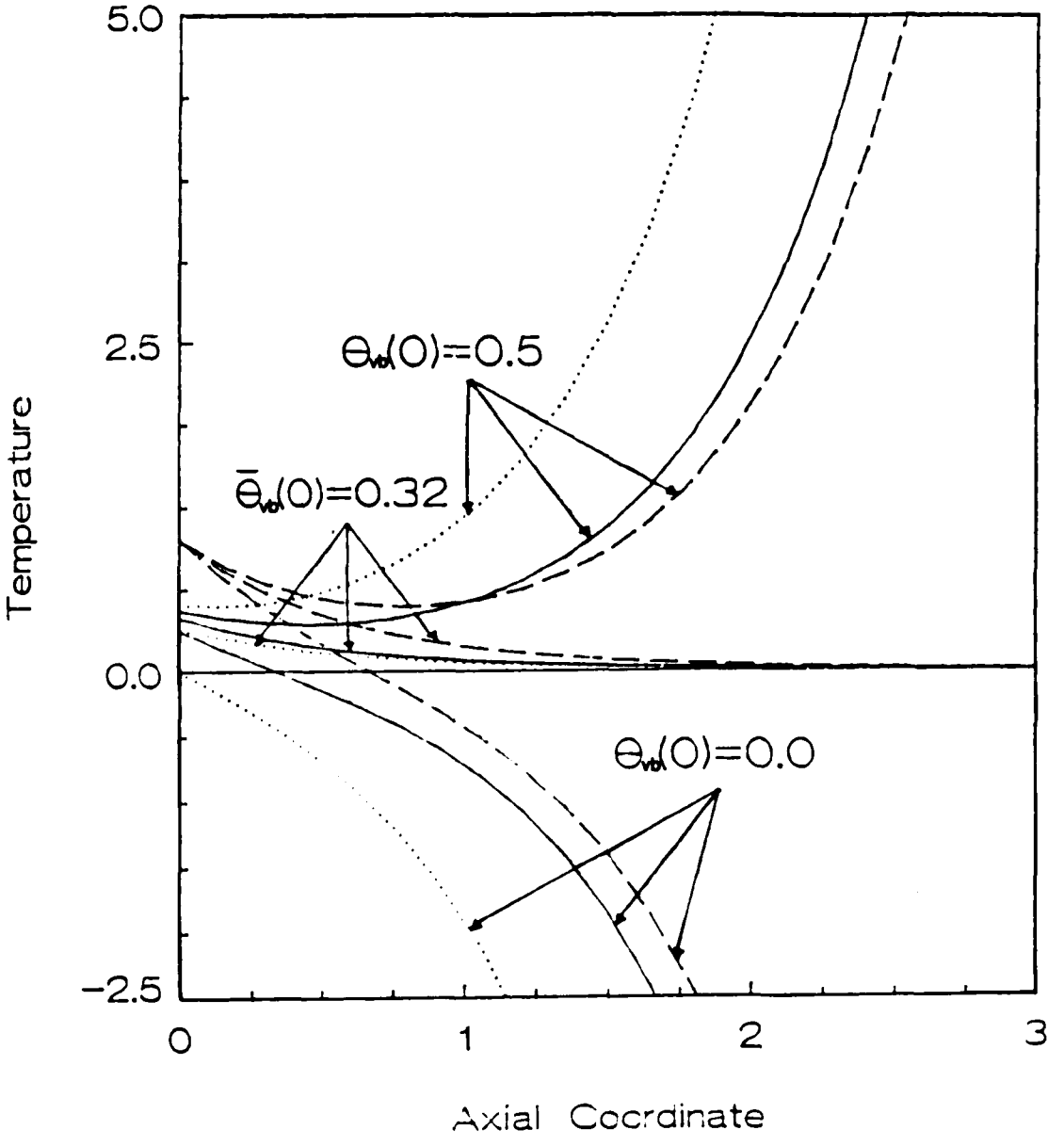

Fig. 7 Bulk temperature distribution in vessels and axial profile of mean tissue temperature for three different axial boundary conditions $\theta_{vb}(0)$. Bi=10, k'=1, $\bar{s}$=2.1, ρ_R=10, $\bar{a}_v$=10
--- artery, ... vein, —— tissue.

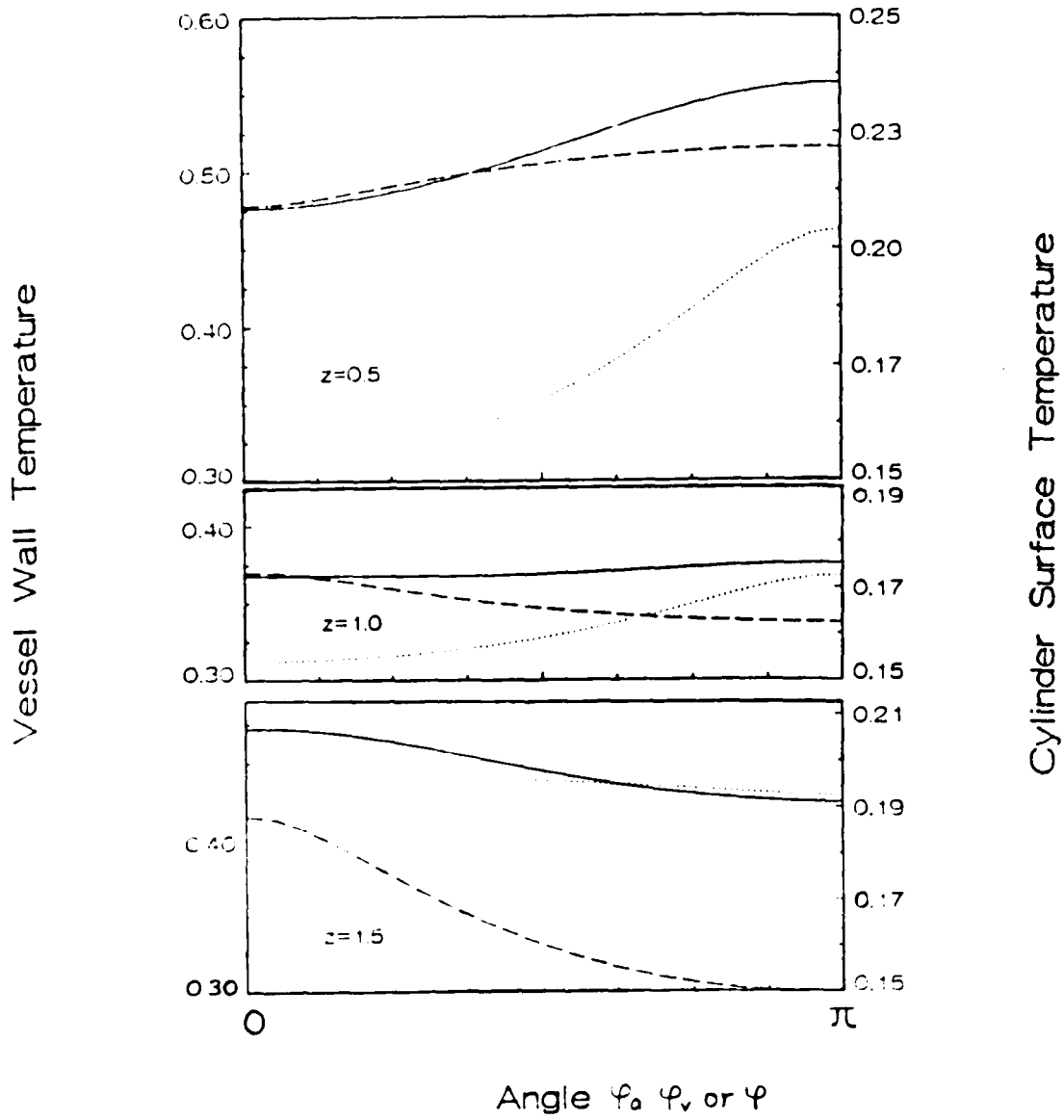

Fig. 8 Angular temperature distribution at vessel walls and cylinder surface under the same conditions of Fig. 6 at three different cross-sections for $s_a=s_v$, $\varphi_{av}=\pi$ and $\theta_{vb}(0)=0.5$. --- artery, ... vein, —— cylinder surface.

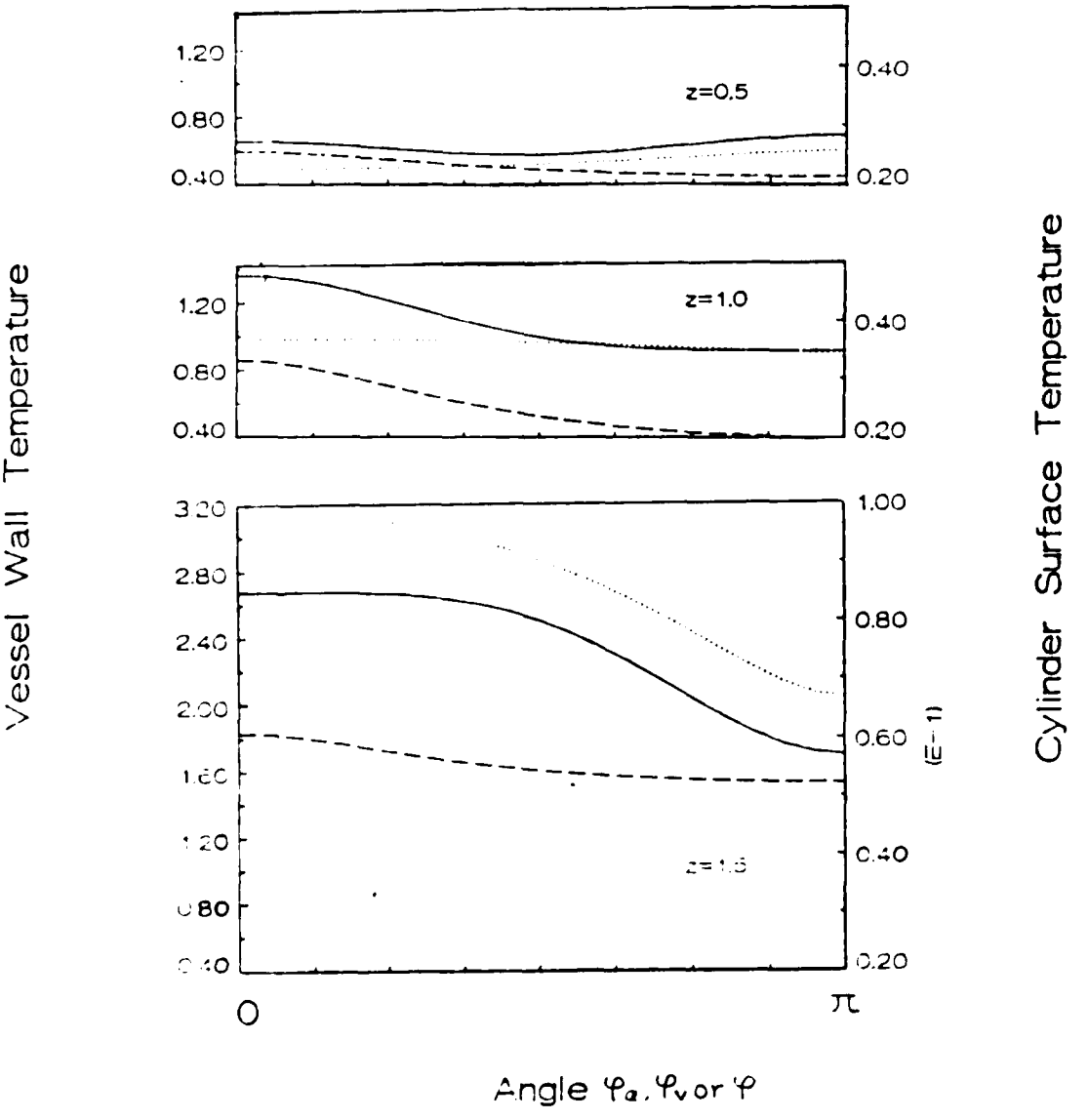

Fig. 9 Angular temperature distribution at vessel walls and cylinder surface under the same conditions of Fig. 7 at three different cross-sections for $s_a=s_v$, $\varphi_{av}=\pi$ and $\theta_{vb}(0)=0.5$. --- artery, ... vein, —— cylinder surface.

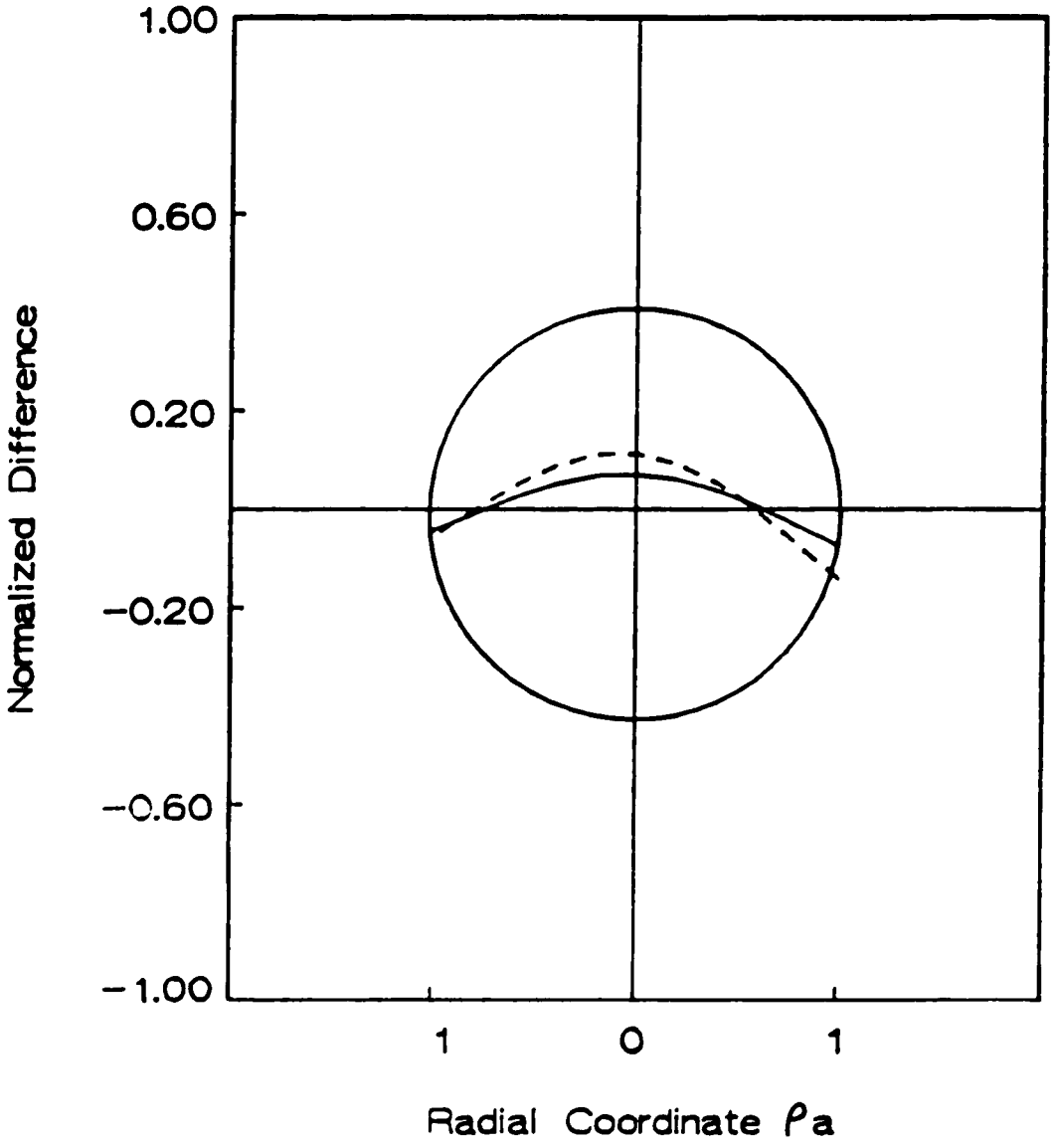

Fig. 10 Variation of normalized difference between bulk and local axial temperature gradients at cross-section z=0. Bi=0.5, k'=1, $\bar{s}$=2.1, ρ_R=10, a_v=1. —— $\theta_{vb}(0)$=0.9, --- $\theta_{vb}(0)$=0.5.

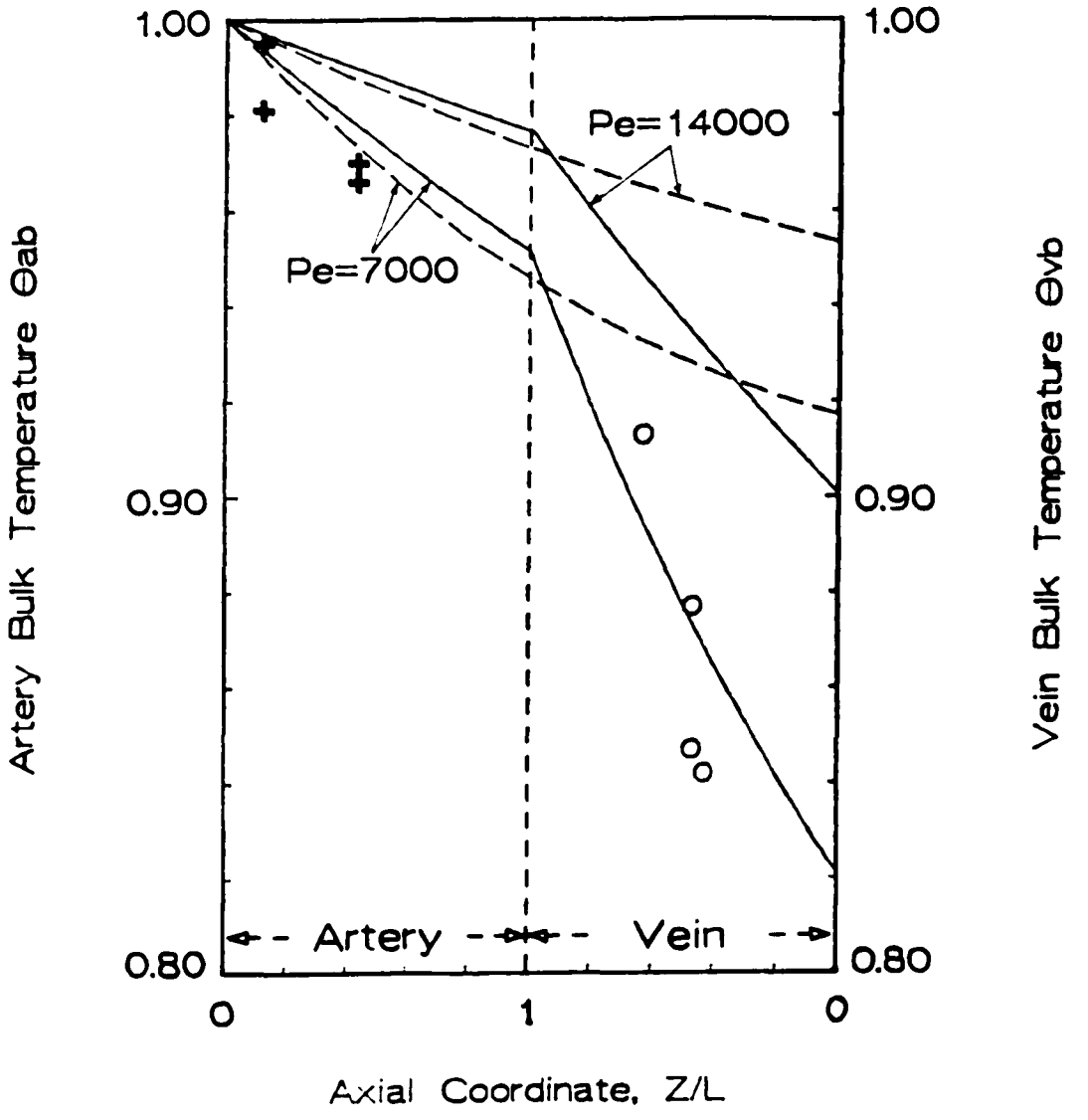

Fig. 11 Comparison of bulk temperature distribution in central vessels of arm predicted by non-taped present model and Mitchell and Myers' model [15] with experimental data of Bazett et al. [19]. $Bi=1.5$, $k'=1$, $s=4$, $a_v=1$, $\rho_R=16$. —— Present model, --- model in [15], + o experimental data in [19].

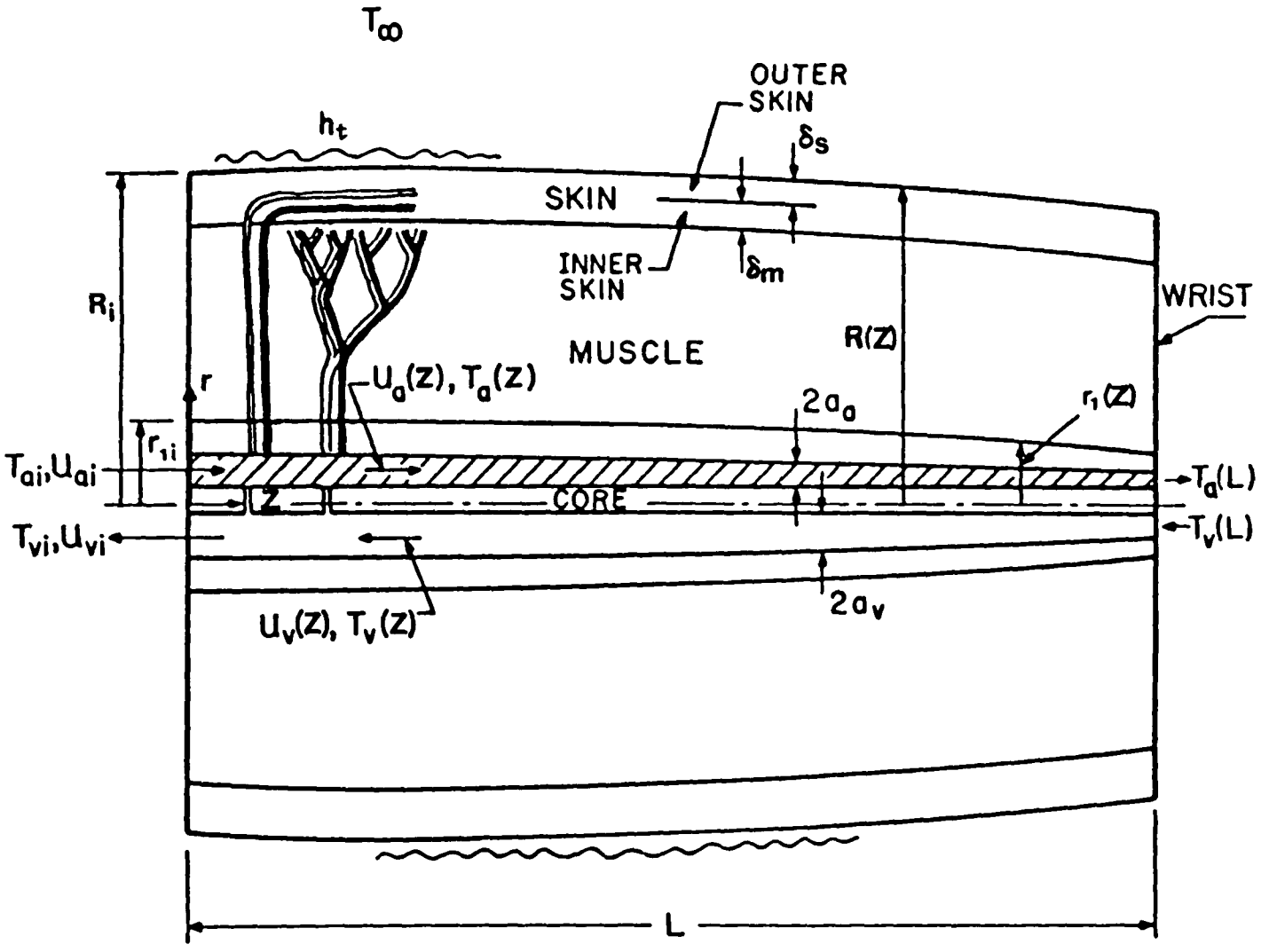

Fig. 12 Schematic of whole limb model

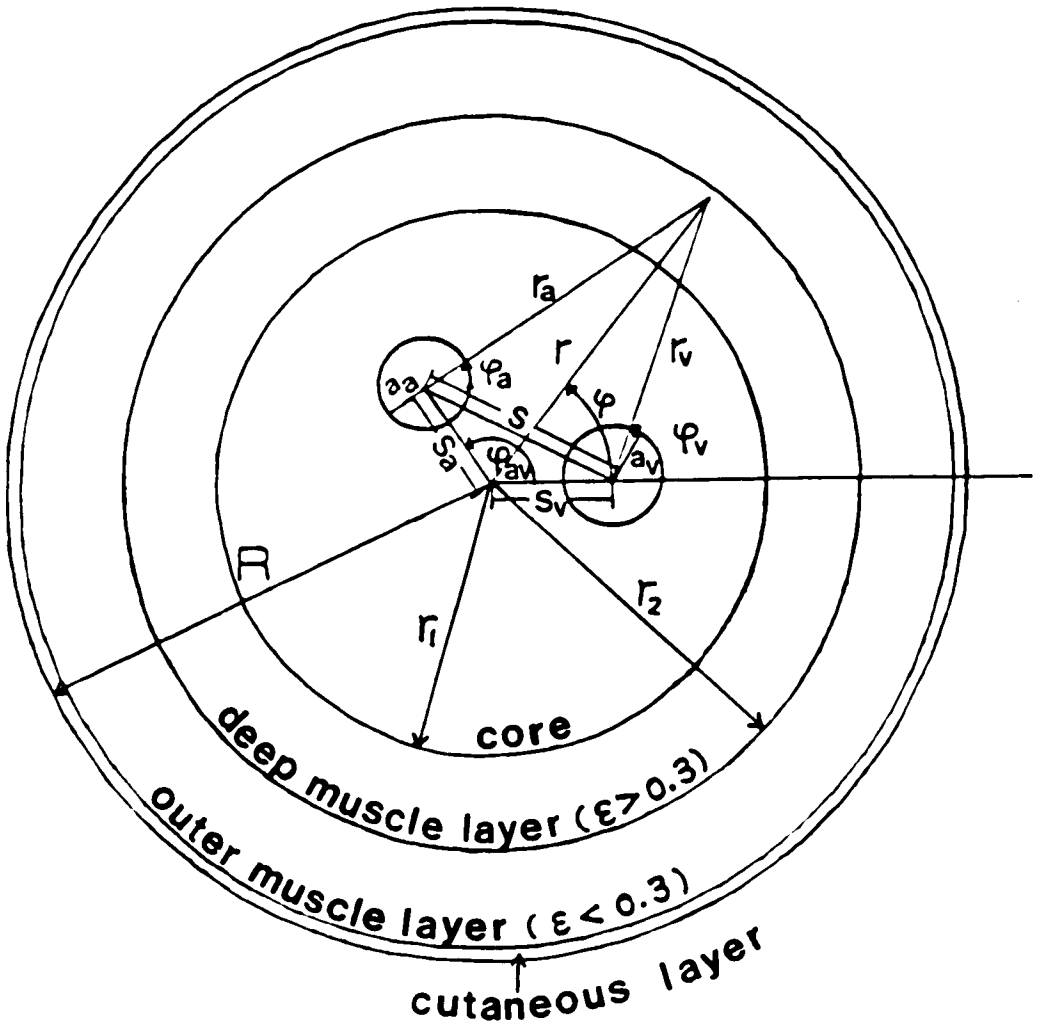

Fig. 13 Schematic of limb cross-section

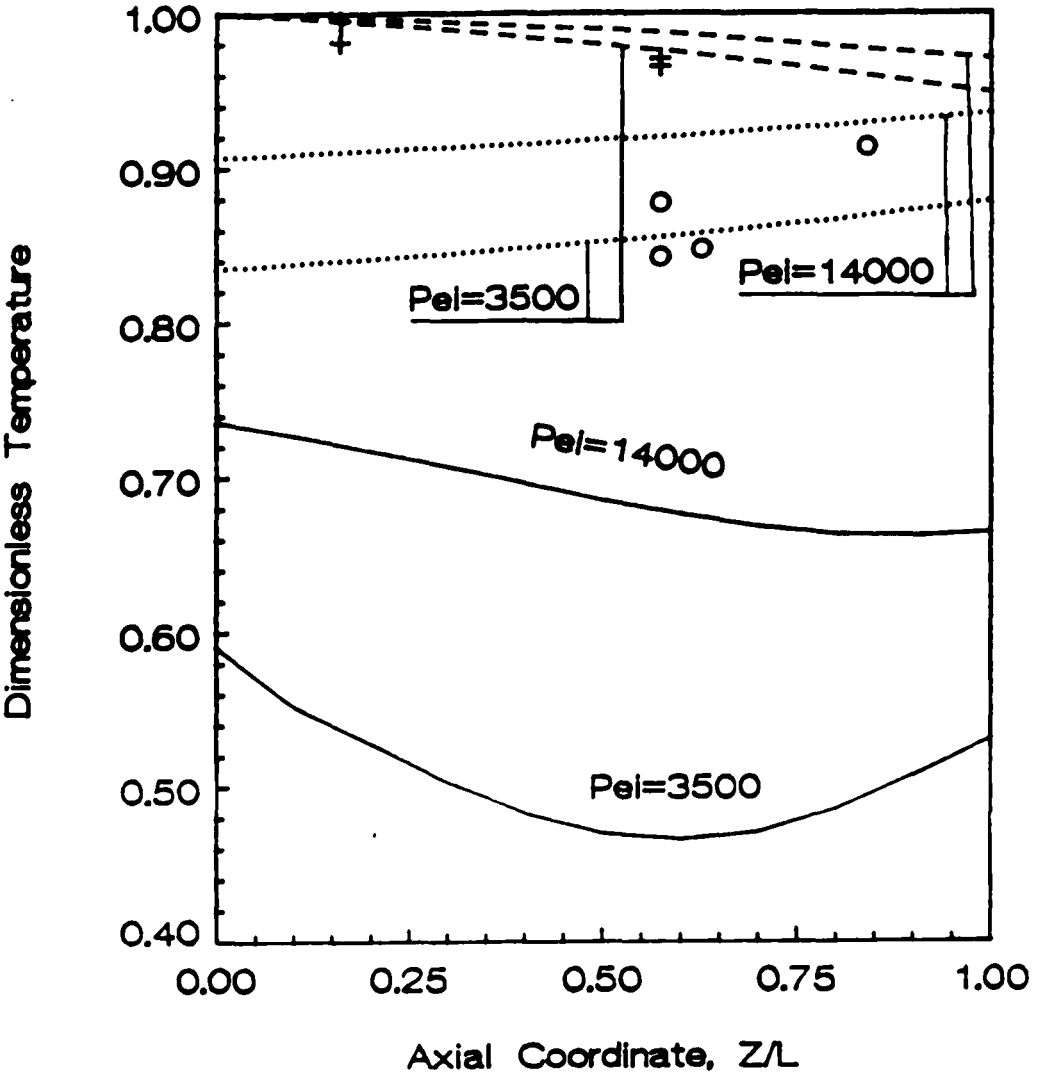

Fig. 14 Effect of inflow Peclet number Pei on central bulk artery, vein and average skin surface temperature profile for ω=0.92, Bit=1.48, ϕ=0.75, γ=1.524X10^{-3} , and the experimental data for central artery and vein temperature in resting state of Bazett et al. [19]. --- artery, ... vein, —— skin surface, + o experimental artery and vein in [19].

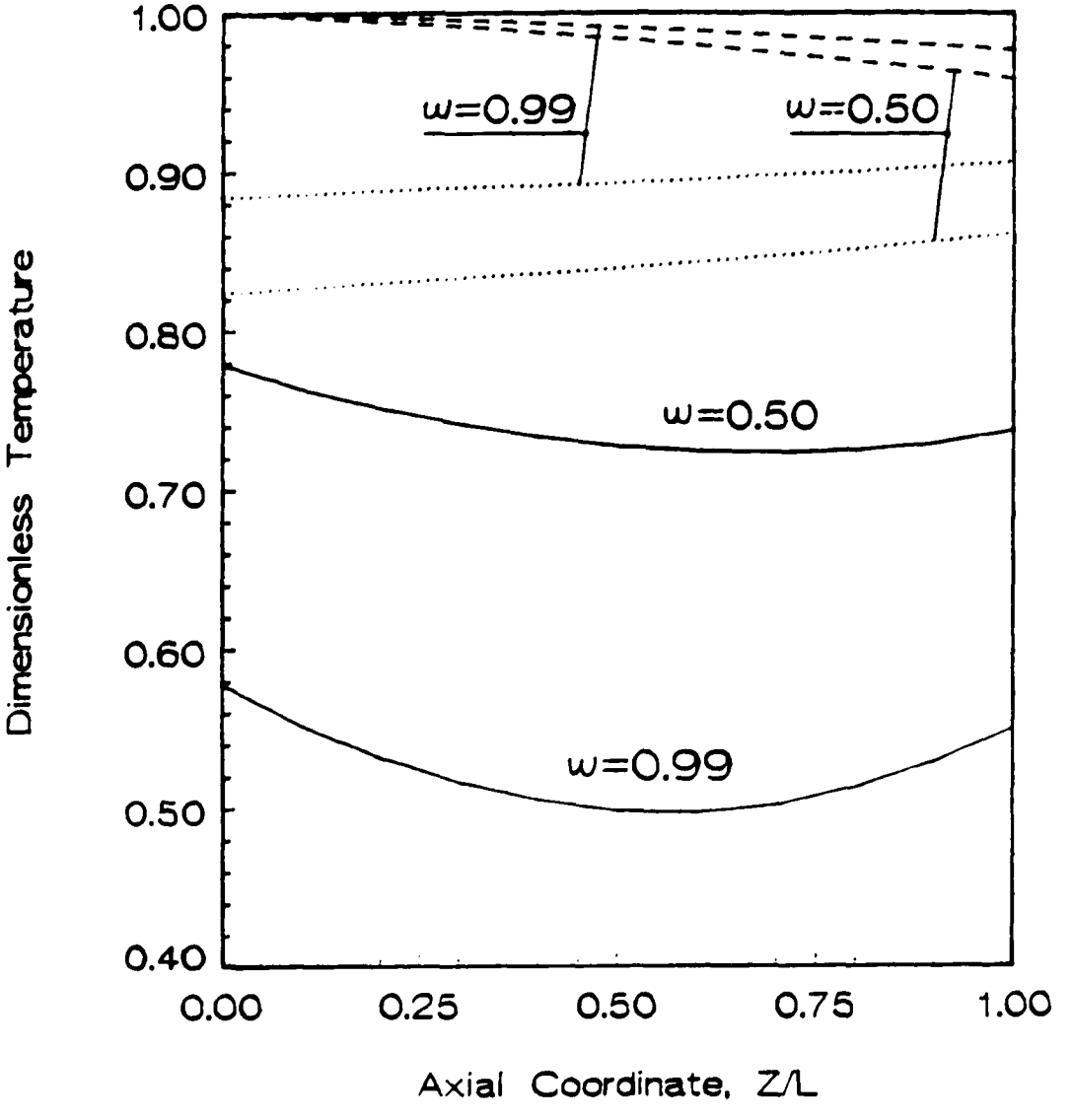

Fig. 15 Effect of blood flow ratio ω on central bulk artery, vein and average skin surface temperature profile for Pei=7000, Bit=1.48, Ψ=0.75, τ=1.524×10^{-3}, --- artery, ··· vein, —— skin surface.

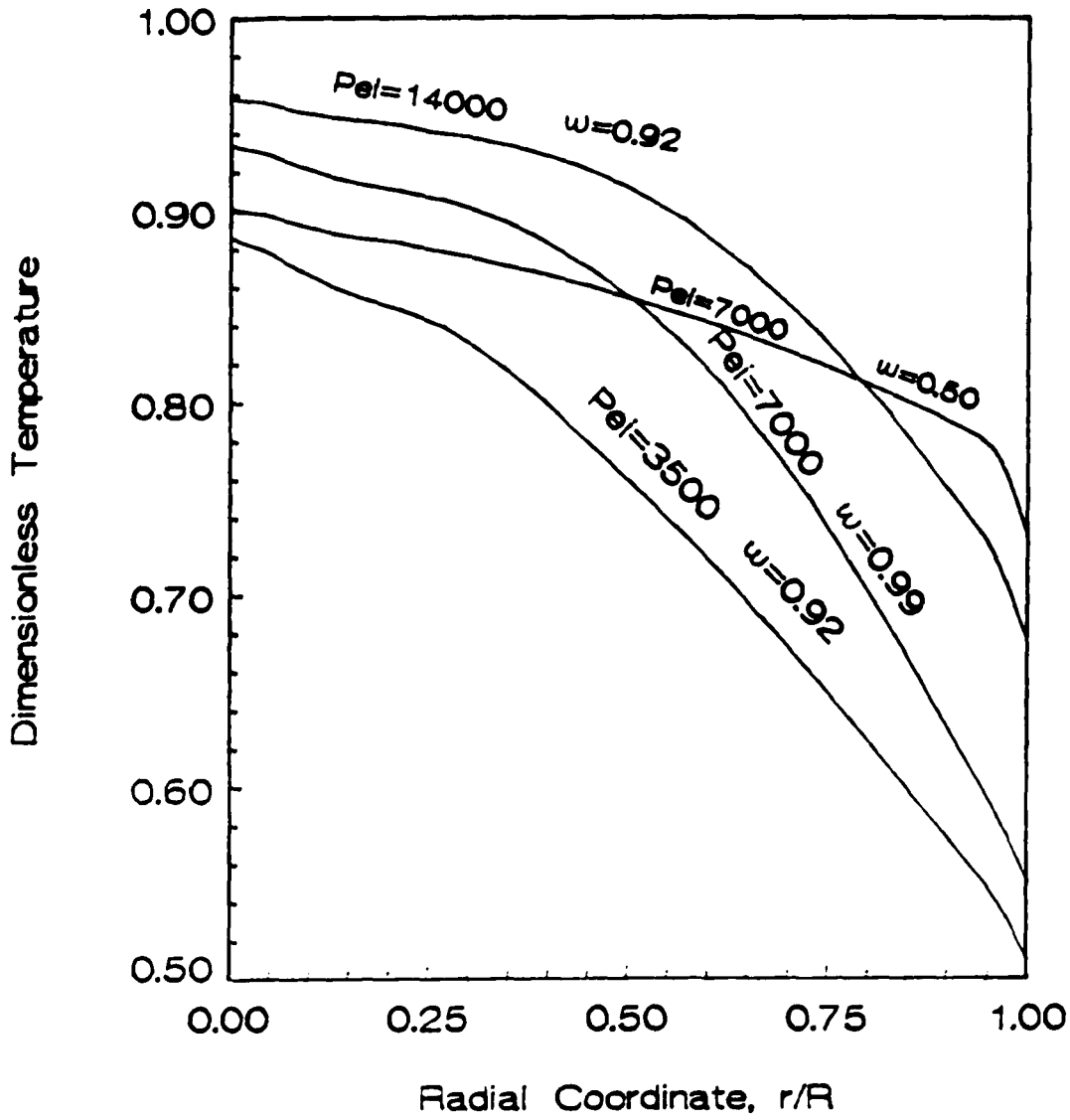

Fig. 16 Radial temperature profile of tissue at Z/L=0.95 for Bi_t=1.48, ψ=0.75, γ=1.524X10^{-3}

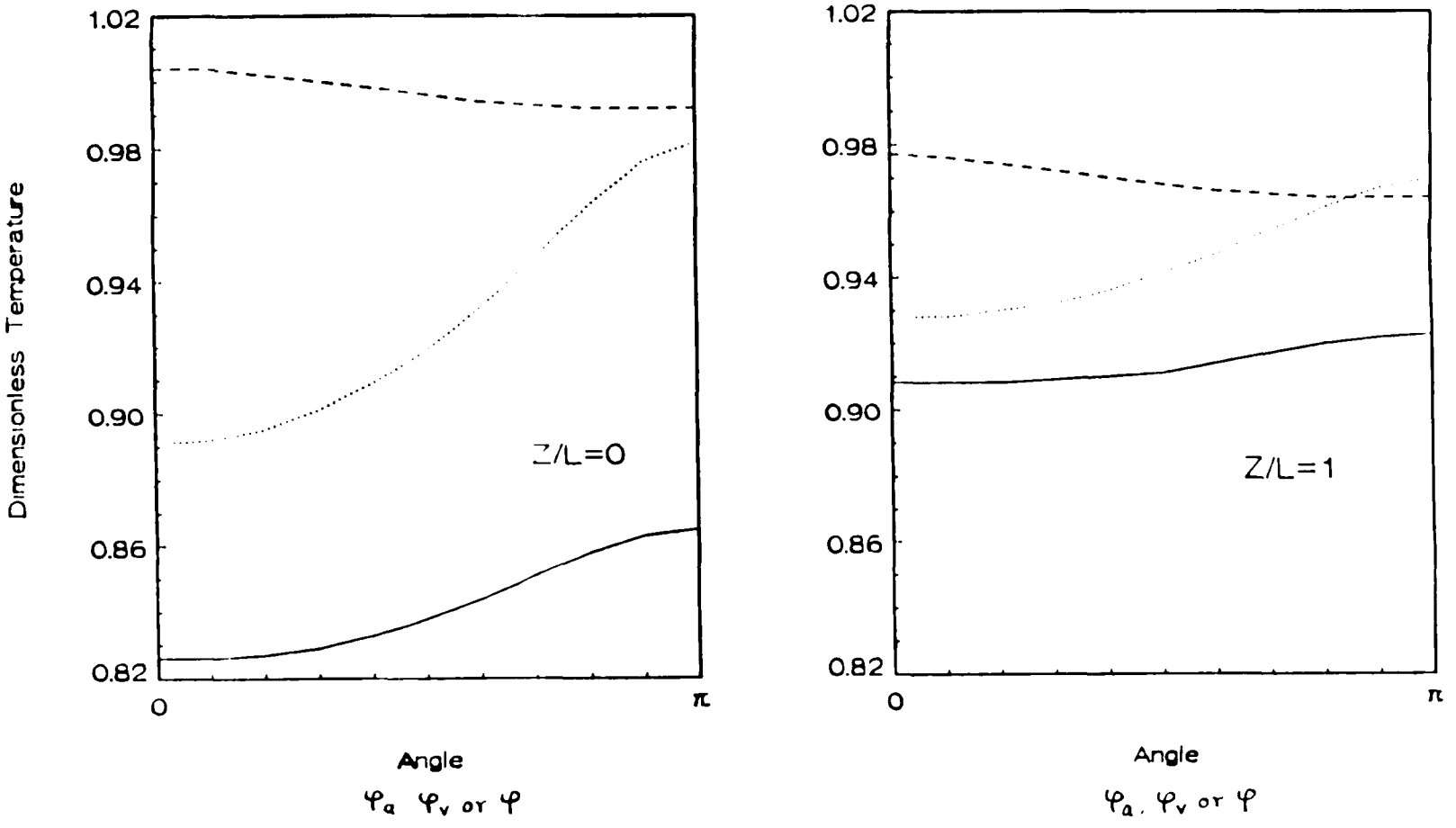

Fig. 17 Angular temperature distribution at central vessel walls and interface between core and muscle for P_{ei}=14,000, ω=0.92, B_{it}=1.48, ϕ=0.75, γ=1.524×10^{-3} at shoulder and wrist cross-sections. --- artery, ... vein, ___ core.

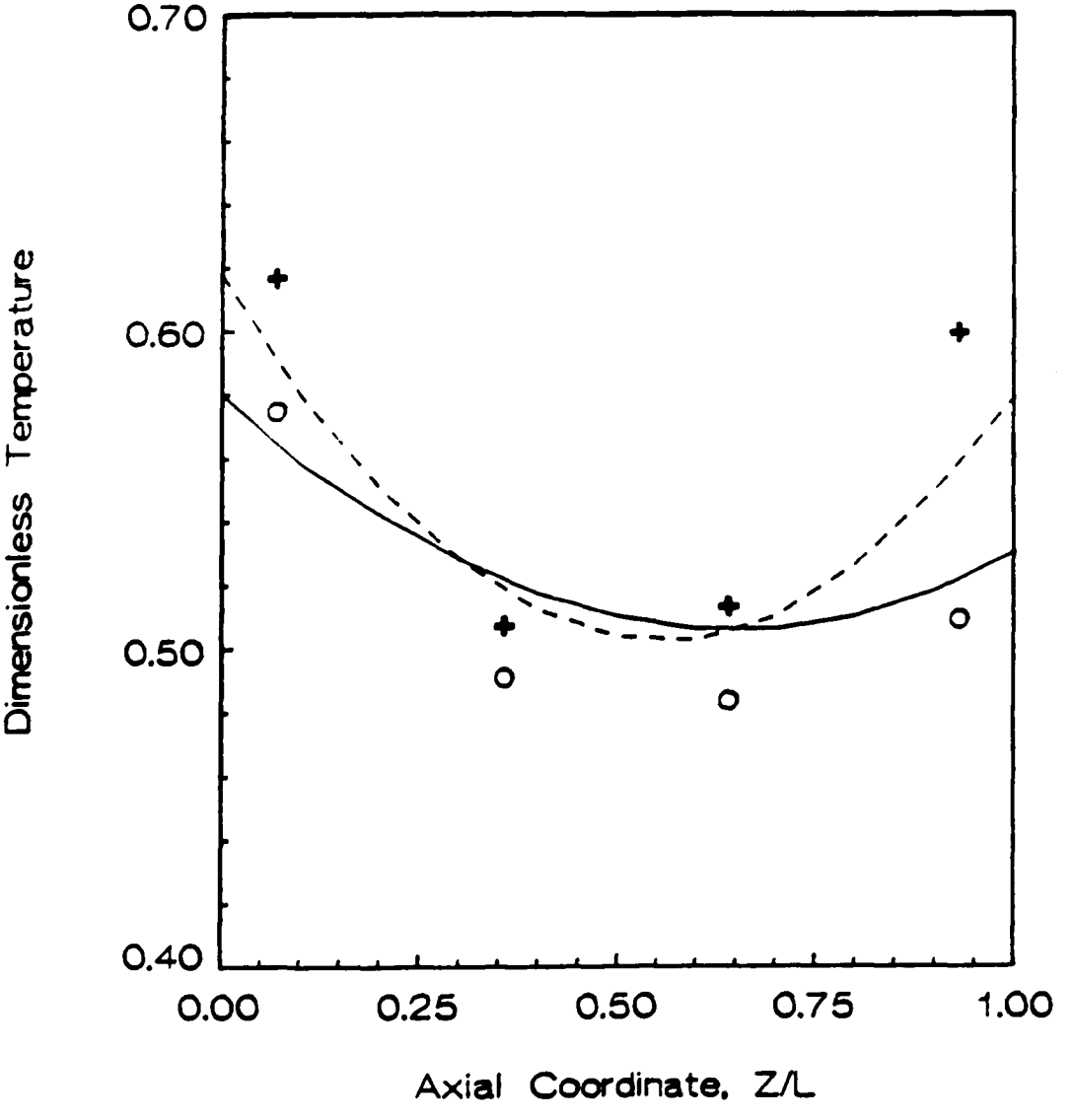

Fig. 18 Comparison of axial skin surface temperature distribution predicted by present model with experimental data for hand in 30°C water(Pe_i=3582, ω=0.92, Bi_t=1.48, ϕ=0.757, q_H=7.35W γ=1.524×10^{-3}) and 35°C water (Pe_i=4215, ω=0.92, Bi_t=1.48, q_H=2.9W, γ=1.524×10^{-3}). —— o theoretical and experimental value for 30°C water, --- + theoretical and experimental value for 35°C water.

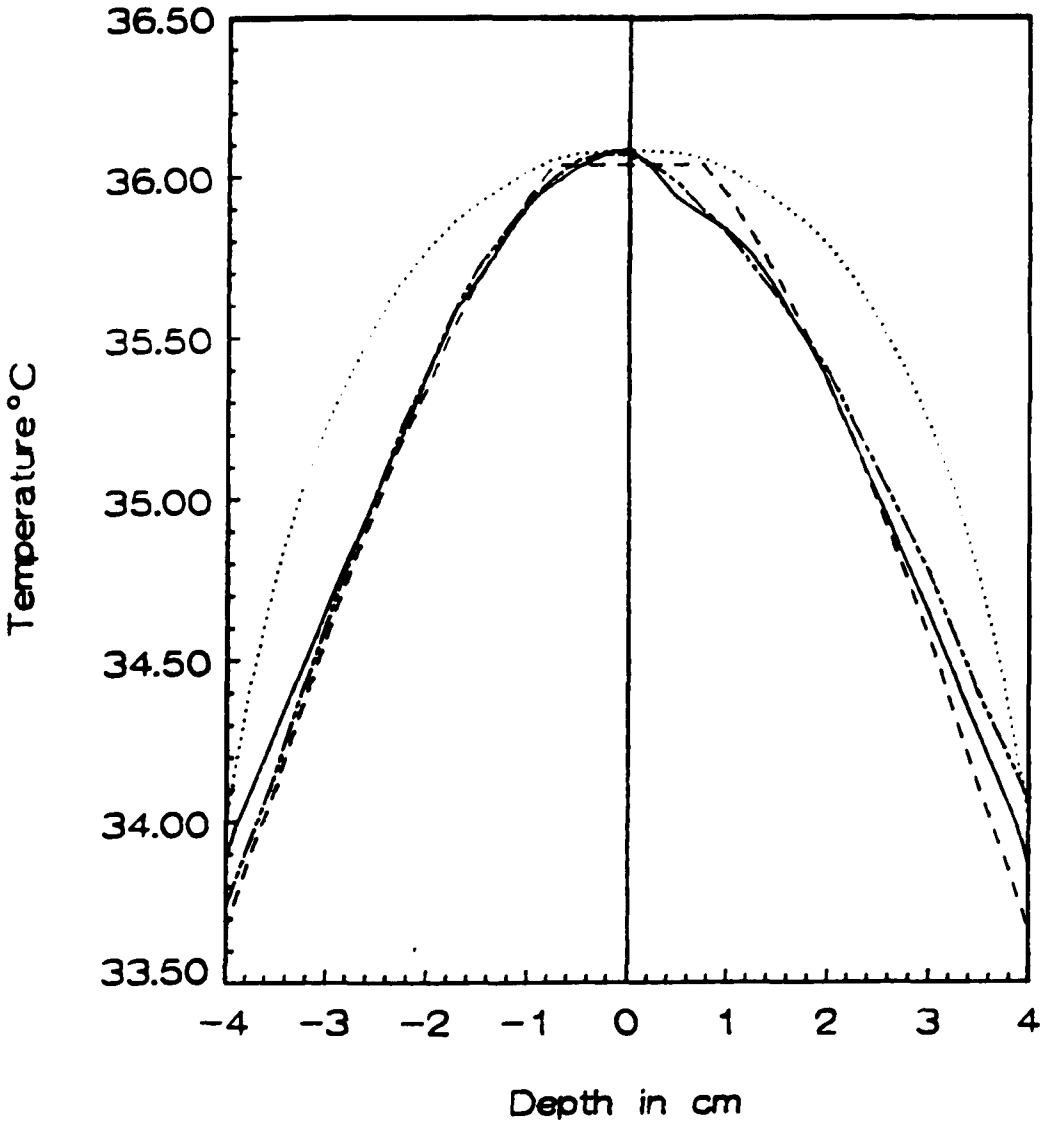

Fig. 19 Comparison between theoretical predictions and experimental measurement for radial tissue temperature profile at Z/L=0.95 in resting state at room temperature 27°C. —— present model, --- model in [14], ··· model in [1], —·— experiment in [1].

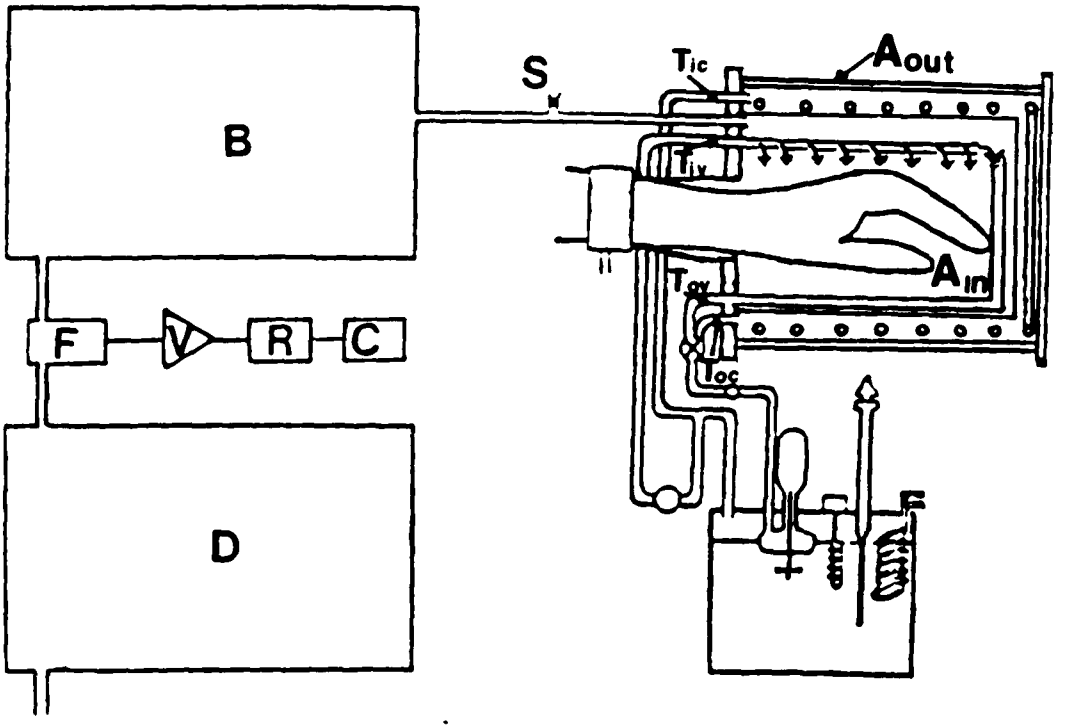

Fig. 20 Schematic of Plethcal apparatus

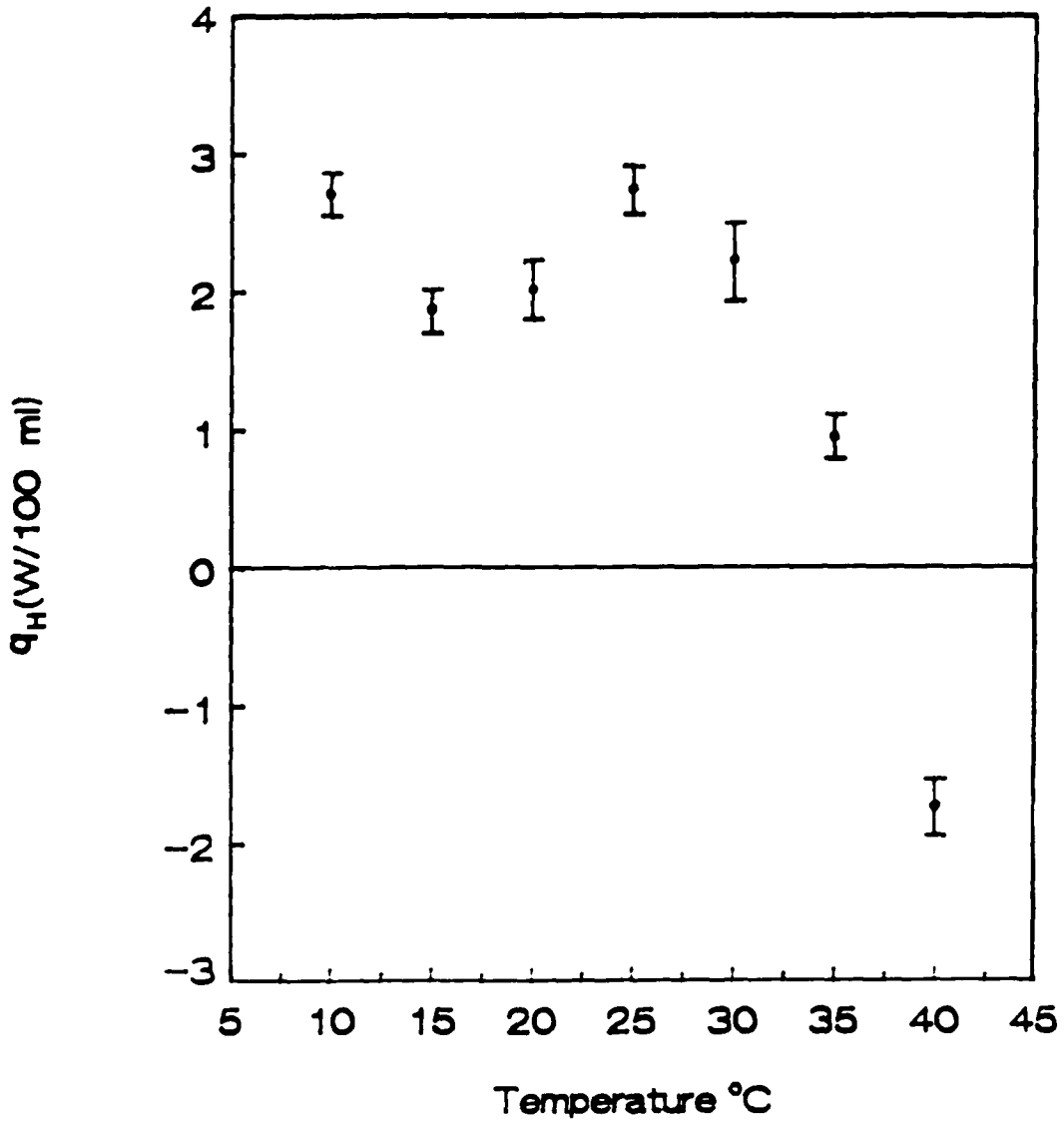

Fig. 21 Heat loss from hand as function of water temperature T_w

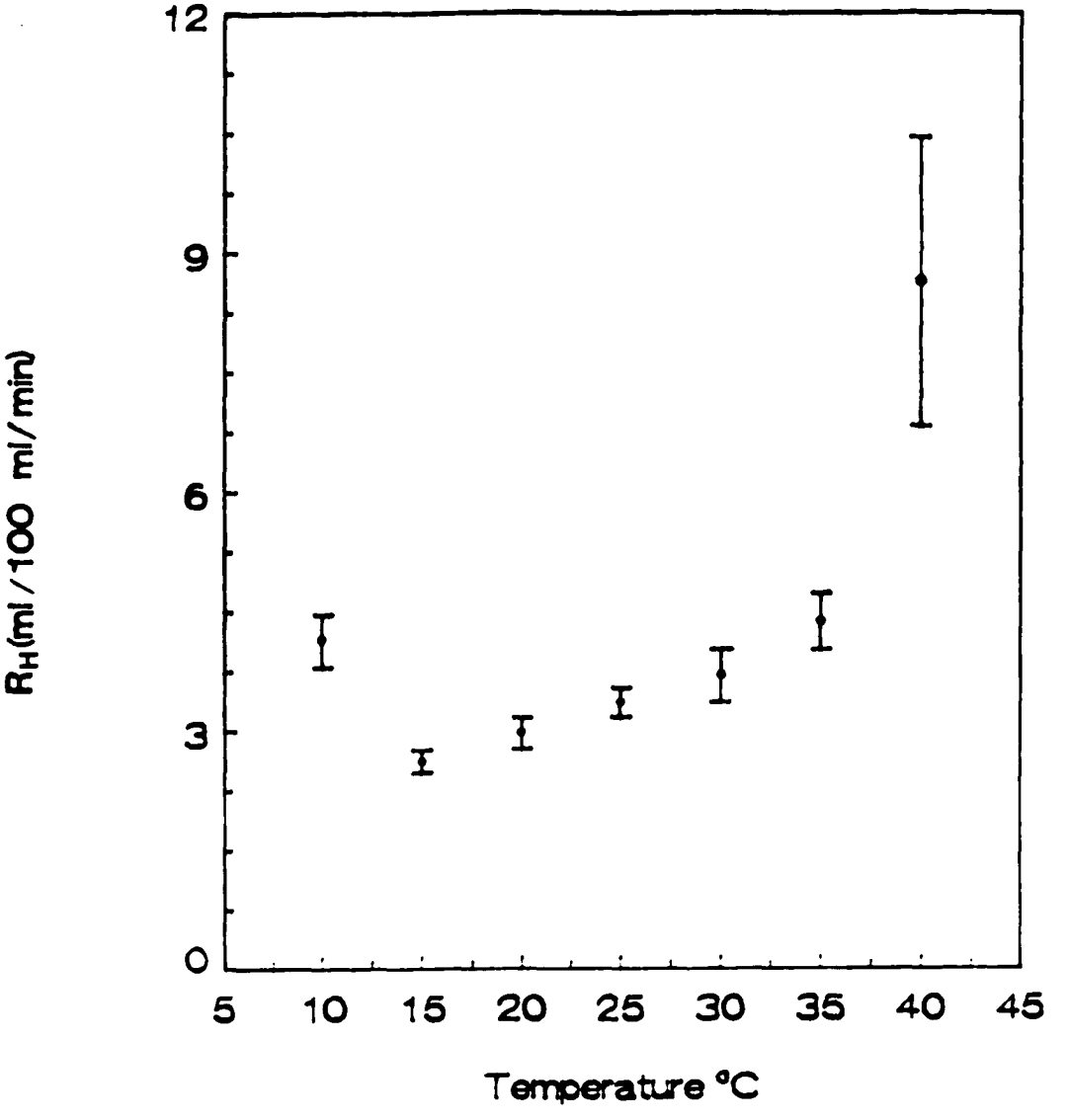

Fig. 22 Hand blood flow rate as function of water temperature T_w

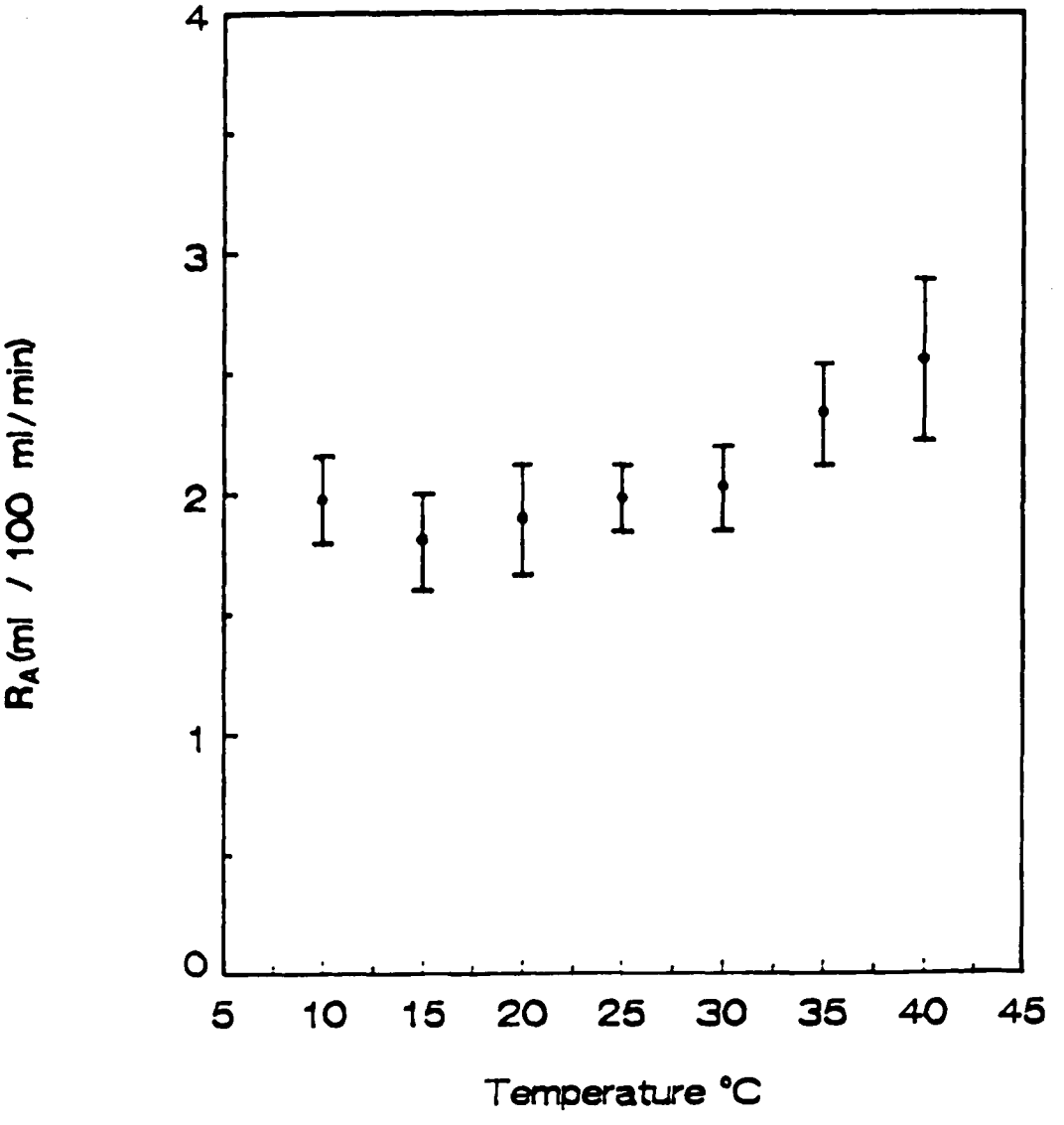

Fig. 23 Arm blood flow rate as function of water temperature T_w

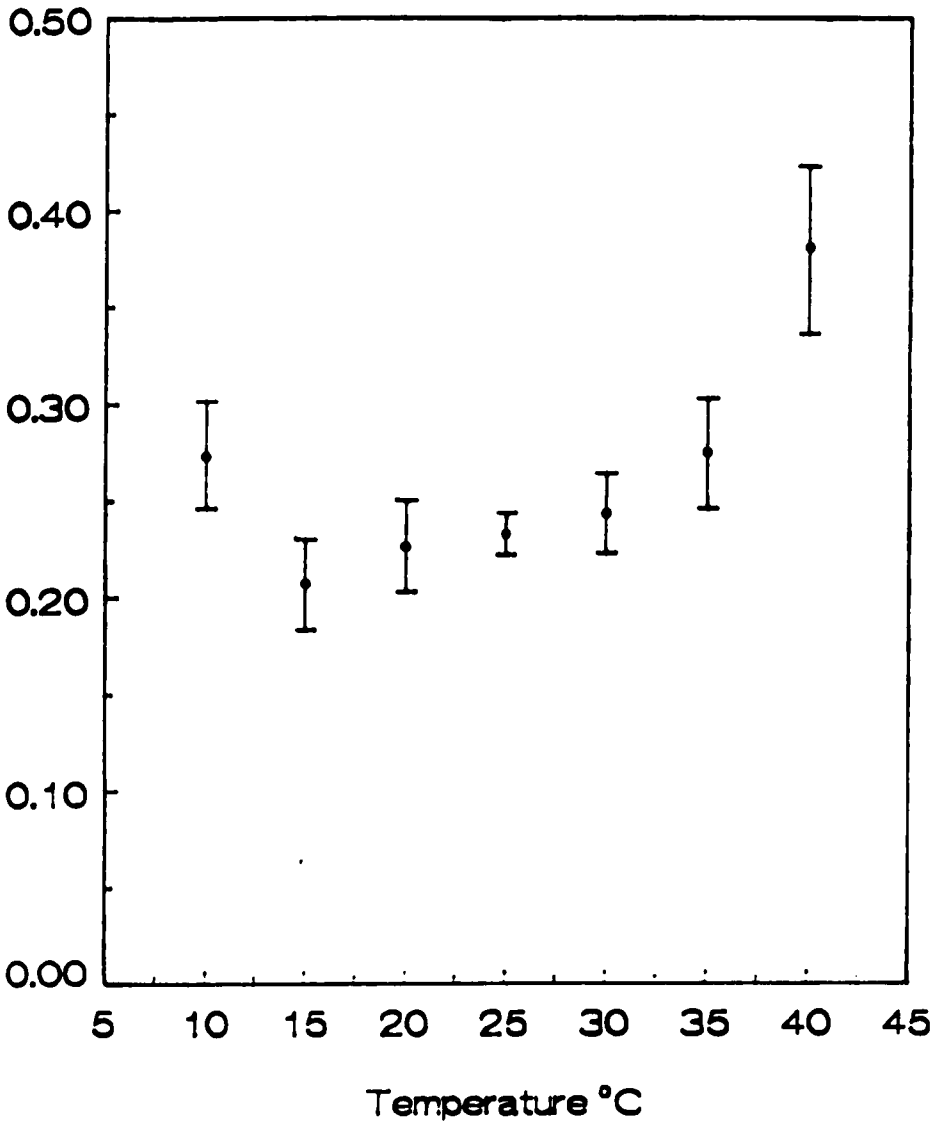

Fig. 24 Blood flow ratio $1-\psi$ as function of water temperature T_w

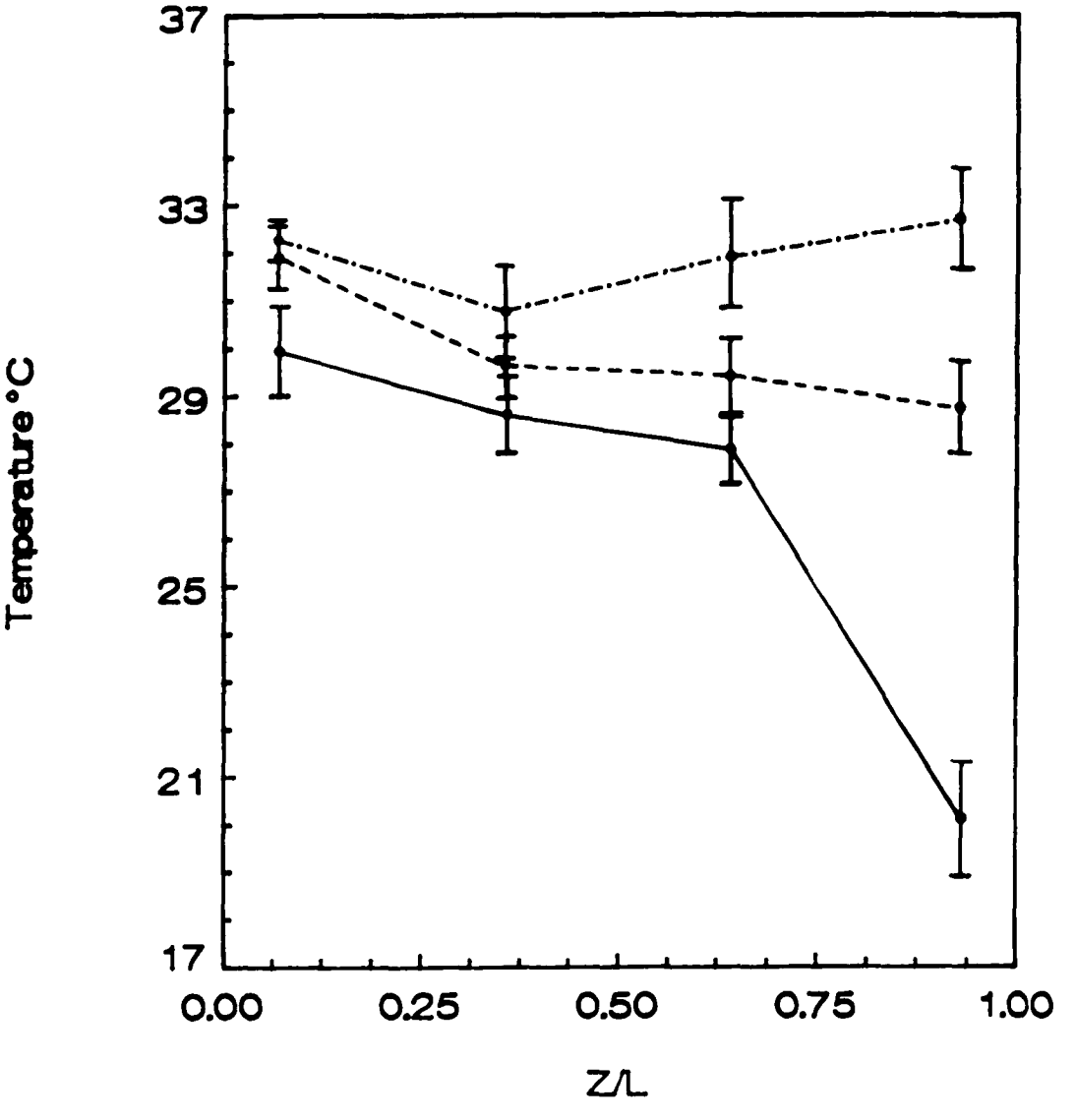

Fig. 25 Axial skin surface temperature profile of arm for hand immersed in three different temperature water. —— 10°C water, --- 25°C water, -·- 40°C water.

BIBLIOGRAPHY

1. Pennes, H.H., "Analysis of Tissue and Arterial Blood temperatures in the Resting Forearm," Journal of Applied Physiology, Vol.1, 1948, pp. 93-122.

2. Shitzer, A. and R.C. Eberhart, Ed., Heat Transfer in Medicine and Biology, Vol.1, Plenum Press, New York, 1985.

3. Wulff, W., "The Energy Conservation Equation for Living Tissue," ISEE Trans. BME-21, No.6, 1974, pp. 494-495.

4. Klinger, H.G., "The Description of Heat Transfer in Biological Tissue, " Proceedings Conference on Thermal Characteristics of Tumors: Applications in Detection and Treatment," New York Academy of Science (Mar. 14-16, 1979).

5. Chen, M.M. and K.R. Holmes, "Microvascular Contributions in Tissue Heat Transfer," Annals of the New York Academy of Science, Vol.355, 1980, pp. 137- 150.

6. Weinbaum, S. and L.M. Jiji, "A New Simplified Bioheat Equation for the Effect of Blood Flow on Local Average Tissue Temperature," ASME Journal of Biomechanical Engineering, Vol. 107, 1985, pp. 131-139.

7. Charny, C.K., S. Weinbaum and R.L. Levin, "An Evaluation of the Weinbaum-Jiji Bioheat Equation for Normal and Hyperthermic Conditions," ASME Journal of Biomechanical Engineering, Vol. 112, 1990, pp. 80-87.

8. Jiji, L.M., S. Weinbaum and D.E. Lemons, "Theory and Experiment for the Effect of Vascular Microstructure on Surface Tissue Heat Transfer. Part II: Model Formulation and Solution," ASME Journal of Biomechanical Engineering, Vol.106, 1984, pp. 331-341.

9. Dagan, Z., S. Weinbaum and L.M. Jiji, "Parametric Studies on the Three Layer Microvascular Model for Surface Energy Exchange," ASME Journal of Biomechanical Engineering, Vol. 108, 1986, pp. 89-96.

10. Lemons, D.E., S. Weinbaum and L.M. Jiji, "Experimental Studies on the Role of the Micro and Macro Vascular System in Tissue Heat Transfer," American Journal of Physiology, Vol.253, 1987, pp. R128-R135.

11. Wissler, E.H., "Comments on the New Bioheat Equation Proposed by Weinbaum and Jiji," ASME Journal of Biomechnical Engineering, Vol.109, 1987, pp. 226-233.

12. Weinbaum, S. and L.M. Jiji, "Discussion of Paper by Wissler and Baish et al. Concerning the Weinbaum-Jiji Bioheat Equation," ASME Journal of Biomechanical Engineering, Vol.109, 1987, pp. 234-237.

13. Song, W.J., S. Weinbaum and L.M. Jiji, "A Theoretical Model for Peripheral Tissue heat transfer Using the New Bioheat Equation of

Weinbaum and Jiji," ASME Journal of Biomechanical Engineering, Vol.109, 1987, pp. 72-78.

14. Song, W.J., S. Weinbaum, L.M. Jiji and D.E. Lemons, "A Combined Macro and Microvascular Model for Whole Limb Heat Transfer," ASME Journal of Biomechanical Engineering, Vol. 110, 1987, pp. 259-268.

15. Mitchell, J.W. and G.E. Myers, "An Analytical Model of the Countercurrent Heat Exchange Phenomena," Biophysical Journal, Vol.8, 1968, pp. 897-911.

16. Raman, E.R. and V.J. Vanhuyse, "Analytical Model for the Temperature Dependence of the Circulation Pattern in Upper Extremities," Rad. and Environmental Biophysics, Vol. 12, 1975, pp. 257-269.

17. Wissler, E.H., "A Mathematical Model of the Human Thermal System," Bulletin of Mathematical Biophysics, Vol.26, 1964, pp. 147-166.

18. Arkin, H. and A. Schitzer, "A Model of Thermoregulation in the Human Body," ASME Winter Annual Meeting, ASME Paper 84-WA/HT-66, 1984.

19. Bazett, H., L. Love, M. Newton, L. Eisenberg, R. Day and R. Forster, "Temperature Changes in Blood Flowing in Arteries and veins in Man," Journal of Applied Physiology, Vol.1, 1948, pp.3-19.

20. Raman, E.R. and V.J. Vanhuyse, "Temperature Dependence of the Circulation Pattern in the Upper Extremities," Journal of Physiology, Vol. 249, 1975, pp. 197-210.

21. Rowell, L.B., Human Circulation, Oxford, New York, 1986

22. Bernard, C., La Chaleur Animale, Paris, 1876

23. Brengelmann, G. and A. Brown, "Temperature Regulation," in Physiology and Biophysics, Eds. Ruch, T., and H. Patton, pp.10-57, Philadelphia-London: Saunders 1965.

24. Raman, E. R. and V. J. Vanhuyse, "Displacement Plethysmograph Allowing Heat Loss Measurements of Extremities," Medical and Biological Engineering, May 1975, pp. 422-424.

25. Vanhuyse, V.J. and E.R. Raman, "Determination of the Efficacy of the Mechanism Changing the Relative Rate of Blood Flow through Cutaneous and Deep Lying Veins with Temperature," Phys. Med. Biology, Vol. 21, 1976, No. 4, pp. 608-615.

26. Ducharme, M.B., Personal communication, 1989

27. Baish, J.W., P.S. Ayyaswamy and K.R. Foster, "Small-Scale Temperature Fluctuations in Perfused Tissue During Local Hyperthermia," ASME Journal of Biomechanical Engineering, Vol.108, 1986, pp. 246-250.

28. Baish, J.W., P.S. Ayyaswamy and K.R. Foster, "Heat Transport Mechanisms in Vascular Tissues: A Model Comparison," ASME Journal of Biomechanical Engineering, Vol.108, 1986, pp. 324-331.

29. Chato, J.C., "Heat Transfer to Blood Vessels," ASME Journal of Biomechanical Engineering, Vol. 102, 1980, pp. 110-118.

30. Weinbaum, S., L.M. Jiji and D.E. Lemons, "Theory and Experiment for the Effect of Vascular Microstructure on Surface Tissue Heat Transfer. Part I: Anatomical Foundation and Model Conceptualization, " ASME Journal of Biomechanical Engineering, Vol.106, 1984, pp. 321-330.

31. Charny, C.K. and R.L. Levin, "Heat Transfer Normal to Paired Arteries and Veins Embedded in Perfused Tissue During Hyperthermia," ASME Journal of Biomechanical Engineering, Vol. 110, 1988, pp. 277-282.

32. Kays, W.M. and A.C. London, Compact Heat Exchangers, McGraw-Hill, 1986.

33. Eckert, E.R.G. and R.M. Drake, Analysis of Heat and Mass Transfer, pp. 98 and 340, McGraw-Hill, 1972.

34. Hahne, E. and U. Grigull, "A Shape Factor Scheme for Point Source Configurations," Int. Journal of Heat and Mass Transfer, Vol. 17, 1974, pp. 267-273.

35. Thiyagarajan and M.M. Yovanovich, "Thermal Resistance of a Buried Cylinder With Constant Flux Boundary Condition," ASME Journal of Heat Transfer, Vol. 96, 1974, pp. 249-250.

36. DiFelice, R.F., Jr. and H.H. Bau, "Conductive Heat Transfer between Eccentric Cylinders with Boundary Conditions of the Third Kind," ASME Journal of Heat Transfer, Vol. 105, 1983, pp. 678-680.

37. Bau, H.H. and S.S. Sadhal, "Heat Losses from a Fluid Flowing in a Buried Pipe," Int. Journal of Heat and Mass Transfer, Vol. 25, 1982, pp. 1621-1629.

38. Wissler, E.H, "An Analytic Solution for Countercurrent Heat Transfer Between Parallel Vessels with a Linear Axial Temperature Gradient," ASME Journal of Biomechanical Engineering, Vol. 110, 1988, pp. 254-256

39. Charny, C.K., Personal communication, 1989

40. Ducharme, M.B., W.P. VanHelder and M.W. Radomski, "Tissue Temperature Profile in the Human Forearm During Thermal Stress," Physiologist, Vol. 32, No. 4, August 1989 pp. 203.

41. Bargeton, D., J. Durand, J. Mensch-Dechene, and J. Decaud, "Exchanges de chaleur de la main," J. Physiol., Paris 51, 1959, pp. 111-150.